Magnetic Sedimentation in Aqueous Ferrofluids

for Magnetic Density Separation

A.M. van Silfhout

ISBN: 978-94-6380-912-2
Doctoral Thesis
Magnetic Sedimentation in Aqueous Ferrofluids
Printed by ProefschriftMaken | www.proefschriftmaken.nl
Cover design by Ron Zijlmans | www.ron.nu

Magnetic Sedimentation in Aqueous Ferrofluids

for Magnetic Density Separation

Magnetische Sedimentatie in Waterige Ferrofluïda

voor Magnetische Dichtheid Scheiding

(met een samenvatting in het Nederlands)

Proefschrift

ter verkrijging van de graad van doctor aan de Universiteit Utrecht op gezag van de rector magnificus, prof. dr. H.R.B.M. Kummeling, ingevolge het besluit van het college voor promoties in het openbaar te verdedigen op maandag 28 september 2020 des middags te 12:45 uur

door

Alexander Marius van Silfhout

geboren op 14 juni 1992 te Ede

Promotor: Prof. dr. A. P. Philipse
Copromotor: Dr. B. H. Erné

This work is part of the research programme P14-07 with project number 3.1, which is (partly) financed by the Dutch Research Council (NWO).

Contents

Chapter 1

General Introduction

Abstract

In 2015, a Dutch national program [1] was started to develop magnetic density separation (MDS) as a recycling technology. This generic method enables the separation of materials from plastics or electronic waste, an essential step in recycling. In the MDS technology as designed in this program, an effective density gradient is realized in a magnetic liquid by applying an external field, and multiple density fractions are separated in a single continuous processing step. This offers significant advantage over sink-float techniques, in which the flow of material can only be separated into two fractions per processing step. The program involves researchers who study material recycling, superconducting magnet design, liquid flow dynamics, and colloidal chemistry of magnetic liquids. The chemical design and sedimentation properties of magnetic liquids suitable for magnetic density separation are the focus of this thesis.

This introductory chapter starts with a short overview of plastic waste—one of the main targets of magnetic density separation—and continues with a presentation of the underlying principle of the technique. This is followed by a basic description of the colloidal and sedimentation properties of magnetic liquids. Finally, the structure of the remaining chapters of the thesis is outlined.

1.1 Plastic Waste

Plastics are widely used in our modern world. Plastics often provide a combination of high strength, low weight and low cost that is superior to most other materials. However, one of the increasingly urgent problems concerning the use of plastics is the end of life of plastic products.

In Europe, plastic waste is collected separately from other household waste. In this way, 29.1 million tons of plastic waste were collected in Europe in 2018 [2]. This waste is processed in three ways: energy recovery, landfill and recycling. The amount of plastics sent to landfill has been lowered from 12.9 Mt in 2006 to 7.2 Mt in 2018. The fraction of plastics waste sent to landfill varies per country, with a total of 24.9% of total European plastic waste. The majority of the plastic waste (42.6%) is used for energy recovery. In energy recovery, waste is burned and the heat is used to generate electricity.

In 2018, 32.5% of European plastic waste was used for recycling. In order to recycle plastics to a purity grade comparable to virgin plastics, different types of plastics must be separated. The composition of plastic products used in Europe in 2017 is given by PlasticsEurope [3]. In their data, 14 categories of plastics are defined. Separation of these fractions can be done via several methods. Pieces of plastic can be sorted manually, by sink-float techniques or using selective dissolution. However, these methods are so expensive in either manual labour or materials that without subsidies, applying them to recycle plastics is not economically viable.

1.2 Magnetic Density Separation

In our program's implementation of magnetic density separation (MDS), a combination of magnetic field and ferrofluid is used to continuously separate flakes of material, based on their mass densities. In contrast to earlier implementations of this principle [4, 5, 6, 7], this technique allows for separation into more than two fractions, offering accurate separation of materials in a single processing step.

The principle behind this application is called magnetic buoyancy [8], which can be explained as follows. If we consider a nonmagnetic particle submerged in a liquid, two major forces are acting on the particle: (1) gravity, which scales with the mass of the particle, shown in equation 1.1 and (2) buoyancy, which scales with the mass of the displaced liquid, shown in equation 1.2. When the liquid is a ferrofluid and is placed in a magnetic field gradient, an additional force is introduced. While there is no direct interaction between the nonmagnetic particle and the magnetic field, the surrounding ferrofluid is attracted in direction of increasing magnetic field. This results in a net force on the nonmagnetic particle towards decreasing magnetic field; the effective magnetic force on the particle appears in equation 1.3.

$$F_{\text{gravity}} = V \cdot \rho_{\text{particle}} \cdot g \tag{1.1}$$

$$F_{\text{buoyancy}} = V \cdot \rho_{\text{liquid}} \cdot g \tag{1.2}$$

$$F_{\text{magnetic}} = V \cdot M_{\text{liquid}} \cdot \mu_0 \cdot \frac{\mathrm{d}H}{\mathrm{d}h} \tag{1.3}$$

Here, V is the volume of the particle, ρ_{particle} the mass density of the particle, ρ_{liquid} the mass density of the liquid, g the gravitational acceleration, M_{liquid} the magnetization of the liquid, μ_0 the permeability of vacuum, and $\mathrm{d}H/\mathrm{d}h$ the magnetic field gradient. When the system is in equilibrium, these forces cancel each other. While the forces of gravity and buoyancy are independent of position, the magnetic force is a function of magnetization and magnetic field gradient, which are position-dependent. The position at which the forces acting on a particle are in equilibrium depends on the density difference between the particle and the liquid, and the spatial dependence of the magnetic field strength. The precise dependence of the equilibrium height on the den-

sity of the particle can be determined by tuning of the magnetic field and the magnetization of the liquid.

In the MDS setup shown in figure 1.1, a stream of nonmagnetic particles is brought into a flow of ferrofluid. After flowing through a laminator in order to prevent turbulence, the mix enters the separation chamber with a well-controlled magnetic field. Here, particles move to the equilibrium heights determined by their density. The flow speed of the liquid is set to allow all particles to reach their equilibrium heights before reaching the end of the chamber. Using blades at predefined positions, different density fractions are collected separately. In the last step, particles in each fraction exit from the liquid, which is brought back to the beginning in a continuous process.

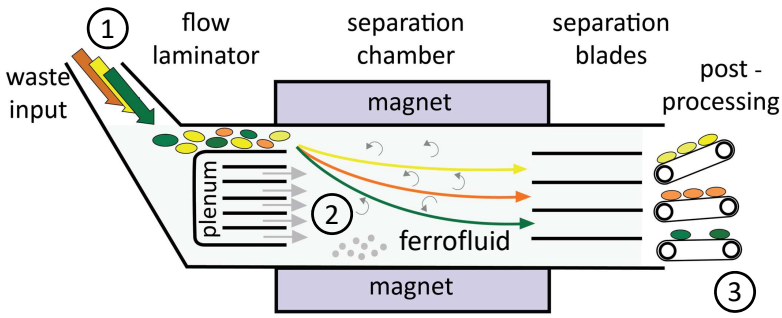

Figure 1.1: Schematic representation of an industrial MDS setup. (1) Nonmagnetic particles are brought into a flow of ferrofluid, after which the mix flows into a separation chamber (2), where particles flow towards an equilibrium height which depends on their density. At the end of the separation chamber, particles are collected in a number of fractions (3) and removed from the liquid, which is reused in a continuous process. Figure provided by S. Tajfirooz [9].

Although such an MDS setup is currently operational in Amsterdam [10] for the separation of plastics, further upscaling of such industrial setups would be beneficial. Additionally, the generic nature of this method allows for the separation of, for instance, materials in electronics with much larger density differences compared to water. However, for both these developments much stronger magnetic fields and field gradients are required, which in turn calls for more research into and development of strong magnets and ultrastable ferrofluids.

1.3 Ferrofluids

In the previous sections, the ferrofluid is described as a continuous medium. In order to achieve this, the fluid should remain homogeneous in magnetic field gradients and should not dissolve or penetrate into plastic particles submerged in it. The most common and inexpensive liquid that does not dissolve or swell most commercially used plastics is water, making it the preferred solvent for the ferrofluid. The magnetic properties of the ferrofluid are provided by dispersing magnetic nanoparticles in the water.

1.3.1 Ferrofluid Magnetism

The magnetic properties of a material at a chosen temperature can be described by its magnetization curve. A magnetization curve describes how strongly a material is magnetized as a function of an external magnetic field. A paramagnetic material like iron chloride, for instance, has atoms with a net magnetic dipole moment that only weakly align with external field. Ferrofluids consist of ultrasmall superparamagnetic nanoparticles (see figure 1.2) that also align with external field, but to much stronger extent than paramagnetic materials. This is because the magnetic particles have a single domain whose dipole moment is much larger than that of a magnetic atom in a paramagnetic material.

Without any external magnetic field, the magnetic nanoparticles in a stable ferrofluid are oriented at random, such that the total magnetic moment of the ferrofluid is zero on average. When an external field is applied, the magnetic nanoparticles tend to align to the field, giving the material a total magnetic moment that scales with the amount of magnetic material that is aligned to the field. The tendency of particles to align to an external magnetic field depends on the magnitude of the field and the magnetic moment of the particles. For an ensemble of superparamagnetic particles that all have the same magnetic moment, the average alignment of particles to the field is given by the Langevin function ranging from 0 to 1 at $H \geq 0$, shown in equation 1.4.

$$L(B) = \coth\left(\frac{\mu_{\text{particle}}\mu_0 H}{k_{\text{B}}T}\right) - \frac{k_{\text{B}}T}{\mu_{\text{particle}}\mu_0 H} \tag{1.4}$$

Here, μ_{particle} is the magnetic dipole moment of a nanoparticle, μ_0 the perme-

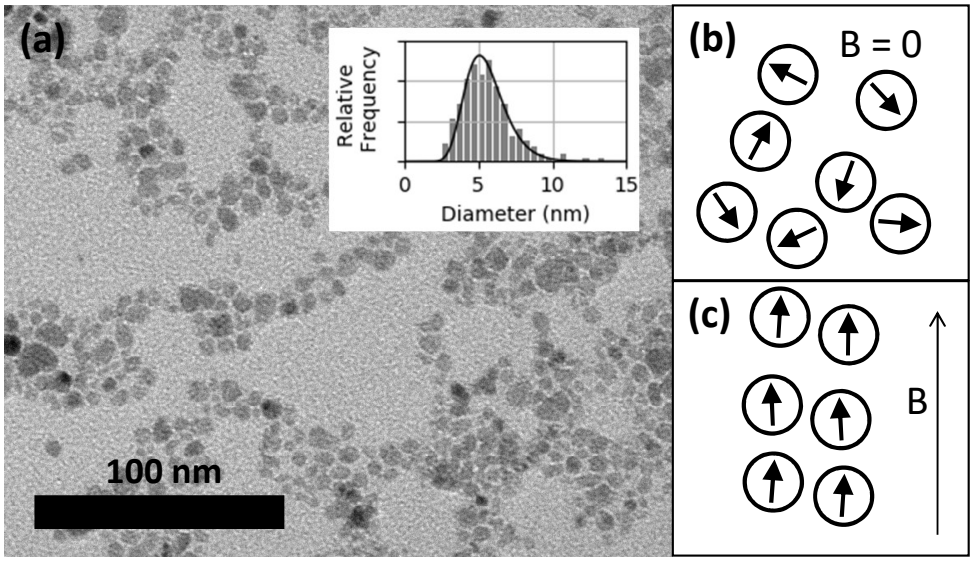

Figure 1.2: (a) Typical transmission electron microscopy (TEM) image of iron oxide nanoparticles prepared by aqueous coprecipitation. Inset shows the size distribution of particles analyzed from TEM. (b) Schematic representation of magnetic nanoparticles randomly oriented without external field. (c) Schematic representation of magnetic nanoparticles aligned to an external field.

ability of vacuum, H the external magnetic field, k_{B} the Boltzmann constant and T the absolute temperature. The magnetic dipole moment of a particle is determined by the volume of the particle and the material. The magnetization of a material is the magnetic moment per unit volume (in Am^2 per m^3, so in A/m), and the bulk magnetization of a material describes the density of magnetic dipole moments in a magnetic domain in a ferri- or ferromagnetic material. The saturation magnetization of a sample is the magnetization extrapolated in the limit of infinitely strong field. For maghemite (γ-Fe_2O_3) particles as featured in this thesis, the bulk magnetization is 430 kA/m [11] and nanoparticles contain a single magnetic domain [12]. If not all particles are the same size, the shape of the magnetization curve corresponds to a sum of the Langevin equations for all particle sizes, with each partial curve weighted by the volume frequency of the corresponding particles. This implies that the magnetization curve informs not only on the average size of the particles, but also on the width of the size distribution. The contribution from large par-

ticles is most pronounced in the low-field part of the curve (see figure 1.3a), while smaller particles are more prominent at higher fields. To illustrate this, figure 1.3b shows the magnetization curves of an ensemble of monodisperse iron oxide particles of 5 nm diameter, compared to a 50/50 vol% mix of 4 nm and 6 nm particles.

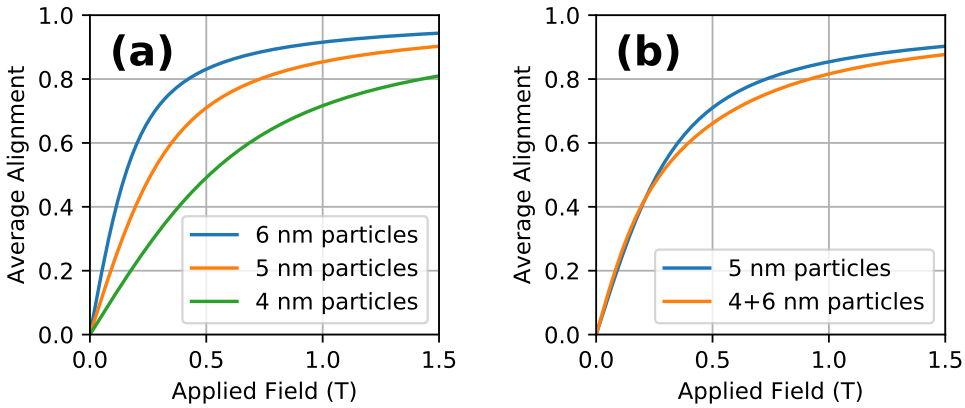

Figure 1.3: (a) Magnetization curves for monodisperse particle populations with spherical particles of 6 (blue), 5 (orange), and 4 (green) nm diameter. Degrees of alignment were calculated via equation 1.4. The bulk magnetization of the particles was set at 430 kA/m. (b) Direct comparison of a collection of monodisperse particles of 5 nm diameter and a mix of 50 vol% 4 nm and 50 vol% 6 nm particles.

1.3.2 Magnetic Sedimentation

In a magnetic field gradient, the ferrofluid will flow towards regions of higher magnetic field strength [8]. However, since this force acts only on the magnetic particles and not on the carrier liquid, the particles might move independently from the rest of the fluid. Here, the size of the particles is crucial. The force on the particles in a given magnetic field gradient depends on the volume of a single particle, while the total force on the ferrofluid scales with the total amount of magnetic material in the liquid.

To illustrate this, when a single magnetic particle with a radius of 1 mm submerged in 1 mL of water is brought close to a magnet, the particle will move towards the magnet while the liquid remains behind. By breaking the particle into many small particles with the same total volume, the total magnetic

force is not affected. However, the force on each of the particles is now much smaller, reducing the velocity of the particles with respect to the liquid. The effect is that the liquid will start to move along with the particles, acting as a continuous ferrofluid as shown in figure 1.4.

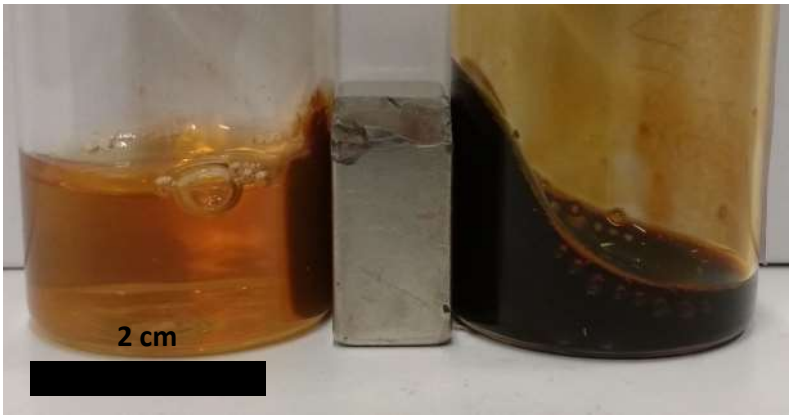

Figure 1.4: Two ferrofluid samples positioned against a magnet. The ferrofluid on the left is destabilized by addition of NaCl, inducing aggregation which increases the effective particle size. This leads to rapid sedimentation of the particles and phase separation between magnetic particles and solvent. The ferrofluid on the right is colloidally stable on this timescale, as can be seen by the motion of the liquid as a whole.

In industrial applications of MDS, sedimentation of magnetic nanoparticles will create a time- and position-dependent concentration of the ferrofluid, leading to deviations from the calculated heights at which each nonmagnetic material floats. If these deviations are significant compared to the scale of the design, this would greatly reduce the purity of the recovered materials, defeating the purpose of separation.

In order to prevent such problems, the timescales of (1) the fluid moving and (2) the particles moving with respect to the fluid need to be separated as far as possible. However, as shown in section 1.3.1, decreasing particle size results in much lower magnetization at low field. Moreover, besides particle size, aggregation also plays a significant role in sedimentation. While the magnetization curve is not influenced much by aggregation [13], the sedimentation of aggregated particles is much faster compared to single particles. The friction force on such particles or aggregates will in this thesis be assumed to follow

Stokes' law [14], i.e. the frictional force is given by $6\pi\eta Rv$, with η the viscosity of the solvent, R the radius of the object, and v the velocity of the object. In contrast, the magnetic force scales with the third power of the radius, and in consequence for a compact cluster of 8 nanoparticles, sedimentation velocity is approximately 4 times faster than the sedimentation velocity of the individual particles.

Aggregation of nanoparticles can be reversible or irreversible, and it can have several causes. For instance, magnetic nanoparticles of approximately 20 nm diameter will spontaneously form chain-like structures [15]. Polymeric compounds may stabilize particles, but may also induce bridging flocculation, where particles are stuck together irreversibly.

1.3.3 Aqueous Magnetic Fluids via Coprecipitation

The synthesis method used for this thesis is based on a protocol by Massart [16], adapted by Dubois et al. [17], known to result in stable ferrofluids. In the first step, the magnetic nanoparticles are precipitated. This is done by raising the pH of a solution of Fe(III) and Fe(II) salts, in a 2:1 molar ratio. Although the precise mechanism of formation is still poorly understood, raising the pH of this solution leads to rapid formation of various iron hydroxides which transform into magnetite (Fe_3O_4) over time [18]. If kept in water without protective atmosphere, the magnetite particles obtained this way are prone to oxidation, resulting in a range of iron oxides with varying magnetic properties [19].

To prevent this, the second step in the procedure is to oxidize the particles in a controlled reaction to form maghemite (γ-Fe_2O_3) particles. Particles are collected by a magnet and transferred to a solution of nitric acid containing Fe(III) salts. This solution is kept at 90 °C for one hour in order to let the transformation to maghemite finish. After this step the surface of the particles is coated by a layer of nitrate ions, but due to the high concentration of salt, the electrical screening length is very short, allowing particles to approach closely where Van der Waals forces dominate [20], resulting in extensive aggregation and rapid sedimentation. Note that the iron oxide nanoparticles do not disappear by dissolution, despite a pH below 0 and an equilibrium solubility of several molar. The reason for this must reside in the kinetics of dissolution,

as it was seen during syntheses for this thesis that if acid treatment was inadvertently much longer than planned, all iron oxide did eventually dissolve, similar to observations published by Tourinho *et al.* [21].

In the third step, the solution is washed with solvent three times in order to remove as much salt as possible. As long as the ionic strength is high, colloidal stability is poor and particles are easily collected by a magnet outside the reaction vessel, allowing removal of the supernatant. Once the ionic strength is lower, typically below 0.5 M, an antisolvent such as acetone has to be added in order to destabilize the dispersion and allow for further washing steps. After washing, the nitrate ions on the particle are displaced by addition of citrate molecules. This is done by adding a solution of citrate to the particles and heating the mix to 90 °C for a few minutes. In this step, the pH of the reaction should be above 2.8, the lowest pK_a of citrate [22], so that the deprotonated carboxylic acid group can attach to the particles.

In the last step, particles are washed multiple times in order to wash away all excess citrate. For the ferrofluids as described in this thesis a solution of 10 mM NaCl is used in these washing steps, so that the ionic strength of the resulting ferrofluid is precisely known.

1.4 Not in this Thesis

Not presented in this thesis—except in this short subsection—is all the work done by bachelor and master thesis students in exploring paths that we did not (yet) follow up, for reasons of time or strategy. Willem Boon [23] implemented an original magnetic analytical centrifugation technique with a magnet in the sample holder and developed the related theory. Cedric Cornelissen [24] developed a new low cost stability analysis approach in which the magnetization of supernatant and sediment of ferrofluids was measured after centrifugation in an Eppendorf cup, and he used quantitative infrared spectroscopy to determine the adsorption isotherm of PPEG on iron oxide. Myrthe Hogeboom [25] used high gradient magnetic separation in an attempt to improve the quality of ferrofluids by removing aggregates. Hannah Oppermann [26] synthesized aqueous ferrofluids stabilized by polyelectrolytes including poly(acrylic acid) and studied their stability as a function of salt concentration. Richard Koschny [27] explored how to evaluate ferrofluid stability using a webcam setup. Kim Dreijer [28] studied the dipolar chaining of nonmagnetic particles under MDS-like conditions. All these studies were valuable in providing preliminary experience with the subject and in helping to guide the choices of research presented in this thesis.

1.5 This Thesis

Characterizing the sedimentation of the magnetic nanoparticles in magnetic field is an essential step in evaluating whether a ferrofluid is sufficiently stable for applications. In this thesis, magnetic sedimentation of the nanoparticles in different aqueous ferrofluids is studied in a number of ways.

In **chapter 2**, sedimentation of the nanoparticles on a neodymium magnet is analyzed by detection of changes in the local magnetic field between the magnet and the ferrofluid. The time-dependent magnetic measurements are interpreted in terms of a simple model, with which indications of the timescale and extent of sedimentation are obtained. Three ferrofluids are studied: one ferrofluid synthesized in the Van 't Hoff laboratory and two ferrofluids obtained from the Urban Mining Corporation (Umincorp), a company working on the commercial development of MDS.

In **chapter 3**, the sedimentation of the same ferrofluids is studied in extremely high magnetic fields, up to 10 tesla. The effects of high magnetic field and high magnetic field gradient on the sedimentation of nanoparticles are studied systematically. By comparing ferrofluids of good and lesser stability, the effects of nanoparticle aggregation on sedimentation velocity are examined.

In **chapter 4**, a theoretical model is presented describing the sedimentation of magnetic nanoparticles in magnetic field gradients. The model is implemented in numerical calculations of sedimentation in a range of fields and field gradients. The numerical results are compared to experimentally obtained data. The model is also used to predict the evolution of concentration gradients at a length scale and under magnetic field conditions typical of industrial MDS.

In **chapter 5**, the way in which our nanoparticles are modelled in the other chapters is examined in more detail, essentially as dipolar hard spheres with a nonmagnetic shell. A stable ferrofluid is analyzed using independent experimental methods, giving insight into the size of the magnetic core, a nonmagnetic iron oxide shell, and a layer of surfactant and less mobile solvent. Validity and limitations of the nanoparticle model are discussed.

In **chapter 6**, the main findings of this thesis are summarized, first in English and then in Dutch.

Chapter 2

Magnetic Detection of Nanoparticle Sedimentation in Magnetized Ferrofluids

Abstract

Colloidal stability in external magnetic field is crucial for applications of ferrofluids. Here, we introduce a magnetic analysis approach to monitor how rapidly magnetic nanoparticles are pulled out of the liquid in an external magnetic field gradient. The motion of the sedimentation front is deduced from the time-dependent field produced by a column of ferrofluid placed on a permanent magnet. Citrate-stabilized nanoparticles in a homemade aqueous ferrofluid are found to sediment at the rate expected of single nanoparticles. More rapid sedimentation occurs in two other types of ferrofluid, indicating that our magnetic sedimentation analysis method can differentiate ferrofluids with respect to their in-field colloidal stability. Our method is further validated by comparison with time-dependent x-ray transmission profiles.

2.1 Introduction

Ferrofluids are concentrated colloidal dispersions of magnetic nanoparticles that behave as liquid magnets in external field. Oil-based ferrofluids are used as lubricants in many applications, with the advantage that they can be magnetically kept in place [8, 29, 30, 31, 32]. Another type of application of ferrofluids exploits the phenomenon of magnetic levitation: a nonmagnetic object that would sink in a normal liquid can be made to levitate in a ferrofluid, whose apparent mass density can be tuned via the magnetization of the fluid and via the magnetic field gradient [8]. Magnetic levitation has been applied for decades in the diamond industry, to separate diamonds from gangue material [4], and currently, magnetic levitation is being developed as a technology to separate solid waste materials for recycling [33]. The separation of plastics by magnetic density separation requires new low-cost high-stability ferrofluids that are water based, to prevent the dissolution of plastic.

For good colloidal stability of a ferrofluid, the magnetic nanoparticles must be dispersed at the single particle level and the pair interaction upon close approach between two nanoparticles must be repulsive. The stability will thus depend on the magnitude of the nanoparticle dipole moments and on the modification of the surface with possibly charged chemical groups or surfactants [34, 35]. Reversible or irreversible nanoparticle structures may already be present in zero field [36, 37], they may grow in external field [15], and isotropic attraction between nanoparticles may result in macroscopic phase separation [17]. To guide the chemical development of new ferrofluids with optimal stability, it is important to have a method to characterize how rapidly the magnetic material settles towards a magnet. Moreover, this characterization should be done at the same magnetic field gradients and relatively high nanoparticle concentrations that are relevant for applications.

The measurement of magnetization curves is a favorite way to characterize ferrofluids, but it is not very informative about their colloidal aggregation state. With magnetic nanoparticles in the 5-10 nm diameter range prepared by coprecipitation, a magnetization curve will be largely the same whether the nanoparticles are single or clustered, as the particles mostly respond to the external field individually [38, 39]. For larger nanoparticles, that form dipolar structures in zero field and which grow in external field, the formed

structures do affect the magnetization curve [40, 13], but still the presence of nanoparticle structures cannot easily be deduced from the magnetization curve alone. Field-induced dipolar structures have been visualized by cryo-TEM [15], but this is neither a routine method nor does it give a macroscopic characterization of stability. Small angle scattering of x-rays [41] or neutrons [42] can reveal dipolar structure formation in the presence or absence of a magnetic field, but it requires access to dedicated beam facilities. Optical imaging of a thin capillary in external field is a useful option that might in principle be used, not only to study sedimentation equilibrium profiles [43] but also to detect whether magnetophoresis is more rapid than expected in the absence of aggregates; this approach will be adopted in chapters 3 and 4.

The approach that we propose here is to monitor the external magnetic field produced by a small bottle of ferrofluid placed on top of a permanent magnet. It is a convenient and simple approach that allows easy comparison of the in-field colloidal stability of different ferrofluids. In the Theory section, the principle of our method is described, together with our mathematical approach to calculate sedimentation rates from the time-dependent magnetic data. Practical aspects of our setup are presented in the experimental section, and the results and discussion compare the colloidal stabilities of a few different ferrofluids in external field.

2.2 Theory

2.2.1 Magnetic Analysis of Sedimentation Front Position

Our approach to characterize the colloidal stability of ferrofluids in external field is summarized in figure 2.1. As a column of ferrofluid is placed on a permanent magnet, the liquid becomes a magnet itself. The dipoles of the magnetic nanoparticles become aligned to an extent that depends on the magnitudes of the dipole moments and on the strength of the external field. For simplicity, a cylindrical permanent magnet is used and we consider only its axial field H, given by [44]

$$H(z) = \frac{M}{2}\left[\frac{z+t}{\sqrt{(z+t)^2+R^2}} - \frac{z}{\sqrt{z^2+R^2}}\right] \tag{2.1}$$

where M is the magnet's (internal) remanent magnetization, z is the distance from the top surface of the magnet, t is the magnet's thickness, and R is its radius.

The dimensions of the initial column of magnetized ferrofluid are given by the height h_0 of the liquid column and the internal radius r of the flask. As the nanoparticles sediment, the geometry changes. As a simple model, we propose to assume that the flask now contains three cylindrical layers: (1) a nonmagnetic top layer that starts at the position h of the sedimentation front, (2) a ferrofluid layer with the same concentration c as at the start of the experiment, and (3) a sediment layer of increased concentration fc. Because of the strong optical absorbance of the dilute ferrofluid in the top layer, the position of the sedimentation front is typically not visible to the naked eye. Nevertheless, the sedimentation can now be monitored from the field measured by a Hall sensor positioned in between the magnet and the column of ferrofluid. The measured field will combine the constant contribution of the permanent magnet and the time-dependent contribution of the sample.

In the framework of our simple model, the measured field originating from the sample consists of two contributions: the field from the sediment and the field from the ferrofluid below the sedimentation front. In terms of equation 2.1, the sediment is a cylindrical magnet that starts at a distance z_0 from the Hall sensor and has a thickness t equal to $(h_0-h)/(f-1)$. The ferrofluid layer

is a second cylindrical magnet, starting at a height $z_0 + (h_0 - h)/(f - 1)$ and with a thickness t equal to $h_0 - (h_0 - h)/(f - 1)$. In both cases, the radius R is the internal radius r of the flask. Finally, the magnetization M scales with c for the ferrofluid and with fc for the sediment. This assumes that the sediment and the ferrofluid are close to magnetic saturation.

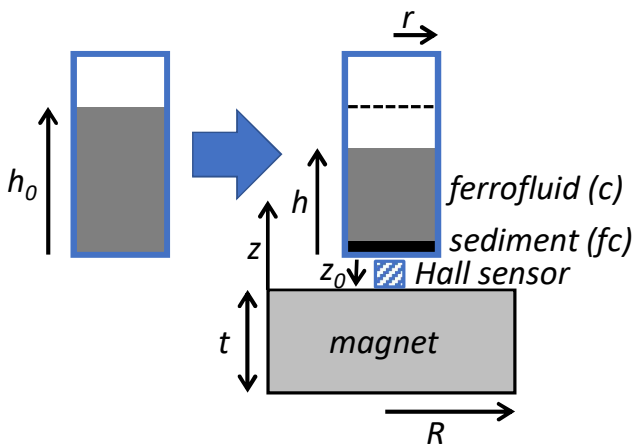

Figure 2.1: Schematic of the proposed approach to monitor the sedimentation of magnetic nanoparticles in a ferrofluid towards a magnet. The ferrofluid of concentration c in a cylindrical flask of internal radius r is magnetized by the permanent magnet below and contributes to the magnetic field measured at a Hall effect sensor positioned between magnet and ferrofluid. In the simplest interpretation of the data, as the position h of the sedimentation front moves, a sediment of concentration fc is formed ($f > 1$), affecting the strength of the measured magnetic field.

Using this relatively simple model, the measured field can be calculated from the position of the sedimentation front, and vice versa. The example calculation in figure 2.2a corresponds to our experimental geometry for a sediment that is more concentrated than the initial ferrofluid by a factor $f = 5$. Once sedimentation is complete, all particles are found in a pellet whose thickness is 1/5 of the initial height of the ferrofluid column, which is $(f - 1) = 4$ times smaller than the resulting supernatant. A numerical expression for the measured field from the sample as a function of the position of the sedimentation front can be solved for h, giving an expression for the position of the sedimentation front in terms of the measured field. Different ferrofluids will have

a different factor f by which the concentration of the sediment is enhanced compared to the initial dispersion, leading to a different final thickness of the sediment and a different final enhancement $H(h)/H(h_0)$ of the measured sample field compared to its initial value. Figure 2.2b shows the final values of $H(h)/H(h_0)$ for f going from 1 to 20 in our measurement geometry; on this basis, the value of f in the case of a particular ferrofluid can be determined from the final value of $H(h)/H(h_0)$.

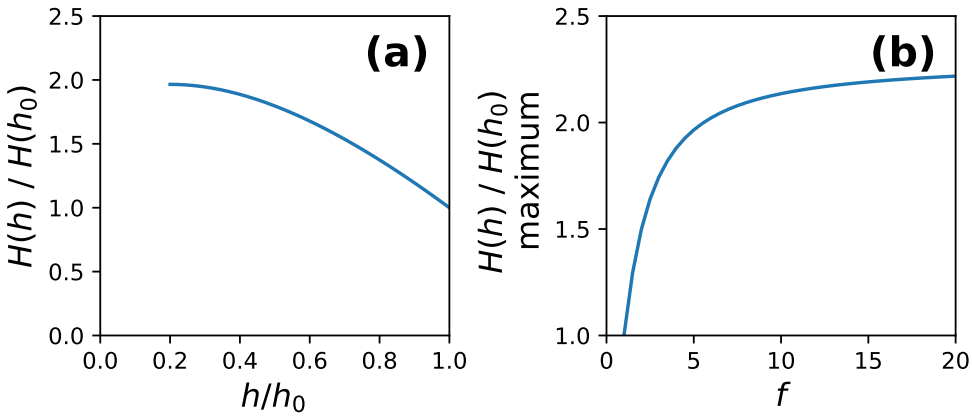

Figure 2.2: (a) Calculation via equation 1 of the field H as a function of the position h of the sedimentation front scaled to the initial value ($h = h_0$) for a sediment whose concentration is increased by a factor $f = 5$ compared to the initial concentration. Dimensions of permanent magnet: 30 mm thickness, 22.5 mm radius. Dimensions of liquid column: 10 mm height, 6.5 mm radius, minimal distance to Hall sensor: 2 mm. (b) Maximum value of $H(h)/H(h_0)$ as a function of f, the relative concentration in the sediment compared to the initial ferrofluid.

2.2.2 Aggregation dependence of sedimentation rate

The sedimentation rate of single or aggregated magnetic nanoparticles in external magnetic field results from a balance between magnetic force and friction. The force of gravity is typically weaker than the magnetic force by two orders of magnitude.

Upon full magnetic alignment of nanoparticle dipoles with external field, the magnetic force F_{mag} on a colloidal particle (single nanoparticle or aggregate) with a magnetic moment m_{colloid} is given by [45]

$$F_{\text{mag}} = \mu_0 m_{\text{colloid}} \mathrm{d}H/\mathrm{d}z \tag{2.2}$$

where μ_0 is the permeability of free space and $\mathrm{d}H/\mathrm{d}z$ is the external magnetic field gradient. In practice, magnetic alignment will not be complete. When all magnetic nanoparticle dipoles are free to rotate thermally in zero field, the average degree of magnetic alignment in an external field H is described by the Langevin function [46]:

$$M/M_{\text{sat}} = \coth(\alpha) - 1/\alpha \tag{2.3}$$

where M is the sample magnetization, M_{sat} is M at magnetic saturation, and $\alpha = \mu_0 m H/(k_{\text{B}}T)$, with m the nanoparticle dipole moment and $k_{\text{B}}T$ the thermal energy. In our case, the gradient is found by taking the derivative of equation 2.1:

$$\frac{\mathrm{d}H}{\mathrm{d}z} = \frac{M}{2}\left[\frac{\sqrt{(z+t)^2+R^2} - (z+t)^2\left[(z+t)^2+R^2\right]^{-\frac{1}{2}}}{(z+t)^2+R^2} - \frac{\sqrt{z^2+R^2} - z^2(z^2+R^2)^{-\frac{1}{2}}}{z^2+R^2}\right] \tag{2.4}$$

The frictional force F_{friction} on a colloidal particle can be modelled in terms of the hydrodynamic radius a of an effective hard sphere [47]:

$$F_{\text{friction}} = 6\pi\eta a v \tag{2.5}$$

where η is the viscosity of the liquid medium on the colloidal particle scale and v is the velocity of the colloidal particle. Effects of nonspherical shape and hydrodynamic interactions are hidden in the value of the effective hydrodynamic radius. Moreover, this approach neglects back-diffusion, that is, diffusion in direction opposite to magnetophoresis due to the concentration gradient created by magnetophoresis; in our experiments, this assumption applies the best to the initial sedimentation rate, when the concentration profile is still far from reaching sedimentation-diffusion equilibrium.

With knowledge of colloidal size, dipole moment, viscosity, and field gradient, the magnetophoretic velocity u can be calculated. Conversely, the size of

colloidal objects can be determined from the sedimentation rate. To obtain a rough estimate, we will assume the presence of colloidal particles of hydrodynamic radius a with an amount of magnetic material equal to a fraction $x_{\mathrm{FeO_x}}$ of the total hydrodynamic volume. From $F_{\mathrm{mag}} = F_{\mathrm{friction}}$, equations 2.2 and 2.5, and $m_{\mathrm{colloid}} = (4/3)\pi a^3 m_b x_{\mathrm{FeO_x}}$ with m_{b} the bulk magnetization of iron oxide, the size of objects with a sedimentation rate u is given by

$$a \cong \sqrt{\frac{9\eta u}{2m_{\mathrm{b}} x_{\mathrm{FeO_x}} \mu_0 (\mathrm{d}H/\mathrm{d}x)}} \tag{2.6}$$

Since the maximum possible fraction of magnetic material in a particle is 1, equation 2.6 gives a minimum effective size of the colloidal objects. Magnetic nanoparticles are expected to have a single magnetic domain, so that the magnetic moment of a particle with a diameter of 7 nm and a bulk magnetization of 430 kA/m [48] will be 7.7×10^{-20} Am^2. Bare single nanoparticles in water (viscosity: 10^{-3} Pa·s) in a gradient of 20 T/m are expected to sediment at a rate on the order of 0.08 mm per hour. From equation 2.6, more rapid sedimentation will indicate the presence of aggregates containing many nanoparticles.

2.3 Experimental Methods

Three different types of water-based ferrofluid were studied. The "FerroTec" ferrofluid was produced by FerroTec (Santa Clara, USA) for use in magnetic density separation by the Urban Mining Corporation (Rotterdam). The "UMinCorp" ferrofluid was produced at a test facility of Urban Mining Corporation. The third ferrofluid, named "Citrate", contained citrate-stabilized maghemite nanoparticles at nearly neutral pH prepared by us via a method by Dubois *et al.*[13]. Magnetization curves were measured using a vibrating sample magnetometer (EZ-9 from Microsense, see example in figure 2.3) and particle sizes were determined using transmission electron microscopy (Tecnai 10, 100 kV). Both vibrating sample magnetometry (VSM) and transmission electron microscopy (TEM) indicated that the UMinCorp and Citrate ferrofluids had particles with an average diameter of about 7 nm and a polydispersity of around 30%, typical for ferrofluids prepared by aqueous coprecipitation [12]. The FerroTec fluid had slightly larger particles, about 11 nm and a polydispersity of around 30%. The viscosity of the samples was measured at 20 °C in a cone-plate geometry (5 cm diameter, 1° cone angle) in the low-shear regime using a Physica Anton Paar MCR-300 rheometer.

A schematic of the setup used for magnetic analysis of ferrofluid sedimentation is shown in figure 2.1. A cylindrical neodymium magnet of 45 mm in diameter and 30 mm in thickness was obtained from SuperMagnete (Gottmadingen, Germany). A transverse Hall sensor probe with a square edge length of 1 mm (HMMT-6J04-VR, Lake Shore Cryotronics, Inc.) was fixed against the center of the magnet inside a thermostatized box consisting of a copper cylinder of 25 cm in diameter and 34 cm in depth kept close to the average temperature of the thermostatized room (typically 19.0 °C): water from a Julabo F25 cryostat was pumped through copper tubing welded onto the copper cylinder, itself contained in an insulated closed wooden box. Thermostatization within 0.1 °C is crucial for a stable background field from the neodymium magnet. Preliminary experiments indicated that the field from the neodymium magnet decreased by about 0.5 mT per temperature rise of 1 °C, and slight corrections were applied to subsequent measurements to take into account small changes in the measured temperature near the Hall probe. The sample consisted of a 4 mL glass vial with screw cap (VWR) 4.5

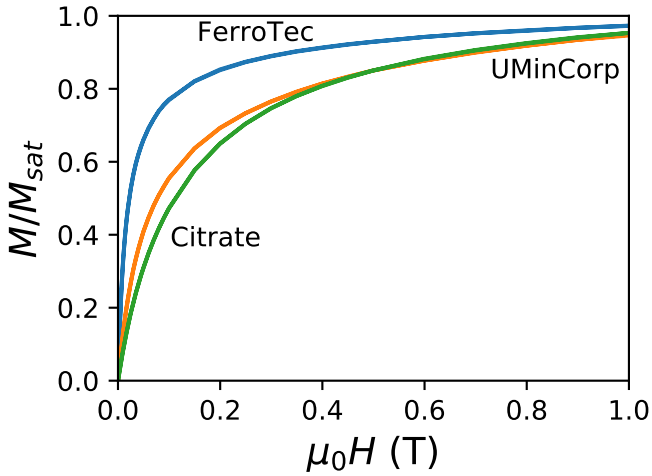

Figure 2.3: Magnetization curve of the ferrofluids measured by VSM. No hysteresis was observed, evidence of the superparamagnetic nature of the ferrofluid. Magnetization is scaled to the saturation magnetization of 12600, 2200, and 1140 A/m for the FerroTec, UMinCorp, and Citrate ferrofluids respectively.

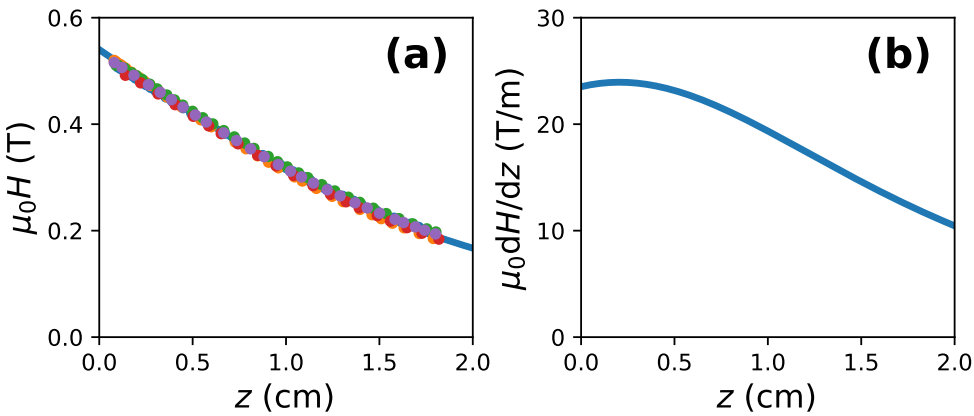

Figure 2.4: (a) Measured axial field from our magnet as a function of the distance z from the surface. The fit is according to equation 2.1 ($\mu_0 M = 1.32$ T, $R = 0.0225$ m, $t = 0.030$ m). (b) Calculated axial magnetic field gradient of our magnet, see equation 2.4.

cm in height and 1.5 cm in external diameter (1.3 cm internal diameter) filled with 1.4 mL of ferrofluid and thermostatized overnight inside the box at 5 cm from the magnet center in lateral direction before it was slided onto the

center of the magnet to start a measurement. The height of the liquid column from the inside bottom of the bottle to the bottom of the meniscus was 1.0 cm. Measurements with sample were performed for 100 hours at 1 point per minute, after which the measurement was continued without sample for a few hours to verify the background field.

Figure 2.4 shows the height-dependent axial field and gradient of our magnet (height dependence obtained by fixing the gauss probe onto a cathetometer with digital readout of the elevation). With the gauss probe positioned against the magnet, the Hall sensor measured a field of 0.53 T, in line with the remanent magnetization of 1.32 T quoted by the supplier and a distance of ∼1 mm between magnet surface and Hall sensor (inside the metal casing of the gauss probe). In the first cm above the magnet surface, the axial field drops to 0.32 T and the gradient is about 20 T/m.

To validate our calculation of magnetophoretic sedimentation rates from magnetic data, we measured x-ray transmission profiles using a LUMiReader X-ray instrument (LUM, Berlin; 17.48 keV molybdenum x-ray source). A liquid column of 1 cm in height inside a plastic disposable cuvette (2 mm optical path length) was placed on the same type of magnet as used for the magnetic experiments. The x-ray absorbance of a water-filled cuvette was subtracted.

2.4 Results and Discussion

Magnetic stability analyses of the FerroTec ferrofluid are shown in figure 2.5, before and after dilution with water by factors of 2, 4, and 8. The initially measured field scales with the initial concentration (figure 2.5a), and the relative increase in field from the sample in 100 hours is the largest at the highest dilution (figure 2.5b). In terms of the model presented in the Theory section, the most concentrated sample exhibits not only the slowest sedimentation but also seems to tend towards a less strongly sedimented sample upon prolonged sedimentation (figure 2.5c). Similar measurements performed on the UMinCopr and Citrate ferrofluids are shown in figure 2.6.

The observed differences in relative field increase as presented in figure 2.5b can be understood by comparing the data to x-ray measurements of the equilibrium concentration profiles in figure 2.7. The profiles in figure 2.7 show that there is no full settling of the particles at the bottom of the sample. The density of the sediments increases towards the bottom, and the highest density is reached in the most concentrated sample. This can be understood in terms of a gradual increase in osmotic pressure towards the bottom of the sediment: repulsive interactions that keep the particles apart gradually yield to the pressure exerted by the column of sediment above it [49, 50].

The trend of increasing initial sedimentation rate upon dilution follows the trend of decreasing viscosity: values of 2.30, 1.46, 1.20, and 1.12 mPa·s were measured for dilution factors of 1, 2, 4, and 8, respectively. For comparison, the UMinCorp and Citrate ferrofluids each had viscosities of 1.10 and 1.08 mPa·s, respectively. As the viscosities were measured without magnetic field and the volume fractions of magnetic material are low (2.6% for the most concentrated sample), the trend in viscosity is ascribed to the presence of excess polymer surfactant. At similar viscosity, the FerroTec (0.23 mm/h) and UMinCorp (0.19 mm/h) ferrofluids show more rapid sedimentation than the Citrate ferrofluid (0.06 mm/h), whose rate is close to that expected for single particles (0.08 mm/h, see section 2.2.1). The more rapid sedimentation in the FerroTec ferrofluid can in part be ascribed to the slightly larger nanoparticles in that system compared to the UMinCorp and Citrate ferrofluids. From equation 2.6, the colloidal objects in the UMinCorp ferrofluid have a radius that is larger than that of single particles by a factor of about 2, suggesting

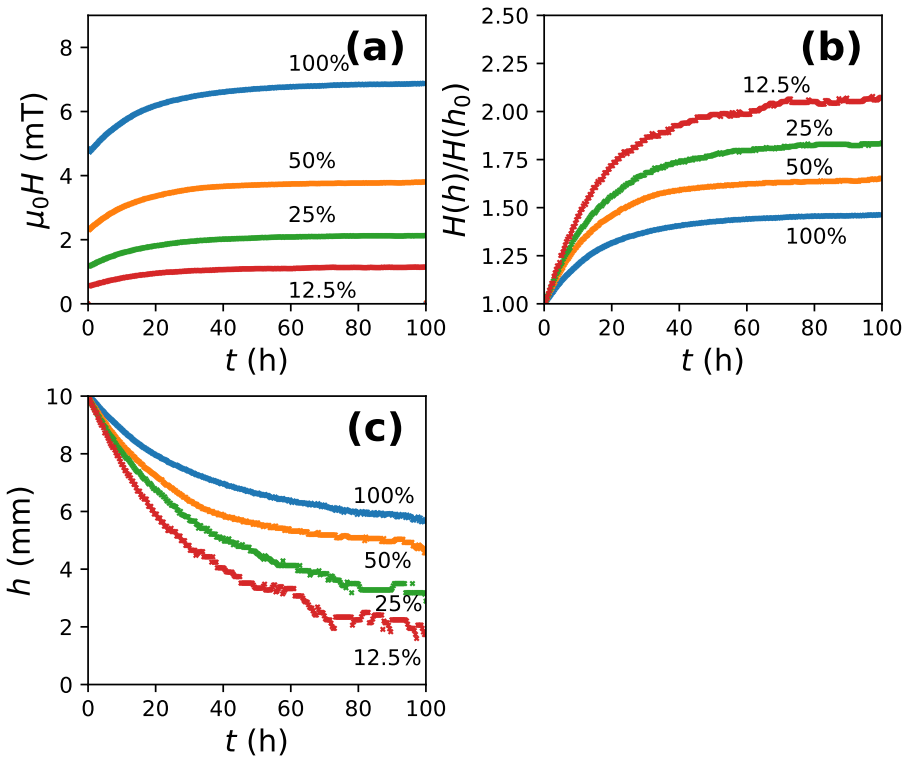

Figure 2.5: (a) Measured fields from samples placed on a magnet, corrected for the background field of the magnet (500.7 mT). Samples are FerroTec fluid before dilution (blue) and after dilution to 50% (orange), 25% (green), and 12.5% (red) of the initial concentration. (b) Measured fields relative to the initial sample field; final values of $H(h)/H(h_0)$ are 1.48, 1.65, 1.78, and 2.06, corresponding to f values of 1.8, 2.5, 3.3, and 6.8, respectively (see figure 2.2b). (c) Position of the sedimentation front as calculated by the model presented in figures 2.1 and 2.2. The initial sedimentation rates of the increasingly dilute samples are 0.13, 0.16, 0.20, and 0.23 mm per hour.

the presence of aggregates of approximately 5-10 nanoparticles.

Time-dependent x-ray transmission profiles of the FerroTec ferrofluid are shown in figure 2.8a. For a comparison with the magnetic measurements, we used equation 2.1 to calculate the contribution from each elevation to the measured field, viewing the sample as a stack of disks each having a thickness given by the distance between two data points in the x-ray profile (about 13 µm) and a magnetization assumed to be linear with the x-ray absorbance

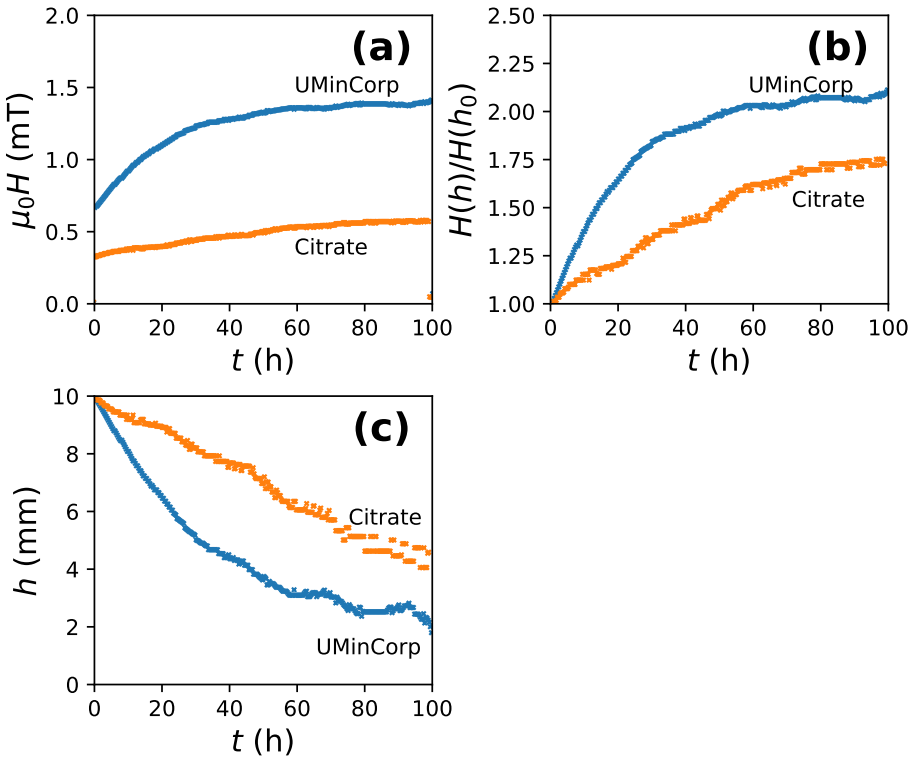

Figure 2.6: As in figure 2.5, but for the UMinCorp (blue) and Citrate (orange) samples: (a) measured field corrected for background (500.7 mT), (b) same data but now scaled to initial sample field, and (c) calculated position of the sedimentation front. In the UMinCorp sample, $H(h)/H(h_0)$ reaches 2.05, corresponding to $f = 6.7$, and we find an initial sedimentation rate of 0.19 mm per hour. In the Citrate sample, $H(h)/H(h_0)$ reaches 1.72 ($f = 3.1$), and we find a sedimentation rate of 0.06 mm per hour.

and initially equal to the magnetization measured by VSM. The resulting predictions of the sample field at the position of the Hall sensor are shown in figure 2.8b.

The time-dependent increase in sample field calculated from x-ray profiles agrees with the magnetic measurement, except for a rapid initial increase in the first hour observed in the x-ray profiles but not in the magnetic measurements (figure 2.8b). This discrepancy does not result from incomplete magnetization of the sample, which causes the field to be about 10% lower than at saturation magnetization from start to finish of the experiment (see figure 2.3). About

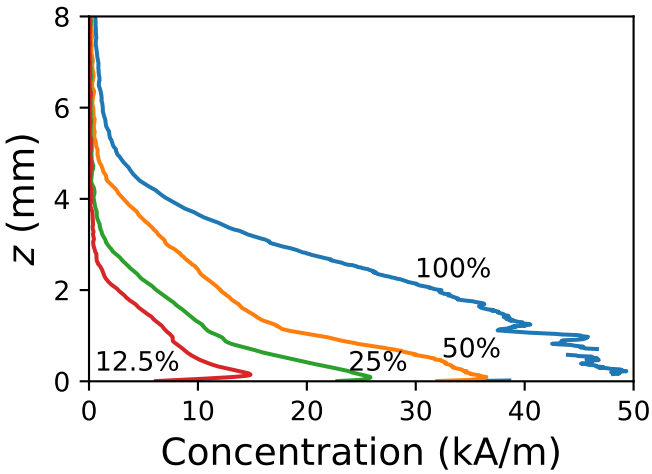

Figure 2.7: Equilibrium concentration profiles of the FerroTec sample before dilution and after dilution by factors of 2, 4, and 8. The undiluted fluid initially had a magnetization of 12600 A/m (initial ferrofluid height: 10 mm). Concentrations are given in terms of saturation magnetization, calculated from x-ray transmission and VSM measurements.

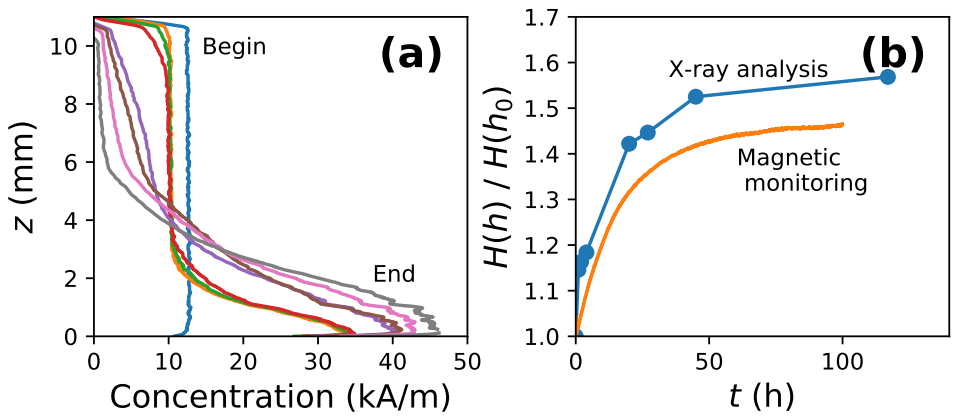

Figure 2.8: (a) Time-dependent concentration profiles of the undiluted FerroTec sample. Each line is an average of two samples. (b) Relative increase in sample field due to sedimentation obtained from direct magnetic monitoring and calculated from the x-ray profiles in part (a) of this figure.

20% of the magnetic material in this unfractionated ferrofluid can apparently easily be removed in external magnetic field before using the remaining fluid in applications. A possible reason why this fraction of the magnetic material

is not observed in the magnetic measurements is that it consists of aggregates that already settle to the bottom during the temperature equilibration performed before starting the magnetic measurements. Lengthy equilibration is necessary for a stable background field from the permanent magnet, a drawback of the magnetic monitoring method. In the future, a way might be found to perform the temperature equilibration with the sample much farther from the magnet.

2.5 Conclusions

Our magnetic approach to characterize the sedimentation rate of ferrofluids seems well suitable to compare the colloidal stability of ferrofluids in external magnetic field. Clear differences were observed between a ferrofluid with citrate-stabilized nanoparticles, which sedimented at the rate expected for single particles, and two commercially available ferrofluids in which sedimentation was more rapid. Moreover, a trend was observed in the sedimentation rate of a ferrofluid as a function of concentration, the slowest sedimentation occurring in the sample with the highest viscosity.

The descriptive model used in the magnetic analysis of sedimentation rates is oversimplified. X-ray transmission profiles indicate that the position of the sedimentation front is not abrupt but spread out and that the sediment does not have a homogeneous concentration but gradually becomes more concentrated towards the bottom. Nevertheless, further development of the magnetic sedimentation analysis method and its interpretation is not a priority. It is a simple method that measures a single parameter in time, the sample's contribution to the measured field, and it interprets the measurement in terms of a single parameter, the effective position of the sedimentation front. Development of a more elaborate model poses the risk of leading to overinterpretation. For more detailed information on the sedimentation process, a better approach seems to measure x-ray transmission profiles. In chapter 4, we aim to focus on the interpretation of such profiles. In theory, they describe not only the kinetics of sedimentation, but also the colloidal interactions between the nanoparticles, since sedimentation equilibrium profiles can be used to calculate the osmotic equation of state [49, 50].

Chapter 3

Colloidal Stability of Aqueous Ferrofluids in Magnetic Fields up to 10 Tesla

Abstract

Applications of ferrofluids require good colloidal stability in an external magnetic field. A case in point is a new recycling technology that separates plastics via magnetic levitation in an aqueous ferrofluid. Large-scale implementation of this technology may require much higher fields than applied to aqueous ferrofluids until now, raising the question whether colloidal stability is maintained under such extreme conditions. Here, we investigate the sedimentation of nanoparticles in aqueous ferrofluids in fields up to 10 T and at gradients up to 100 T/m. Sedimentation is observed by optical transmission imaging of thin capillaries containing ferrofluids, placed in the bore of a 30 T Bitter magnet. The field strength and gradient are controlled by tuning the current through the magnet and the distance of the capillaries from the zero gradient position. In one ferrofluid, sedimentation occurs at the velocity expected of separate nanoparticles, indicating optimal colloidal stability. More rapid sedimentation, as observed in two other ferrofluids, is ascribed to the presence of nanoparticle aggregates assembling into dipolar structures in an external field. From comparison with earlier results, it is concluded that sedimentation on a neodymium magnet is predictive of ferrofluid stability in much stronger fields.

3.1 Introduction

Ferrofluids are colloidal dispersions of magnetic nanoparticles that behave like liquid magnets in external magnetic field [8]. This property is exploited in many applications where a ferrofluid acts as a lubricant that is magnetically held in place, for instance in rotary shafts and loudspeakers [32, 29]. A less widely applied property of ferrofluids is their ability to create magnetic buoyancy: nonmagnetic objects submersed in ferrofluids are effectively repelled from a magnet. The main application of this phenomenon has long been in the separation of diamonds from other minerals [4], but it is now also used in magnetic density separation (MDS), an emerging recycling technology. In MDS, an external field generates an effective density gradient in a ferrofluid, and materials are separated into many fractions in a single continuous processing step [51, 52]. While MDS is already operational industrially [53], larger scale implementation is under development, requiring gradients on the order of 10 T/m applied across tens of centimeters, which implies that the magnet must produce fields of several tesla. Practical challenges include the development of suitable magnets with low operating costs and proper engineering of the hydrodynamics of nonmagnetic particle separation. For the separation of plastics, a further requirement is that the ferrofluids must be water-based, to prevent degradation or dissolution of plastics as occurs in oil-based ferrofluids. A major concern is whether existing aqueous ferrofluids will remain colloidally stable in magnetic fields of several tesla, an issue not studied before.

In principle, the magnetic nanoparticles in a ferrofluid will always move towards increasing magnetic field. If the ferrofluid is stable and sufficiently concentrated, magnetophoresis does not lead to a strong concentration gradient of the magnetic nanoparticles, since their motion with respect to the carrier liquid is counteracted by a strong opposing osmotic force [54, 55]. In MDS, however, the ferrofluids are quite dilute, typically at a concentration of 0.1 volume percent of magnetic material [33]; in this case, prolonged exposure to an external magnetic field does lead to an inhomogeneous particle distribution across the liquid [43]; this is undesirable for the application, in which the magnetic density gradient must be constant over time. Magnetophoresis of the nanoparticles cannot be avoided, but it can be minimized by preparing the ferrofluid in such a way that the nanoparticles remain separate from each

other in external field. The presence of aggregates of the nanoparticles must be prevented, since their magnetophoresis is much more rapid than that of separate nanoparticles.

To ensure that nanoparticles remain separate from each other, corresponding to optimal colloidal stability, direct contact of two nanoparticles must be prevented. One type of measure that can be taken is to prepare nanoparticles that repel each other. In principle, this can be done by control of the surface chemistry of the nanoparticles, via electrically charged chemical surface groups [21, 17], adsorbed lyophilic organic molecules [56, 57], or adsorbed polyelectrolytes [58, 34]. Colloidal stability of ferrofluids without magnetic field has been studied extensively using techniques such as optical scattering [59], neutron scattering [60, 61] or x-ray scattering [62]. For relatively small magnetic iron oxide nanoparticles with a diameter of, for instance, 7 to 10 nm as in the present work, the magnetic dipole moment of the particles is small; the dipolar attraction of two particles in head-to-tail configuration is not enough to overcome thermal energy and to induce dipolar structure formation [63]. However, for larger magnetic iron oxide nanoparticles, with a diameter of, for instance, 16 to 20 nm and no thick steric stabilization layer, the single magnetic domain has a much larger dipole moment, and dipolar structures spontaneously form in zero field [15]. The effect of an external magnetic field on the stability and structure formation in ferrofluids has been studied theoretically [64] and experimentally in relatively low fields, both in uniform fields [65, 66, 67, 68] and in field gradients [43]. Depending on the particle size and initial aggregation state, field-induced structure formation can even be optically resolved [69].

Here the magnetic sedimentation of three types of aqueous ferrofluid is investigated at magnetic field strengths up to 10 T and gradients of 0 – 100 T/m. The preparation and characterization of the ferrofluids are presented in the Experimental section, as well as the setup used in the study of magnetic sedimentation. The Results and Discussion section starts with a preliminary characterization of the ferrofluids, from electron microscopy and magnetization curves. Then the initial sedimentation behavior is described, which occurs just after the magnet is turned on. Finally, the sedimentation velocity on longer time scales is analyzed in greater detail.

3.2 Experimental

3.2.1 Ferrofluids Preparation and Characterization

Three different types of ferrofluid were prepared. All three were aqueous dispersions of magnetic iron oxide nanoparticles, whose shapes and sizes were characterized via transmission electron microscopy (Tecnai 20, 200 kV).

The "Citrate ferrofluid" was synthesized following a protocol adapted from Massart [16, 17]. Milli-Q water was used and all other chemicals were of pro analysis grade (from Merck, except for the iron salts, which were from Sigma-Aldrich). 2.0 g of NaOH in 20 mL of water was added under heavy stirring to a solution of 3.46 g of $FeCl_3 \cdot 6H_2O$ and 1.28 g of $FeCl_2 \cdot 4H_2O$ in 80 mL of water. After 5 more minutes of stirring, the black precipitate was collected with a handheld magnet placed outside the flask until the supernatant was clear. The supernatant was removed, the particles were dispersed in 16 mL of 2 M HNO_3, a solution of 2.28 g of $FeCl_3 \cdot 6H_2O$ in 24 mL of water was added, and the mixture was stirred at 90 °C under reflux conditions for 1 hour. Next, particles were collected with a handheld magnet and the supernatant was removed. The particles were washed three times by dispersing them in 2 M HNO_3 and collecting them with a handheld magnet. The particles were dispersed in 10 mL of water, 2 mL of 1 M trisodium citrate was added, and the suspension was stirred for 15 minutes at 90 °C under reflux conditions. In the last steps, the particles were precipitated by adding acetone, collected with a handheld magnet, and dispersed in an aqueous solution of 10 mM NaCl; this was repeated four more times. The NaCl was added to set a well-defined ionic strength.

The two other ferrofluids were of commercial origin. The "FerroTec ferrofluid" was produced by FerroTec (Santa Clara, USA) for use in magnetic density separation by the Urban Mining Corporation (Rotterdam, the Netherlands). The "UMinCorp ferrofluid" was produced at a test facility of the Urban Mining Corporation. Both commercial ferrofluids were diluted by us with water to obtain a saturation magnetization on the order of 2200 A/m, similar to that of our Citrate ferrofluid.

The magnetization of the fluids was measured at room temperature up to 1.5 T with a Microsense EZ-9 vibrating sample magnetometer (VSM) on

weighed samples of about 60 µL held in plastic sample cups. Saturation magnetizations and magnetic size distributions were calculated by fitting magnetization curves on the basis of lognormal particle size distributions using an approach as published by Luigjes *et al.* [12].

3.2.2 Magnetic Sedimentation Setup

Total field strengths up to 10 T and gradients from 0 – 100 T/m were set using a 30 T Bitter magnet (High Field Magnet Laboratory Nijmegen, cell 1 [70]). Ferrofluid samples were positioned in the central bore of the magnet, and by setting the current through the magnet and adjusting how far the samples were from the field center, field strength and gradient were chosen separately, see figure 3.1. In a typical experiment, the current was 18.3 kA and the samples were 95 mm above the field center, resulting in a field of 15.1 T in the center and in a field of 10 T and a downward gradient of 100 T/m at the sample position. A full overview of the experimental details can be found in table 3.1. The bore of the magnet, where the samples were placed, was thermostatized at 25 °C using a Julabo FP-50 HE.

Table 3.1: Overview of magnetic fields and magnetic field gradients at which sedimentation experiments were performed. For each of the combinations below, at least one experiment with a set of 7 capillaries was performed.

B_{center} (T)	*Elevation* (mm)	B_{sample} (T)	∇B_{sample} (T/m)
3.8	93	2.6	25
5.8	58	5.2	25
7.6	95	5.2	50
10.0	0	10	0
10.5	39	10	25
11.3	59	10	50
15.1	95	10	100

The ferrofluids were contained in thin flat capillaries that were imaged via an optical setup, see figure 3.1a. The Rectangle Boro Tubing capillaries from CM Scientific had an internal cross section of 0.05 mm × 1 mm and were cut to approximately 20 mm in length. They were mounted on a sample holder designed to hold up to 7 capillaries in channels spaced 400 μm apart, and they were sealed using two-component epoxy glue (Bison Kombi). The

capillaries were oriented horizontally along their 20 mm axis, and their 1 mm axis was vertical, which was the axis along which sedimentation occurred. Light from a white LED reflected on a diffusive mirror and lit the back side of the capillaries, and after an optical path length of 0.05 mm through the ferrofluids, the transmitted light was led via further mirrors and a Thorlabs AC254-500-A lens to a Sony dxc-990p ccd camera with YH18x6.7 KRS SX7 lens outside of the magnet, see figure 3.1a. Images were taken at intervals of 1 second or more, depending on the experiment.

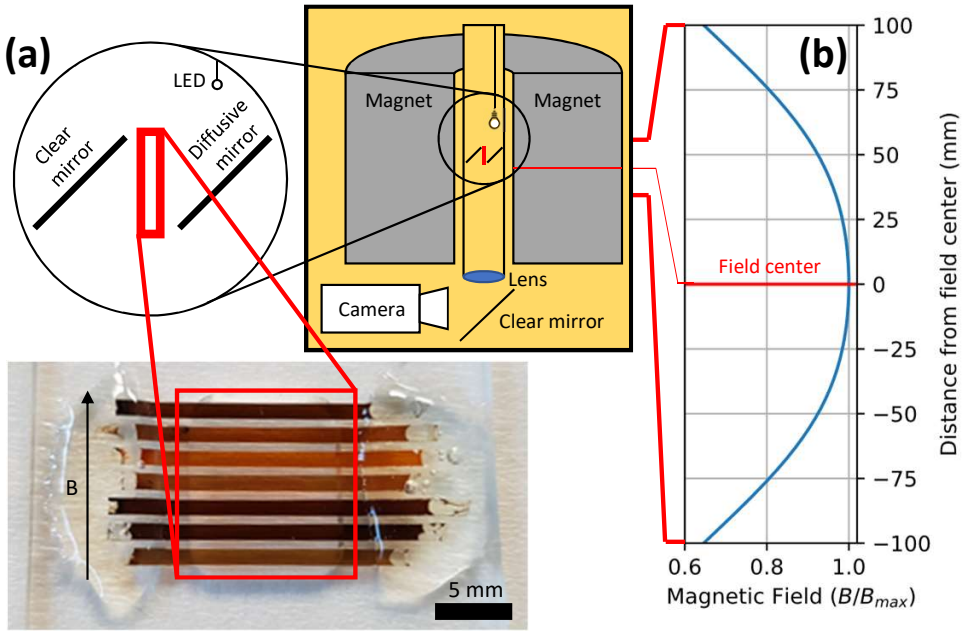

Figure 3.1: (a) Schematic view of the sedimentation setup. Inside the bore of a 30 T Bitter magnet, a height-adjustable sample holder is backlit by a white LED light via a diffusive mirror. Through a combination of a lens and clear mirrors, the transmitted light is imaged by a camera outside the magnet. (b) Profile of the magnetic field inside the bore of the magnet as a function of position [4]. Magnetic field strength is expressed relative to that in the field center. The central field and the distance from the field center thus determine field and gradient at the sample position.

For numerical data analysis, the intensity of the green channel of the RGB images was used. Vertically and horizontally, there were 51 pixels per mm. At every elevation, the intensity of a horizontal row of 50 pixels was averaged

and taken as a measure of the transmitted light intensity. From this transmitted light, the pixel value measured when the LED was off was subtracted. Fluctuations in LED light intensity were corrected for by dividing the pixel intensities at each elevation by the average pixel intensity resulting from light passing between the top two capillaries. At each elevation, the transmittance T was calculated by dividing the thus corrected pixel intensity by that of a water-filled capillary. The reported absorbances are equal to $-\log_{10}(T)$, and absorbance was found to be linear with the concentration of homogeneous samples of the same ferrofluids, as expected from the Lambert-Beer law. In a few cases where the image of water-filled capillaries was overexposed, the height-dependent 100% transmittance level was calculated by extrapolation on the basis of the position-independent extinction coefficient of the ferrofluids and the known initial concentration of the sample.

3.3 Results and Discussion

3.3.1 Preliminary Characterization of the Ferrofluids

Transmission electron microscopy of nanoparticles in the three ferrofluids indicates 30 – 50% polydispersity and an average particle size of approximately 7 nm (Citrate, UMinCorp) or 10 nm (FerroTec), see typical images in figure 3.2.

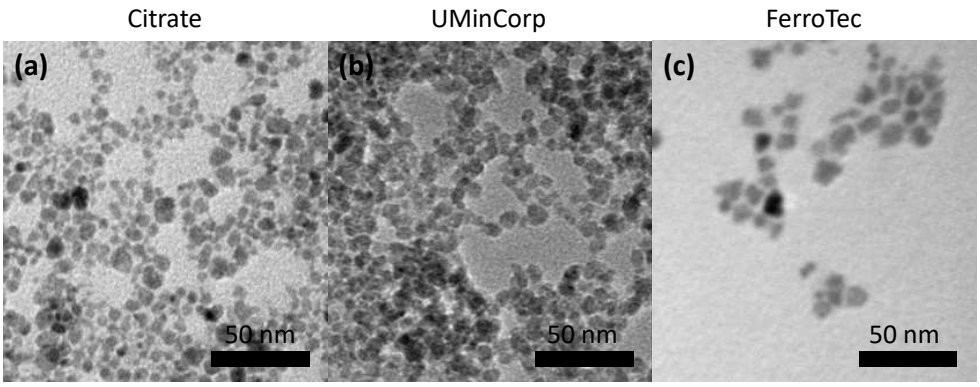

Figure 3.2: Transmission electron microscopy images of (a) the Citrate ferrofluid, (b) the UMinCorp ferrofluid and (c) the FerroTec ferrofluid. The scalebar is 50 nm in all panels.

Magnetization curves of the ferrofluids indicate that the particles are superparamagnetic: magnetization becomes strong in an external field, without any hysteresis upon scanning from +1.5 T to –1.5 T and in reverse direction, see figure 3.3. Fitting on the basis of a lognormal particle size distribution reveals magnetic domain sizes on the same order as particle size found by TEM, as expected for nanoparticles with a single magnetic domain, see inset in figure 3.3. The presented curves are extrapolated to 10 T on the basis of the same size distributions, to illustrate that the particles were largely under magnetic saturation conditions during the sedimentation experiments in the Bitter magnet setup.

In chapter 2, the magnetic sedimentation of the same three ferrofluids was studied at lower fields of 0.3 to 0.5 T and gradients of about 20 T/m, using neodymium magnets [71]. This indicated that the Citrate ferrofluid consisted of individually dispersed particles while the other two ferrofluids contained small aggregates.

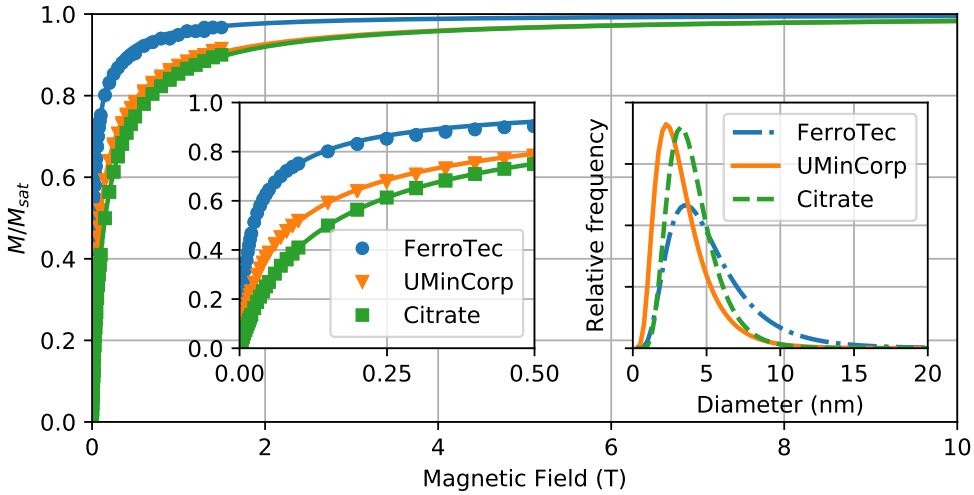

Figure 3.3: Magnetization curves for the three ferrofluids studied, with the magnetization M scaled to saturation magnetization M_{sat}. Solid lines are extrapolations fitted through measured points. Left inset: enlarged view of the initial part of the magnetization curves. Right inset: number frequencies of particle size used to extrapolate the magnetization curves to high field.

3.3.2 Initial Optical Response to Magnetic Field

In the sedimentation experiments (setup in figure 3.1), the Bitter magnet cannot be turned on instantaneously, but the current has to be built up at a rate of 80 A/s, corresponding to 65 mT/s in the field center. In an experiment in the center of the field, i.e. in a uniform field, a strong difference in optical response is observed for the three ferrofluids, as soon as the current starts to flow in the magnet, see figure 3.4. The two commercial ferrofluids become much darker rightaway, whereas the Citrate ferrofluid keeps its initial transmission.

The response of the commercial fluids to the magnetic field is further illustrated in figure 3.5, where the average transmittance of the samples is shown versus time. Even though the concentrations are chosen such that the saturation magnetization is approximately the same for the three fluids (∼2200 A/m), their initial transmittances are not the same. This is mainly due to the presence of aggregates which increase scattering of light and the presence of undisclosed colored surfactant molecules in the commercial fluids, whereas no such surfactants are present in the Citrate ferrofluid. The drop in transmission through the commercial fluids starts precisely at the moment when the

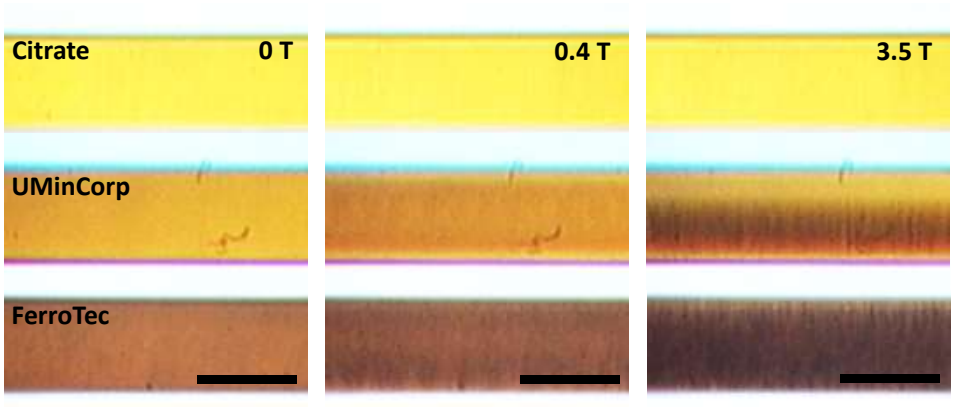

Figure 3.4: Typical set of images with enhanced contrast for visibility. The scale bar represents 1 mm. For the FerroTec and UMinCorp fluids, a decrease in transmission is visible in the second and third panels, while in the third panel macroscopic structures can be observed. In contrast, the transmission of the Citrate fluid remains unchanged across the three panels. All images were taken at zero field gradient, in the center of the magnet.

magnet is turned on, within the 1 s time resolution of the measurements.

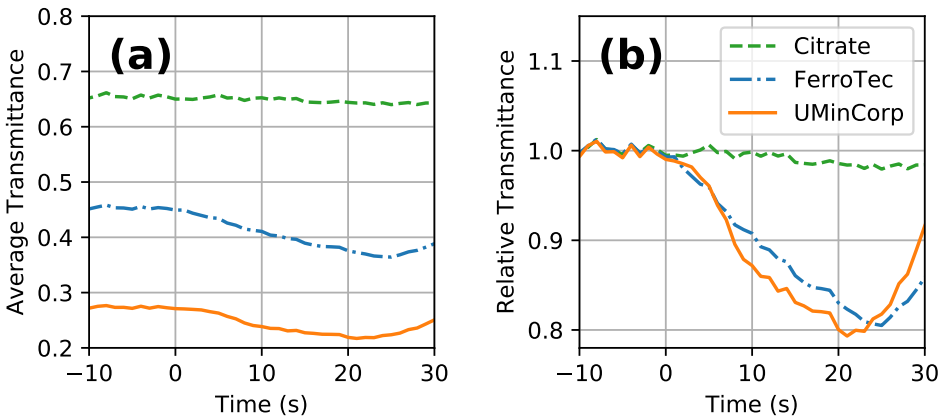

Figure 3.5: Average transmittance of each ferrofluid in a magnetic field increasing linearly with time at 65 mT/s in the field center, starting at time 0. (a) Average transmittance over the entire capillary. (b) Average transmittance over the entire capillary, scaled to initial transmittance.

We ascribe the initial decrease in transmittance observed in the FerroTec and UMinCorp ferrofluids to field-induced dipolar structure formation. These large structures can vaguely be discerned in the images in figure 3.4; bands of

particles with dimensions that must be several tens of micrometers in width (considering the resolution of the images) and that span a large part of the 1 mm vertical range. Because the optical scattering of light scales with the sixth power of the object radius whereas the absorbance only scales with the third power, these large structures lead to an increase in optical scattering in other directions than the camera, thus decreasing the detected light intensity. The "absorbances" later reported for the FerroTec and UMinCorp fluids are thus not pure absorbances but also involve the turbidities of those samples, and their height-integral values are not necessarily conserved during the experiments.

Dipolar structures are known to be present and to grow into larger bands in an external magnetic field when the contact interaction of magnetic nanoparticles or irreversible clusters exceeds the thermal energy [15]. The reversibility of field-induced structure formation, on short timescales where sedimentation does not yet have great effect, is demonstrated by the reversibility of the optical transmission upon alternatingly turning the magnetic field on and off, see figure 3.6a. The optical effect becomes stronger at increasingly stronger fields, see figure 3.6b.

3.3.3 Time-Dependent Optical Profiles

The sedimentation behavior is now examined in greater detail by calculating height-dependent absorbance profiles from the images, see figure 3.7. Heights were measured from the lower outside edge of the capillary, but to correct for glass thickness and because reflections precluded measurements near the edges, heights reported in the figures were set equal to 0.50 mm at the center of the optically accessible range. Due to small deviations in sample positioning between different measurements, the 100% transmittance intensity is most accurate in the middle part of each capillary, in a height range from 0.2 mm to 0.8 mm.

All three ferrofluids initially have a height-independent concentration. In the FerroTec and UMinCorp ferrofluids, large changes are observed within the first minutes after application of the magnetic field. The initial darkening as presented in section 3.3.2 is not visible here, because the timescale for this phenomenon is on the order of seconds. However, the formation of these dipo-

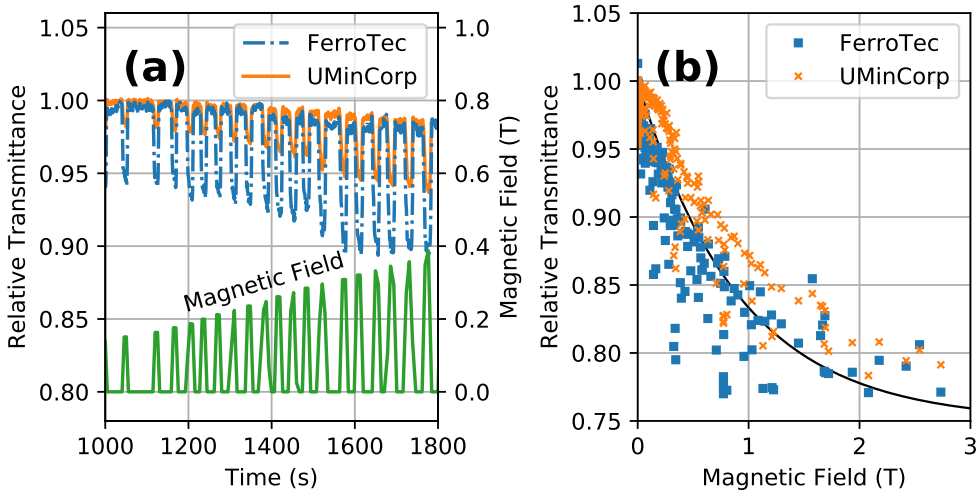

Figure 3.6: (a) Average transmittance through the entire height of the sample capillary scaled to the initial transmittance, plotted along with the magnetic field over time. The decrease in transmittance correlates with the increase of the magnetic field within the time resolution of the measurement. Measurements were performed in the field center. (b) Average transmittance scaled to the initial transmittance plotted against absolute field strength. A line is added to guide the eye.

lar structures accounts for the rapid subsequent sedimentation. The magnetic force on large field-induced structures is the sum of the magnetic force on all individual particles inside the structures, leading to sedimentation velocities that are much higher than those for single particles. After rapid sedimentation of a first fraction of particles, the remaining particles sediment much more slowly. The sedimentation velocity is then still higher than that found in the Citrate ferrofluid, implying that the remaining fraction of particles that continue to sediment in the FerroTec and UMinCorp ferrofluids consists of small aggregates of nanoparticles. Over time, the absorbance in the top part of the capillary tends to zero, indicating the absence of particles. After prolonged exposure to the field, the sediment still reaches a height of about 0.2 mm. The particles then do not form a compact layer, since they are confined to about 20% of the capillary while the overall volume concentration of particles is merely 0.5%. The reason why the average particle height no longer decreases is probably because they form vertical dipolar structures that repel each other, as can be surmised from the images in figure 3.4. The transmission

of light through the gaps between non-transmissive vertical bands of particles could also explain why the integral absorbance of the whole capillary is not conserved upon sedimentation.

In the Citrate fluid, the sedimentation is much slower. Over time the sample tends towards a sedimentation-diffusion equilibrium of individual particles. This can be concluded from the slope of a plot of the logarithm of absorbance versus height. For a Boltzmann distribution of the height-dependent concentration of single magnetic nanoparticles in external field gradient, this slope is approximately equal to $-\mu_{NP}(\mathrm{d}B/\mathrm{d}h)/(k_\mathrm{B}T)$, where $\mu_{NP} \sim 1 \times 10^{-19}\mathrm{Am}^2$ is the average magnetic dipole moment of the nanoparticles (assumed to be fully aligned with field), $\mathrm{d}B/\mathrm{d}h$ is the B-field gradient, and $k_\mathrm{B}T$ the thermal energy [4]. We will demonstrate in chapter 4 via numerical simulations that the profiles obtained in this chapter at high fields agree with the size distributions obtained from earlier measured equilibrium profiles at lower fields.

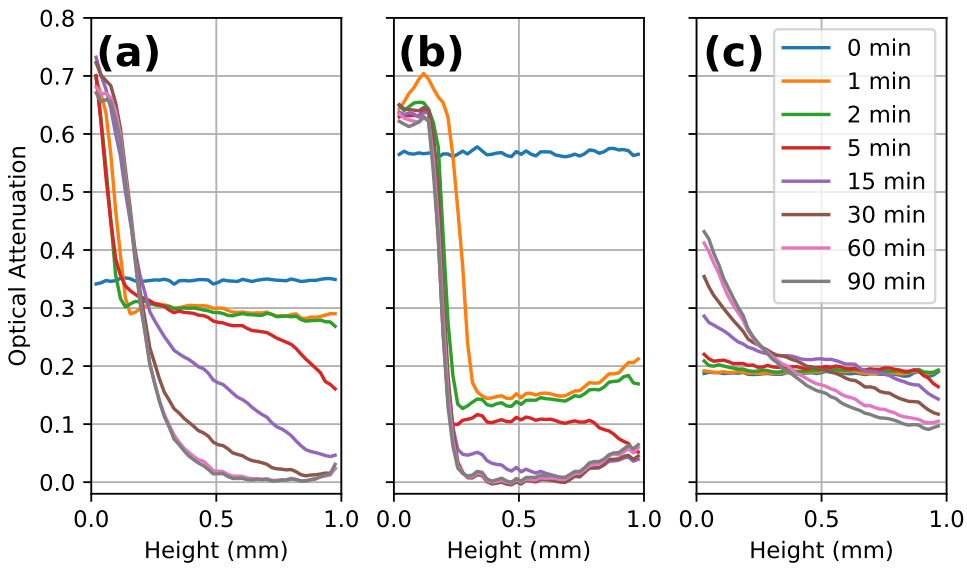

Figure 3.7: Absorbance profiles over time, measured at 10 T and 100 T/m. Starting at time 0, the field was ramped up to the final magnitude with 65 mT/s in the field center, corresponding to 44 mT/s at the sample location. Shown absorbance profiles were measured at 0, 1, 2, 5, 15, 30, 60 and 90 minutes for all samples. (a) FerroTec with an initial saturation magnetization of 2200 A/m. (b) UMinCorp with an initial saturation magnetization of 2500 A/m. (c) Citrate with an initial saturation magnetization of 2200 A/m.

3.3.4 Sedimentation Velocity Analysis

In order to obtain a measure of the colloidal particle velocity from the time-dependent profiles, we adopt the following approach: the absorbance-weighted average height of the particles is calculated for each measured profile using equation 3.1, with $h_{\max}$ and $h_{\min}$ the outermost heights of the profile.

$$< h >= \frac{\int_{h_{\min}}^{h_{\max}} A(h) \cdot h \mathrm{d}h}{\int_{h_{\min}}^{h_{\max}} A(h) \mathrm{d}h} \tag{3.1}$$

As particles migrate towards the bottom of the capillary, the average particle height decreases. In the initial situation all the particles are free to move and the velocity of the average position is identical to the average velocity of the particles (see Appendix). Consequently, the time derivative of $< h >$ as described in equation 3.1 can be considered as a measure of the average sedimentation rate. In figure 3.8, the average particle height is given as a function of time for all three ferrofluids at a magnetic field of 10 T and a gradient of 100 T/m.

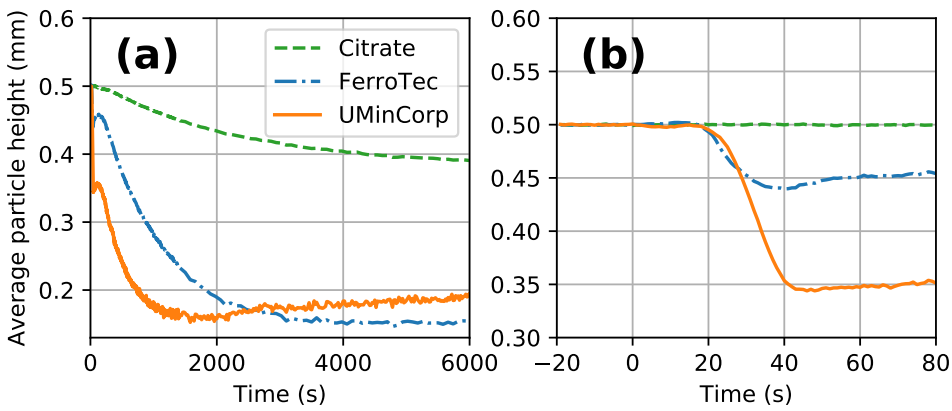

Figure 3.8: Absorbance-weighted average particle height for all three ferrofluids in a 10 T magnetic field with a 100 T/m gradient. Starting at time 0 the magnet is ramped up with 44 mT/s (at the sample location) until preset field is reached. (a) Full length of the experiment. (b) Enlarged view of the initial seconds of the experiment.

For the Citrate ferrofluid, the average particle velocity reaches a maximum shortly after powering up the magnet. As sedimentation progresses in time,

the concentration decreases towards the top and increases towards the bottom, and the resulting concentration gradient generates back-diffusion which lowers the average particle velocity. The initial slope in figure 3.8 corresponds to an initial sedimentation velocity of roughly 70 nm/s. On this basis, an average hydrodynamic size can be calculated, allowing us to conclude whether the sedimenting entities are single particles or larger structures. It is assumed that the sedimenting entities are spheres of diameter D on which acts a magnetic force $m \cdot \mathrm{d}B/\mathrm{d}h$, with $m = (\pi D^3/6)m_\mathrm{b}$ the magnetic dipole moment, $m_\mathrm{b} = 430$ kA/m the bulk magnetization of maghemite [11], and $\mathrm{d}B/\mathrm{d}h$ the magnetic field gradient; it is also assumed that the frictional force follows Stokes' law and thus is equal to $3\pi\eta Dv$ [14], with $\eta = 8.9 \times 10^{-4}$ Pa·s the viscosity of water at 25 °C [72], and v the sedimentation velocity. By setting the magnetic force equal to the frictional force, it can be calculated that a sedimentation velocity of 70 nm/s in a gradient of 100 T/m corresponds to an average hydrodynamic diameter $D = 5.1$ nm of the sedimenting entities. This is of the same order of magnitude as the single particle size from TEM (figure 3.2) and VSM (figure 3.3), indicating that the sedimenting entities are likely to be single nanoparticles. The sedimentation velocity will be analyzed in more detail in chapter 4.

For the Citrate ferrofluid, the initial sedimentation velocity is presented as a function of the magnetic field strength and field gradient in figure 3.9. The sedimentation velocity at 10 T is linearly proportional with the field gradient; this agrees with the presence of single particles on which the magnetic force is $m \cdot \mathrm{d}B/\mathrm{d}h$. At a fixed gradient of 25 T/m, the sedimentation velocity tends to a maximum value as the total field strength is increased from 2.5 T to 10 T; qualitatively, this is as expected from the increase in magnetic alignment that still occurs in this field range, see figure 3.3. Due to the shape and size of the magnet, it was not possible to measure samples at a gradient of 25 T/m in magnetic fields below 2.6 T.

In the FerroTec and UMinCorp ferrofluids, rapid sedimentation occurs already in the first few seconds while the magnet is being turned on, so that a systematic study of the effects of field strength and field gradient would not provide much further information. Nevertheless, after the initial minutes when large dipolar structure sedimented rapidly, sedimentation of remaining

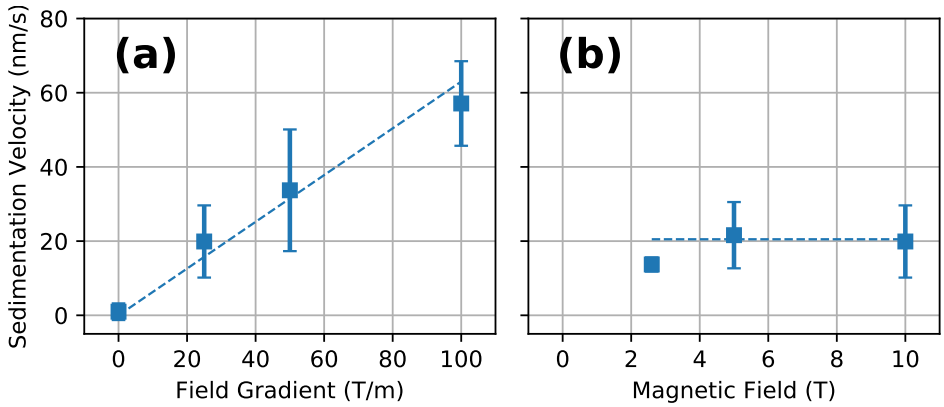

Figure 3.9: Maximum sedimentation velocity in the Citrate ferrofluid. Each point is an average of up to 10 capillaries measured at the same field and field gradient, with the error bars indicating the standard deviation between measurements. Dashed lines are added to guide the eye. (a) Velocities measured in a range of field gradients at a constant field of 10 T. (b) Velocities measured at a range of field strengths with a constant gradient of 25 T/m.

particles continued at a slower rate that was still higher than for the Citrate ferrofluid by about a factor of 6 (figure 3.8). Since the sedimentation rate of spheres scales with the square of the diameter, it is estimated that the entities whose sedimentation was monitored after the first few minutes were aggregates with on the order of 15 nanoparticles.

The results found here at fields of 2.5 – 10 T and gradients of 0 – 100 T/m are comparable to those that we found in chapter 2 at fields of 0.3 – 0.5 T and gradients of about 20 T/m. In the latter experiments, the field was from a neodymium magnet and concentration profiles were determined from x-ray transmission. With the Citrate ferrofluid, the sedimentation-diffusion equilibrium profiles correspond to the size distribution from TEM and VSM, and the average sedimentation rate agrees with the average size of single nanoparticles. With the two commercial aqueous ferrofluids, the sedimentation-diffusion equilibrium profiles and sedimentation rate correspond to the presence of clusters of around 10 particles. The results of the initial rapid sedimentation were also observed by x-ray analysis, but the shortest time between two measurements was 1 hour, so that the initial few minutes were not observed in the same detail as in the present chapter.

3.4 Conclusions

Two types of behavior were observed in our sedimentation experiments on aqueous ferrofluids in magnetic fields up to 10 T and gradients of 0 – 100 T/m. The Citrate ferrofluid consists of nanoparticles dispersed individually which sedimented at the rate expected of single particles, in agreement with our earlier findings at fields of 0.3 to 0.5 T and gradients of about 20 T/m. In contrast, the commercial aqueous ferrofluids contain aggregates, which leads to dipolar structure formation and rapid sedimentation, both here and in our earlier work at lower fields and gradients. An important practical implication is that sedimentation rates at fields obtainable by readily accessible neodymium magnets are predictive of the colloidal stability of ferrofluids at much higher fields and gradients. If sedimentation is much more rapid than expected of single particles at 0.3 to 0.5 T and 20 T/m, this will also be the case at much higher fields and gradients. For the use of aqueous ferrofluids in magnetic density separation or other applications, the presence of aggregates should clearly be prevented. Ferrofluids that are colloidally stable at 0.5 T are likely to remain stable also at much stronger fields. The particles are already oriented magnetically to a large extent at 0.5 T, and the main effect of a further increase in field strength may merely be a further minor increase in degree of magnetic orientation. As such, the challenge of preparing aqueous ferrofluids with good colloidal stability at several tesla, as may be necessary in large-scale implementation of the magnetic density separation technology, may limit itself to the optimalization of existing chemical recipes that yield ferrofluids with good colloidal stability at 0.3 – 0.5 T.

3.5 Appendix: Interpretation of Equation 3.1

The time derivative of $< h >$, the absorbance-weighted or concentration-weighted average height, is equal to the average sedimentation rate at the start of the experiment. This can be seen as follows. As time t progresses, $\mathrm{d} < h > /\mathrm{d}t$ decreases in magnitude due to a fraction ft of particles of a given size accumulating in the sediment, so that a fraction $(1 - ft)$ of particles remains in a column of height $(1-ft)h_0$ above the sediment. The concentration-weighted average height of this column is $(1 - ft)h_0/2$. The concentration-weighted average height of the entire sample, including sediment, is thus given by $(1 - ft)^2 h_0/2 = [1 - 2ft + (ft)^2]h_0/2$, which evolves with sedimentation rate fh_0 in the limit of small ft. The bottom is reached when $ft = 1$.

Chapter 4

Measurement and Modelling of Magnetophoresis of Polydisperse Nanoparticles in Dilute Ferrofluids

Abstract

Dilute ferrofluids have important applications in the separation of materials via magnetic levitation. However, dilute ferrofluids pose an additional challenge compared to concentrated ones. Migration of the magnetic nanoparticles towards a magnet is not well counteracted by a buildup of an osmotic pressure gradient, and consequently, homogeneity of the fluid is gradually lost. Here, we investigate this phenomenon by measuring and numerically modelling time-dependent concentration profiles. Spatial dependence of magnetic field and polydispersity of the particles are taken into account. The magnetic sedimentation rate in our most stable ferrofluids can be understood in terms of the magnetophoresis of separate nanoparticles, a best-case scenario when it comes to applications.

4.1 Introduction

Ferrofluids are liquid dispersions of superparamagnetic nanoparticles that combine properties of liquids and magnets [8]. Many applications, from loudspeakers to rotary seals [29, 32, 73], require ferrofluids with a high volume fraction of the magnetic nanoparticles. The concentration of such ferrofluids remains relatively homogeneous in external fields, because magnetic sedimentation is balanced by back-diffusion of the particles relatively quickly [54, 55]. In dilute ferrofluids, however, sedimentation proceeds much longer before the sedimentation-diffusion equilibrium is approached and by then much of the magnetic material has settled towards the magnet. Dilute ferrofluids have applications in the separation of materials via magnetic levitation in magnetohydrostatic separators, for instance in the separation of diamonds [4], minerals [6], waste metals [74], and plant seeds [52]. Moreover, waste plastics can be separated into different fractions in a single continuous processing step via magnetic density separation [51]. Sedimentation is a clear drawback of dilute ferrofluids, since it renders their magnetic density separation performance time dependent. Nevertheless, the sedimentation rate can be kept as low as possible, by using small magnetic nanoparticles and by preventing aggregation [75].

The presence of aggregates in ferrofluids is detrimental for the performance of the ferrofluid, because they sediment much more rapidly than single particles. Sedimentation is driven by forces that scale with particle volume, whereas the frictional force on a colloidal particle, Stokes drag, scales with particle diameter, resulting in sedimentation rates that increase quadratically with particle size, assuming a spherical particle shape [76]. In a magnetic field, sedimentation can be further accelerated by the magnetically induced growth of aggregates. This does not occur for sufficiently small and separate nanoparticles. For instance, when two magnetic iron oxide particles in the 5–10 nm range collide with each other, they experience a magnetic coupling energy that is smaller than the thermal energy. However, for larger particles or magnetically aligned aggregates of magnetic nanoparticles, the magnetic coupling energy is much stronger. This can lead to formation of large dipolar structures that sediment rapidly [15].

Experimentally, the magnetic sedimentation of nanoparticles has been

studied in different ways, for instance using optical transmission [43, 49], magnetic detection, [71, 77] and density measurements [78]. Not only sedimentation rates were determined, but also sedimentation-diffusion equilibrium profiles, to deduce the size distribution of polydisperse particles [43] or the interactions of monodisperse particles [50]. However, to our knowledge, experimental time-dependent concentration profiles in magnetic fields have not yet been compared to theoretical calculations.

In this work, a model is presented that describes time-dependent concentration profiles of polydisperse ferrofluids in magnetic fields. The model's validity is demonstrated through comparison with experimental data, obtained at different magnetic field strengths and gradients. The studied dispersions are two model ferrofluids, with reportedly good colloidal stability, and for comparison, two commercial ferrofluids expected to have somewhat lower stability. Finally, time-dependent profiles are calculated for sedimentation across distances typical for the industrial separation of plastics via magnetic density separation.

4.2 Theory

In our experiments, the main measured quantities are the saturation magnetization of the sample and a time- and height-dependent measure of the nanoparticle volume fraction. For this reason, we present the experimental time-dependent concentration profiles as a height-dependent saturation magnetization. For comparison, theoretical time-dependent profiles are calculated as follows.

A lognormal distribution of nanoparticle size is assumed. The probability of finding a particle of diameter D is defined in equation 4.1.

$$P(D, \tilde{D}, s) = \frac{1}{\sqrt{2\pi}\beta(s)D} \cdot \exp\left(-\frac{\ln^2(D/\tilde{D})}{2\beta(s)^2}\right) \tag{4.1}$$

Here, $\tilde{D}$ is the median diameter and $\beta(s) = \sqrt{ln(1+s^2)}$, with s the standard deviation divided by the average diameter. Time-dependent concentration profiles are calculated for each particle size separately and added together, with weights corresponding to the overall volume fraction of particles of each size. This assumes a lack of interactions between the particles, in line with the relatively dilute concentrations accessible in our measurements.

In the numerical calculations, space is discretized in bins of height $\mathrm{d}h$. Transfer of particles between bins is calculated according to the average velocity of particles in a bin, which results from a balance of forces on the particles:

$$F_{\mathrm{mag}} + F_{\mathrm{g}} = F_{\mathrm{osm}} + F_{\mathrm{fric}} \tag{4.2}$$

where F_{mag}, F_{g}, F_{osm} and F_{fric} are the magnetic, gravitational, osmotic, and frictional forces, respectively. The average magnetic force on a particle is found by multiplying the magnetic field gradient at height h by the magnetic moment μ_{np} of the nanoparticle [79]:

$$F_{\mathrm{mag}}(h, D) = \mu_{\mathrm{np}}(D) \cdot L(B(h)) \cdot \frac{\mathrm{d}\vec{B}(h)}{\mathrm{d}h} \tag{4.3}$$

where $L(B(h))$ is the average degree of magnetic alignment of magnetic particles with the external field and $\mathrm{d}\vec{B}(h)/\mathrm{d}h$ is the magnetic field gradient. To find the dipole moment of the particles, the volume of the particle is multiplied

by the bulk magnetization m_s of the material:

$$\mu_\mathrm{np}(D) = \frac{\pi D^3 m_\mathrm{s}}{6} \tag{4.4}$$

where D is the diameter of the nanoparticle. The average degree of alignment of magnetic moments to the external field is described by the Langevin function $L(B)$:

$$L(B) = \coth\left(\frac{\mu_\mathrm{np} B}{k_\mathrm{B} T}\right) - \frac{k_\mathrm{B} T}{\mu_\mathrm{np} B} \tag{4.5}$$

where $k_\mathrm{B}T$ is the thermal energy of a particle.

In principle, the gravitational force on a particle can be calculated from $\Delta\rho$, the mass density difference between the nanoparticle and the solvent, and g, the gravitational acceleration:

$$F_\mathrm{g}(D) = \frac{\pi D^3 \Delta\rho}{6} \cdot g \tag{4.6}$$

However, the gravitational force will be neglected, since it is smaller than the magnetic force by two orders of magnitude ($\Delta\rho \cdot g << m_\mathrm{s} \cdot L(B(h)) \cdot \mathrm{d}B/\mathrm{d}h$).

For the osmotic force that counteracts magnetophoresis, the local osmotic pressure is assumed to be that of an ideal solution, neglecting any interactions between the particles:

$$F_\mathrm{chem}(h) = \frac{\mathrm{d}c(h)}{\mathrm{d}h} \frac{k_\mathrm{B} T}{c(h)} \tag{4.7}$$

Here, $c(h)$ is the particle number concentration and $\mathrm{d}c(h)/\mathrm{d}h$ is the number concentration gradient, calculated from the concentrations in neighboring bins, each of height $\mathrm{d}h$.

For the frictional force, the Stokes drag on a spherical particle is assumed [14]:

$$F_\mathrm{drag} = 3\pi\eta D_\mathrm{h} v \tag{4.8}$$

where η is the viscosity of the solvent, v the average velocity of the particles and D_h the hydrodynamic diameter. Note that the hydrodynamic diameter D_h is treated separately from the magnetic core diameter D, allowing for the

modelling of a shell of nonmagnetic material —such as a surfactant— around the magnetic core. An expression for the average velocity of all particles in a bin at height h is found by combining and rewriting equations 4.2, 4.3, 4.7, and 4.8:

$$v(h) = \frac{\frac{\mathrm{d}B(h)}{\mathrm{d}h} \cdot \mu_{\mathrm{np}}(D) \cdot L(B(h)) - \frac{\mathrm{d}c(h)}{\mathrm{d}h} \frac{k_{\mathrm{B}}T}{c(h)}}{3\pi\eta D_{\mathrm{h}}} \tag{4.9}$$

Time-dependent concentration profiles are computed numerically by starting from a homogeneous concentration profile and computing the number n of particles transferred between neighboring segments in discrete time steps $\mathrm{d}t$:

$$n(h) = \frac{v(h) \cdot c(h)}{\mathrm{d}h} \mathrm{d}t \tag{4.10}$$

Equation 4.10 is first calculated for every elevation, before the calculated numbers of particles are transferred at once, resulting in a new concentration profile. Since the outermost bins can only exchange particles towards one side, particles cannot flow out of the system, and the total number of particles remains constant throughout the simulation.

The saturation magnetization profile of the polydisperse system at time t is obtained by summation of the profiles for each particle size, taking into account the number concentrations $c_D(h)$ of particles of diameter D at each height h, as well as the particle volumes and bulk magnetization of the material:

$$m_{\mathrm{sat}}(h) = \int_{D_{\mathrm{min}}}^{D_{\mathrm{max}}} c_D(h) \cdot P(D, \tilde{D}, s) \cdot \frac{\pi D^3}{6} \cdot m_{\mathrm{s}} \cdot \mathrm{d}D \tag{4.11}$$

Here, m_{sat} is the concentration expressed as a saturation magnetization, calculated for direct comparison with the experimental data. A step size $\mathrm{d}D = 1$ nm is used.

The equilibrium concentration profile obtained after prolonged sedimentation can also be computed directly, without tracking profiles during time-dependent sedimentation. At equilibrium, for each particle size, the magnetic and osmotic forces (equations 4.3 and 4.7) are equal at every height:

$$\frac{\mu_{\mathrm{np}}(D)}{k_{\mathrm{B}}T} \cdot L(B(h)) \cdot \frac{\mathrm{d}B(h)}{\mathrm{d}h} = \frac{\mathrm{d}c(h)}{\mathrm{d}h} \frac{1}{c(h)} \tag{4.12}$$

The equilibrium profile is obtained by first calculating relative number concentrations of particles with diameter D in each bin according to equation 4.12, after which the total profile is scaled to agree with the total number of particles of diameter D in the system. Equation 4.11 is finally used to find the equilibrium profile for the entire system. By fitting this theoretical profile to the experimental equilibrium profile, a median particle size and standard deviation (equation 4.1) are found that we use to compute time-dependent concentration profiles that are consistent with the equilibrium profile.

4.3 Experimental

4.3.1 Ferrofluid Preparation

Maghemite (γ-Fe_2O_3) nanoparticles were prepared by coprecipitation of Fe(II) and Fe(III) salts, following a variation on the protocol presented by Massart [16, 17]. Iron chloride salts of p.a. grade were obtained from Sigma-Aldrich. All other chemicals, also of p.a. grade, were obtained from Merck. Water used in this protocol was Milli-Q water. In short, 5.19 g of $FeCl_3 \cdot 6H_2O$ and 1.92 g of $FeCl_2 \cdot 4H_2O$ were dissolved in 130 mL of water and 3.0 g of NaOH in 20 mL of water was added rapidly under heavy stirring. After 5 minutes of stirring, the precipitate was gathered using a hand-held magnet and the supernatant was poured off. The sediment was redispersed in 24 mL of 2M HNO_3 and 3.42 g of $FeCl_3 \cdot 6H_2O$ in 36 mL of water was added, after which the suspension was refluxed at 90 °C for 1 hour. After refluxing, particles were gathered by hand-held magnet, supernatant was poured off, and particles were redispersed in 2M HNO_3. This washing step was repeated twice. Here, the batch was split into two equal parts: (1) part of the sediment (batch PPEG) was redispersed in 2 mL of 30 mg/mL poly(ethylene glycol) monophosphate (M_w = 2000 g/mol) and (2) the remainder of the particles (batch Citrate) was redispersed in 8 mL of 375 mM trisodium citrate and refluxed at 90 °C for 20 minutes. After cooling down, particles were precipitated by addition of acetone, and transferred to a 10 mM NaCl solution. Particles were washed with 10 mM NaCl four times to a final volume of 2 mL.

Two commercial ferrofluids of undisclosed precise composition (sterically stabilized magnetic iron oxide in water) were also used in the experiments.

One ferrofluid was produced by FerroTec (Santa Clara, USA) for Urban Mining Corporation (Rotterdam, the Netherlands) for use in magnetic density separation. The other ferrofluid was produced at a test facility of Urban Mining Corporation.

4.3.2 Surfactant Preparation

Poly(ethylene glycol) monophosphate (M_w = 2000 g/mol) was synthesized following a variation on published protocols [80, 81, 82]. To a solution of 5 g of poly(ethylene glycol) methyl ether (M_w = 2000 g/mol) in 7.5 mL of THF, 0.41 g of $POCl_3$ was added under stirring. The solution was stirred overnight, after which the reaction was stopped by addition of 5 mL of water. THF and water were evaporated at reduced pressure. The product was purified by dissolving it in 5 mL of $CHCl_3$ and running it through a column (40 mm diameter, approximately 15 cm height) filled with silica particles (mesh size 200-425). The eluent was a mixture of $CHCl_3$ and methanol, where the volume fraction of methanol was linearly increased from 0 to 3.5%. Upon reaching 3.5% volume fraction of methanol, the column was flushed with 10% methanol solution. Collected fractions were analyzed by TLC plates using Dragendorff reagent [83] as indicator, which stains all poly(ethylene glycol) compounds. All fractions containing poly(ethylene glycol) compounds were analyzed by ^{1}H and ^{31}P NMR, after which the fractions containing poly(ethylene glycol) monophosphate were collected and solvent was evaporated under reduced pressure. The final product was dissolved in water to a final concentration of 30 mg/mL.

4.3.3 Sample Characterization

Magnetic characterization was done by vibrating sample magnetometry using a Microsense EZ-9. Measurements were performed up to 1.5 T on weighed samples containing approximately 60 µL in a plastic cup. Magnetization curves were used to fit lognormal particle size distributions, which is accurate for the systems investigated here [84]. Transmission electron microscopy was done using a Tecnai 10 at 100 kV. For size distributions from TEM images, at least 120 particles were measured for each sample.

4.3.4 Magnet Characterization

Sedimentation experiments were carried out in well-characterized magnetic fields. Calibration data for the Bitter magnet used for high-field measurements is publicly available from the HFML website [70]. Calibration measurements for the low-field permanent magnet setup, containing cylindrical neodymium magnets of 30 mm thickness and 45 mm diameter (Supermagnete GmbH), show excellent agreement with theoretical predictions for the magnetic field along the axial direction of a cylindrical permanent magnet [48], see chapter 2, equation 2.1. Magnetic field profiles for both setups are shown in figure 4.1.

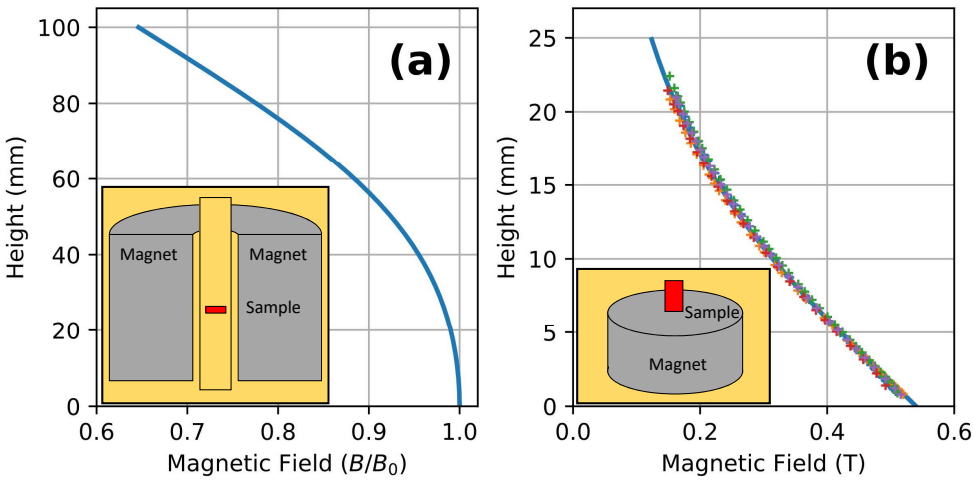

Figure 4.1: (a) Magnetic field as a function of height inside the bore of the 30 T Bitter magnet used in this research. Field is expressed in units of B_0, the magnetic field in the center of the magnet, which is adjustable from 0 to 30 T. Height is defined relative to the center of the field. The inset shows a schematic of the measurements setup; vertical sample position is adjustable within the bore of the magnet. (b) Magnetic field as a function of height for a cylindrical magnet of 30 mm thickness and 45 mm diameter. The solid line represents theoretical field, and the marks indicate measurements done on several magnets [48]. The inset shows a schematic of the measurements setup.

4.3.5 Sedimentation Experiments

Low-field sedimentation experiments were done in polycarbonate cuvettes with a cross section of 2 mm by 9 mm filled to 10 mm height, closed by a cap

to prevent evaporation. Cuvettes were placed on the mentioned neodymium magnets. Position of samples with respect to the magnets was controlled precisely by custom built magnet holders with a cutout for sample placement.

Measurements of concentration profiles in the low field setup was done ex situ, using a LUMiReader X-Ray. Samples were carefully taken from the magnet and placed in the LUMiReader X-Ray, where x-ray transmission profiles were measured at 17.48 keV with a spatial resolution on the order of 100 µm. Each measurement was an average of 11 scans. After measurements, samples were carefully placed back on the magnets. In order to check for disturbances in the concentration profiles due to movement of the sample, all low-field measurements were performed as duplicate or triplicate experiments.

In a back-diffusion experiment, ferrofluid was allowed to reach the equilibrium concentration profile on a magnet. Subsequently the sample was taken away from the magnet and placed in the LUMiReader X-ray, where magnetic field is negligible. Concentration profiles were measured every 15 minutes until the sample approached a homogeneous concentration profile.

High-field sedimentation experiments were performed at the High Field Magnet Laboratory in Nijmegen [70]. Samples were placed in the bore of a 30 T Bitter magnet using a custom made sample holder, adjustable in height (see chapter 3, figure 3.1). By changing the position of the samples with respect to the center of the magnetic field and the current through the magnet, magnetic field strength and gradient could be separately adjusted. Up to 7 capillaries at a time were positioned horizontally in the sample holder. Rectangular capillaries with internal cross section of 50 µm $\times$ 1 mm were used, positioned such that the sedimentation took place over a total height of 1 mm. Using optical imaging, the sedimentation was followed in situ.

4.4 Results and Discussion

4.4.1 Particle Size Distributions

Before measuring and modelling magnetic sedimentation rates, we will present size distributions of the particles as determined in three different ways: from magnetometry (figure 4.2), from electron microscopy (figure 4.3), and from the analysis of sedimentation-diffusion equilibrium profiles.

The magnetization curves (figure 4.2) displayed no hysteresis, confirming the presence of superparamagnetic particles. Size distributions were obtained by fitting according to equations 4.1 and 4.5. The volume magnetization of the material used to calculate particle size distributions was 430 kA/m for the homemade maghemite particles [11]. For the commercial particles, we concluded from magnetometry and density measurements with a pycnometer that they probably consisted largely of magnetite, with a volume magnetization of 480 kA/m [85].

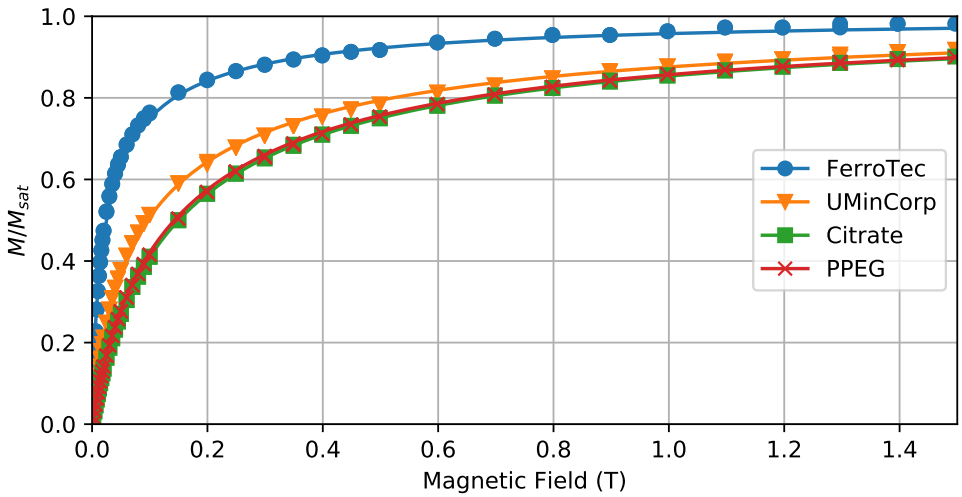

Figure 4.2: Magnetization curves for all tested ferrofluids, scaled to saturation magnetization. No hysteresis was observed and for clarity, only the positive part of the measured curves is shown.

Equilibrium concentration profiles in the low-field sedimentation setup were typically obtained after 200 hours of equilibration. In the approach presented in the theory section, particle interactions are neglected, which implies that there should be no effect of initial concentration on the shape of the

equilibrium profile. Sedimentation experiments were performed for a range of initial concentrations, and a selection of the results is shown in figure 4.4. Each plotted profile represents the average of duplicate or triplicate measurements on different samples of the same fluids. No significant differences were found between multiple experiments with similar initial conditions.

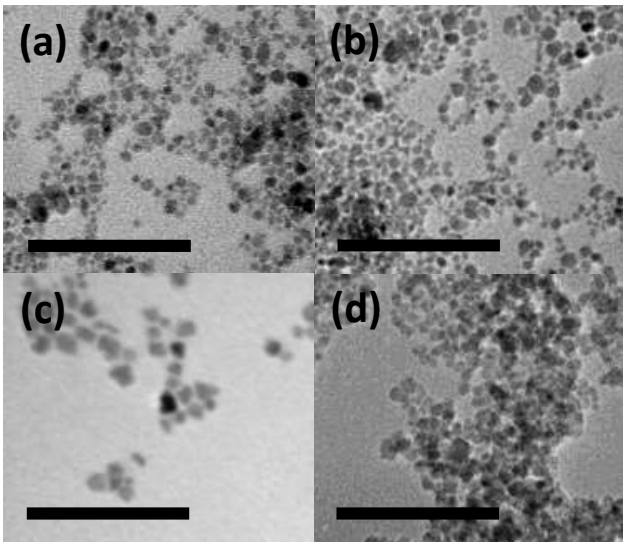

Figure 4.3: Typical TEM images for (a) Citrate ferrofluid, (b) PPEG ferrofluid, (c) FerroTec ferrofluid, and (d) UMinCorp ferrofluid. Scale bars represent 100 nm in all images.

Particle size distributions were calculated by fitting equilibrium concentration profiles to lognormal particle size distributions (see section 4.2, in particular equations 4.1, 4.11, and 4.12). For the PPEG and Citrate ferrofluids, the measurements with the highest initial concentration were used, as they provide the best signal-to-noise ratio. Since the equilibrium profiles for the FerroTec fluid show a concentration dependence, the most dilute sample was used for the fitting. For the UMinCorp fluid, the sample with saturation magnetization of 1100 A/m was used for fitting. These samples were chosen because effects of particle interactions are expected to decrease with lower concentration.

The particle size distributions found by the three methods agree fairly well with each other in the case of the Citrate and PPEG ferrofluids (figure 4.5 and table 4.1). The particle size as measured by TEM is larger than obtained

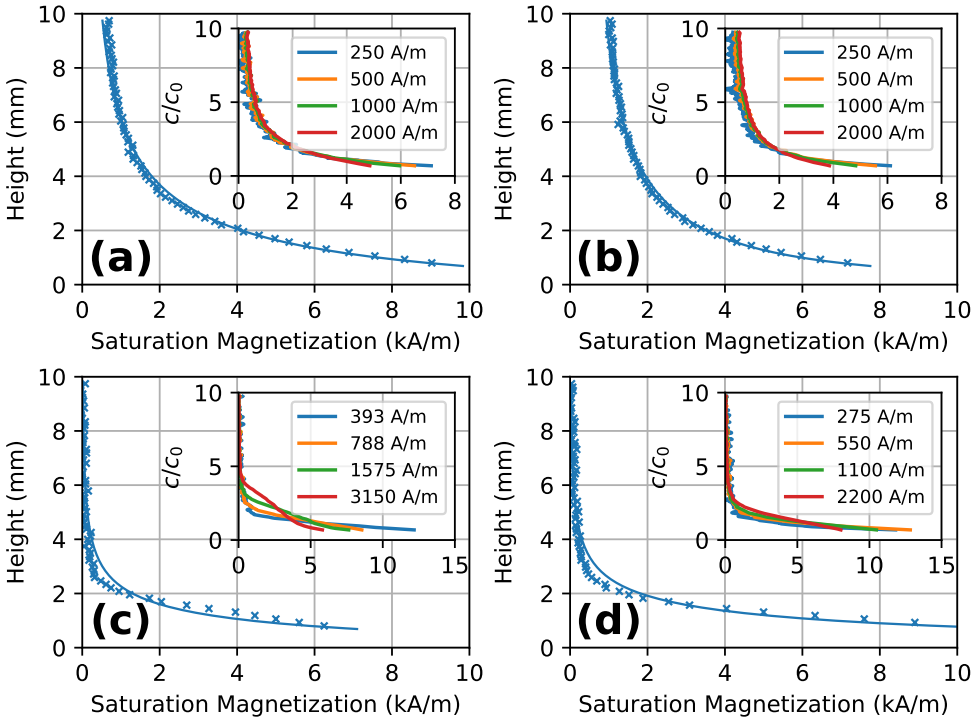

Figure 4.4: Equilibrium concentration profiles in the low field setup as measured (crosses) and fitted according to equation 4.12 (lines). Concentration profiles are (a) Citrate ferrofluid with initial saturation magnetization 2000 A/m, (b) PPEG ferrofluid with initial saturation magnetization 2000 A/m, (c) FerroTec ferrofluid with initial saturation magnetization 788 A/m, and (d) UMinCorp ferrofluid with initial saturation magnetization 1100 A/m. Insets show measured equilibrium concentration profiles for a range of concentrations c, scaled to their initial concentration c_0. Height is defined relative to the surface of the magnet.

by magnetic methods, since the particle contains a magnetic core and a layer of nonmagnetic iron oxide. In the case of the FerroTec and UMinCorp fluids (figure 4.4), more discrepancy is found between the particle size distributions from sedimentation equilibrium analysis and data from the other methods, and the fitted concentration profiles deviate from the measured concentration profiles. In the case of the FerroTec fluid, the largest particles seen by TEM disappear from the sedimentation equilibrium profile, particles that presumably aggregated and rapidly sedimented beyond the experimentally accessible

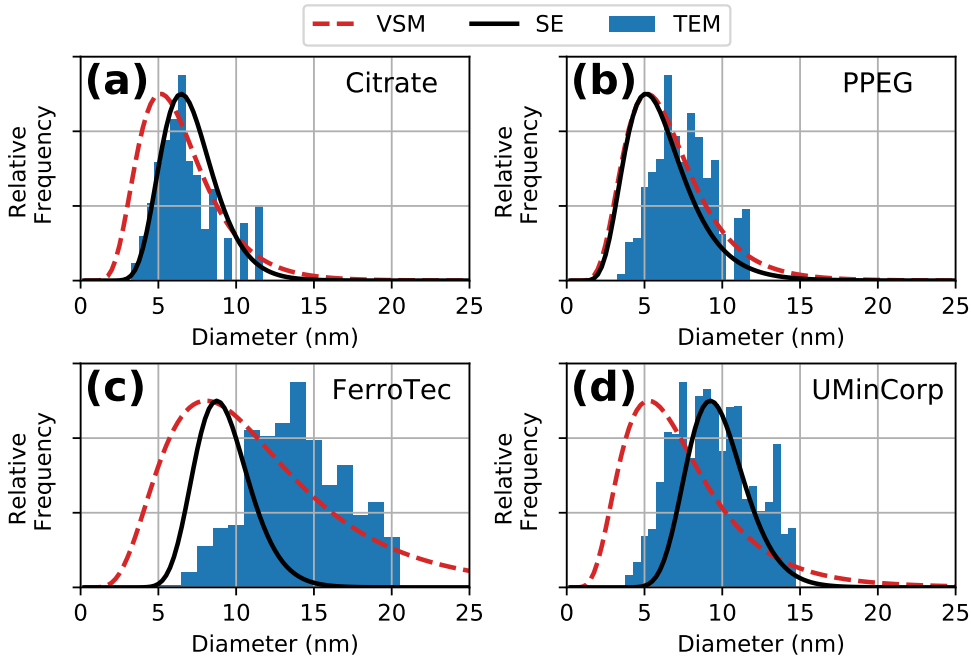

Figure 4.5: Volume-weighted particle size distributions as found by TEM analysis (blue histograms), VSM analysis (dashed red lines) and the sedimentation equilibrium fit (solid black lines) for (a) Citrate ferrofluid, (b) PPEG ferrofluid, (c) FerroTec ferrofluid and (d) UMinCorp ferrofluid.

concentration range. In the case of the UMinCorp fluid, the entities detected in the equilibrium profile show agreement with the particle sizes determined by TEM, but are significantly larger than those found by VSM, possibly indicating small aggregates or multidomain particles.

Table 4.1: Overview of volume-weighted particle size distributions found by VSM measurements, TEM images and magnetic sedimentation experiments (average sizes and standard deviations in nm).

Sample	VSM	TEM	Sedimentation
Citrate	6.0 ± 2.5	6.6 ± 1.5	6.9 ± 1.8
PPEG	6.1 ± 2.6	7.5 ± 1.9	5.8 ± 2.1
FerroTec	10.5 ± 5.8	14.0 ± 3.5	9.1 ± 1.8
UMinCorp	6.7 ± 3.5	8.1 ± 2.1	9.6 ± 1.9

4.4.2 Time-Resolved Sedimentation

4.4.2.1 Time-Resolved Concentration Profiles

Concentration profiles were measured at several times during the sedimentation process. However due to the ex situ nature of the analysis in the low-field sedimentation experiments, concentrations profiles could be measured only once every several hours (figure 4.6a). In the high-field setup (figure 4.6c), depending on the experiments, measurements were taken in situ at intervals of a few seconds.

4.4.2.2 Time-Dependent Average Heights

Since there is no sharply defined sedimentation front to be monitored, we describe the average sedimentation velocity of the particles in a different way. For each measured profile, the concentration-weighted average particle height is calculated using equation 4.13, with $h_{\max}$ and $h_{\min}$ the outermost points of the measured profile.

$$< h >= \frac{\int_{h_{\min}}^{h_{\max}} c(h) \cdot h \mathrm{d}h}{\int_{h_{\min}}^{h_{\max}} c(h) \mathrm{d}h} \tag{4.13}$$

The rate at which the average particle height changes is an average sedimentation velocity of all particles in the system. This average velocity starts at a maximum, decreasing as the system tends toward sedimentation-diffusion equilibrium. This is shown for a selection of experiments in figure 4.7.

Although this representation of the data is less informative than plotting full concentration profiles, it does provide a clear indication of both the magnitude and the timescale at which sedimentation occurs. Using the approach presented in the theory section, concentration profiles were simulated. The particle size distribution found from the equilibrium profile was used for the magnetic size of the particles, and the hydrodynamic radius was varied to fit the measured data. The hydrodynamic radius was taken as the magnetic radius plus an additional shell of fixed thickness, independent of the magnetic radius, see below. The simulation parameters $\mathrm{d}t$ and $\mathrm{d}h$ were chosen sufficiently small that the results are independent of their precise values, while keeping computation time for a single set of parameters and particle size lim-

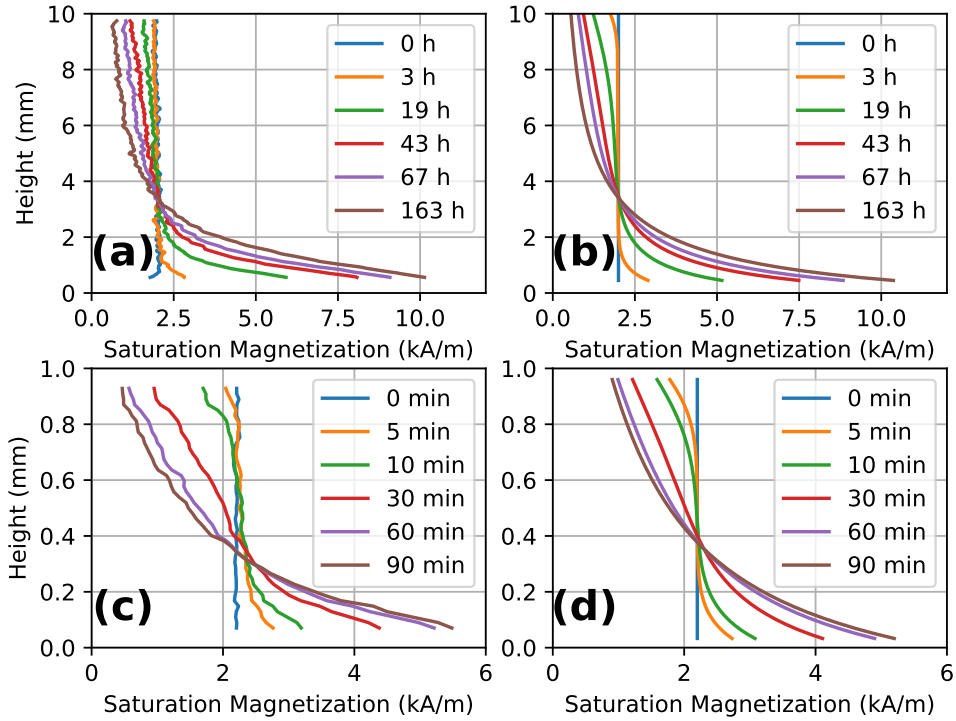

Figure 4.6: (a) A selection of measured concentration profiles for the Citrate ferrofluid (initial concentration 2000 A/m) as measured with the low-field setup using x-ray transmission. Profiles shown are averages of measurements on three samples. (b) Simulated concentration profiles using the particle size distribution obtained by fitting the equilibrium concentration profile, with a 3 nm nonmagnetic shell (see section 4.2). (c) A selection of measured concentration profiles for the Citrate ferrofluid (initial concentration 2200 A/m) as measured in the high-field setup at 10 T and 100 T/m using optical transmission. (d) Simulated concentration profiles using the same particle size distribution as in panel (b). Profiles are shown at the same timepoints as in panel (c).

ited to approximately 4 hours on a personal computer with an Intel Core i5-6400 processor. For the low-field simulations, dt was 200 ms and dh was 20 µm (figures 4.6b and 4.7a), whereas for the high-field experiments simulations, dt was 10 ms and dh was 10 µm (figures 4.6d and 4.7b).

For the PPEG and the Citrate ferrofluids, the simulated sedimentation behavior agrees quantitatively with the experimental data when a shell thickness of 3 nm is assumed. Since a compact physical shell of 3 nm thickness is

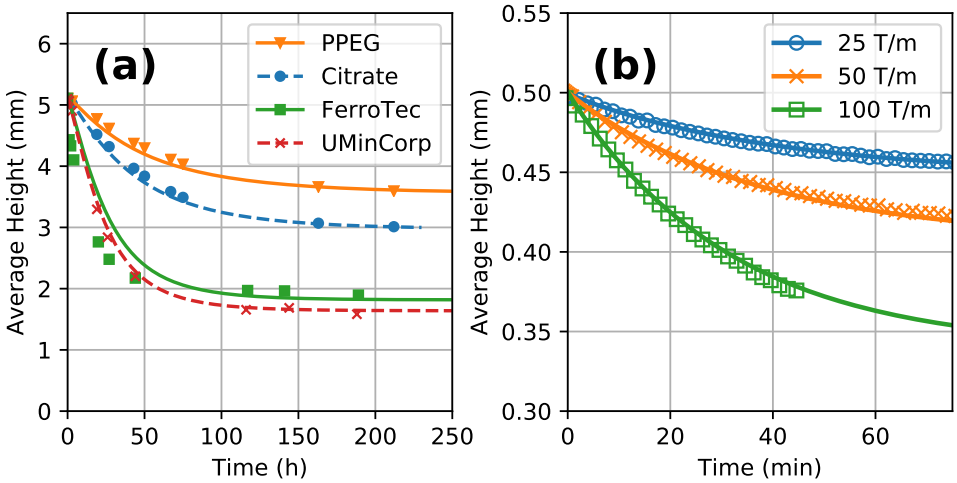

Figure 4.7: (a) Concentration-weighted average particle height in the low field setup plotted as a function of time for the four ferrofluids. (b) Concentration-weighted average particle height in the high field setup plotted as a function of time; the latter experiments were performed using the Citrate ferrofluid in a magnetic field of 10 T, with different magnetic field gradients. Symbols represent measurements, lines represent simulations on the basis of size distributions from sedimentation equilibrium profiles plus, in the case of the PPEG and Citrate fluids, a nonmagnetic shell of 3 nm in thickness.

unlikely for citrate-stabilized particles, considering the small size of the stabilizer molecules, we attribute this to a combination of a thin shell and a friction factor that is higher than that of a sphere. The shell around a particle is likely to consist of a layer of nonmagnetic iron oxide near the surface and a layer of stabilizing organic material. The friction factor of nonspherical particles is known to be different from that of spheres [86]. A cube, for instance, has an approximately 8% lower terminal velocity than a sphere of equal volume [87]. In chapter 5, the core-shell model of the citrate-stabilized particles will be investigated in more detail.

The UMinCorp ferrofluid shows agreement with experimental data if the simulations are performed without a shell around the particles, even though these particles are likely to have a stabilizing layer. Apparently, even though the equilibrium concentration profile was not fitted well, the calculated effective particle size distribution does give a good description of the sedimentation rate.

For the FerroTec ferrofluid, sedimentation in experiments is faster than that in simulations. The largest deviation between simulations and experiments is in the initial part of the experiment, pointing to the presence of aggregates and field-induced structures.

4.4.2.3 Back-Diffusion

From the presented theory, the height-dependence of concentration obtained in magnetic field should disappear upon removal of the field. This prediction was tested experimentally. A sample of the citrate ferrofluid was left on a neodymium magnet until equilibrium was reached, after which it was placed in the LUMiReader X-ray. Concentration profiles were measured every 15 minutes, for a total time of 225 hours. The back-diffusion experiment was carried out with one sample, while two other identical samples were left to re-equilibrate outside of the LUMiReader X-ray. After 225 hours, profiles for all three samples were compared and were found to be largely the same.

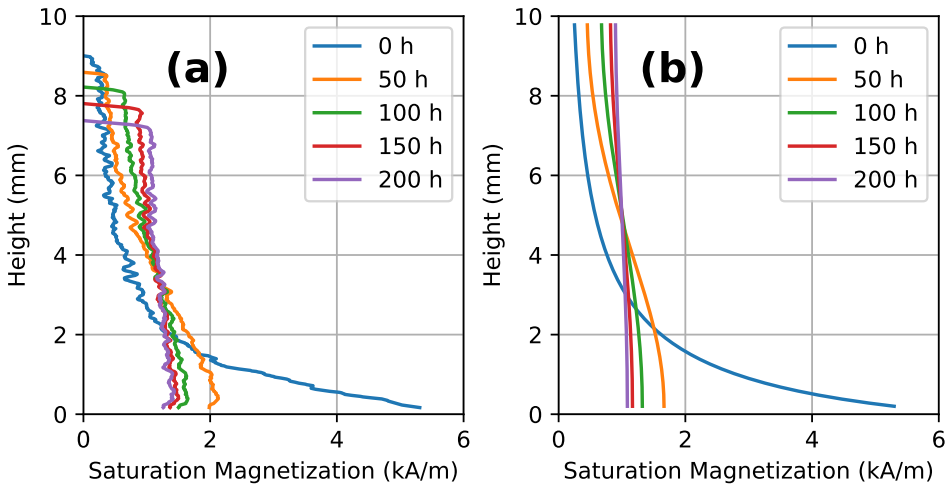

Figure 4.8: (a) A selection of measured concentration profiles for the Citrate ferrofluid (initial concentration 1000 A/m) as measured by x-ray transmission in the absence of a magnetic field. The profile at time 0 is a single measurement, all other profiles are averages of 16 measurements. (b) Simulated concentration profiles using the particle size distribution obtained by fitting the equilibrium concentration profile. Profiles are shown at the same time-points as in panel (a).

Figure 4.8 shows that indeed, starting from a non-homogeneous concentration profile, particles tend to return to a homogeneous concentration profile through diffusion in the absence of a magnetic field. The model presented in this work describes the observed back diffusion process relatively well (figure 4.8b). Although the noise level in these measurements is high and a bit of solvent evaporated despite the cuvette being sealed, the timescale indicated by the simulations is similar to that observed in the experiments.

4.4.2.4 Prediction of Sedimentation across a few Decimeters

The presented model was tested experimentally on millimeter scale, but it can also be used to predict sedimentation across larger distances. In a magnetic density separation setup on industrial scale, magnetic field gradients might be on the order of 10 T/m across several tens of cm. A simulation of the sedimentation of particles in our Citrate ferrofluid was performed for a sample height of 30 cm, a magnetic field of 4 T at the bottom of the fluid, a constant gradient of 10 T/m, and simulation parameters dt and dh of 1 s and 100 µm, respectively. Results are shown in figure 4.9.

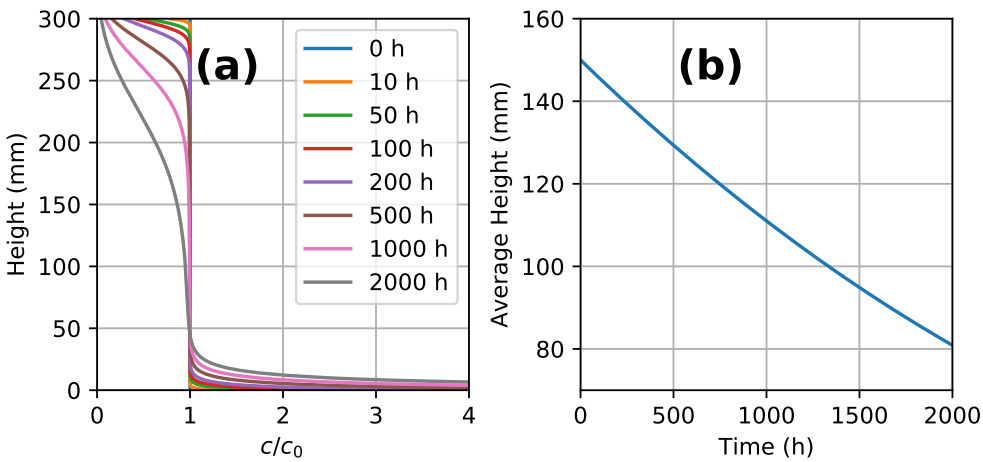

Figure 4.9: (a) A selection of concentration profiles as found by a simulation for typical MDS conditions: a gradient of 10 T/m across an experimental space of 30 cm. Simulation parameters dt and dh were set at 1 s and 1 mm, respectively. The particle size distribution of the citrate ferrofluid was used. (b) Concentration-weighted average particle height versus time for the full duration of the simulation.

The calculated profiles indicate that it takes several weeks to approach sedimentation equilibrium. However, the formation of a dense sediment at the bottom of the experimental space starts within hours. On the one hand, a ferrofluid with nanoparticles in the size range of 5-10 nm diameter dispersed as single particles is a best case scenario, since sedimentation will be much faster with larger particles or aggregates. On the other hand, the calculations do not take into account convection, which may cause homogenization of the fluid and therefore mitigate the effects of sedimentation. For industrial separation of materials using dilute magnetic fluids, magnetic sedimentation may well be a manageable problem, as long as aggregation of the magnetic nanoparticles can be prevented.

4.5 Conclusions

Particle size distributions of dilute polydisperse ferrofluids are deduced from equilibrium concentration profiles measured in well-characterized magnetic fields. On the basis of these size distributions, time-dependent concentration profiles are calculated. In the case of ferrofluids with particles in the 5-10 nm diameter range without aggregation, sedimentation rates agree quantitatively with the presented theory. The same theoretical model seems applicable to other stable ferrofluids in other experimental geometries and on other length scales. Magnetic sedimentation in dilute ferrofluids cannot be prevented, because of the weak osmotic pressures in such systems. However, sedimentation is slow, and possibly a bit of convection may suffice to keep the ferrofluid much more homogeneous than predicted by the presented model.

Chapter 5

Core-Shell-Shell Model of Citrate-Stabilized Maghemite Particles in Aqueous Ferrofluids

Abstract

In previous chapters, discrepancies between the size of magnetic domains inside particles and hydrodynamic size were attributed to a combination of nonmagnetic iron oxide, non-sphericity and a layer of surfactant and immobilized solvent around the particle. In this chapter, the significance of each of these effects is examined by comparing results obtained by different experimental methods applied to aqueous citrate-stabilized maghemite nanoparticles. Besides electron microscopy, magnetometry, and determination of magnetic sedimentation rates and equilibria, two additional techniques are applied here to provide more information on the hydrodynamic size: analytical centrifugation and dynamic light scattering. The overall results are summarized via a core-shell-shell model. The iron oxide core of the particles is assumed to consist of a magnetic sphere surrounded by a nonmagnetic shell. A second, outer shell represents the citrate molecules adsorbed on the surface and a layer of solvent that is immobilized around the particle.

5.1 Introduction

Many applications of ferrofluids, such as speakers or hard drives [88, 89], require high magnetization, obtained by having a high concentration of magnetic nanoparticles. When such concentrated ferrofluids are subject to magnetic field gradients, the magnetophoresis of particles is counteracted by their high osmotic pressure, preventing sedimentation. However, in applications of dilute ferrofluids such as magnetic density separation (MDS) [51], the osmotic pressure is not enough to prevent sedimentation. The best scenario is to have sedimentation to be as slow as possible.

The sedimentation rate of superparamagnetic nanoparticles in magnetic field gradient results from the magnetic and frictional forces on the particles. Both magnetic force and friction factor depend on particle size, but differently. The magnetic force scales with the in-field component of the magnetic dipole moment of a particle and is proportional to the volume of the magnetic material in the particle in the limit of saturating field. Since viscous forces dominate over inertial forces (the so-called Stokes regime), the friction factor scales with the radius of the particle, including nonmagnetic material such as nonmagnetic iron oxide or surfactant material. In order to gain more insight into the sedimentation velocity in magnetic field gradients, here we study the structure of the particles in more detail using several methods that inform on the particle size in different ways.

Particle size analysis from transmission electron microscopy (TEM) measurements provides direct number-weighted statistics in which no bias towards small or large particles is present, provided that the sample size is large enough and samples are carefully prepared [90]. In contrast, dynamic light scattering (DLS) experiments detect the intensity of scattered light, which scales with the sixth power of the particle radius. DLS is thus much more sensitive for the larger particles than for the smaller particles in the sample. Although intensity-weighted distributions from DLS can be mathematically transformed to give volume- or number-weighted particle size distributions, it is a model-dependent operation that may not be fully reliable for systems with high polydispersity. Moreover, values reported by DLS are dependent on scattering angle and concentration of nanoparticles [91, 92].

In sedimentation experiments, there are two main approaches: time-dependent

sedimentation measurements [93] or sedimentation-diffusion equilibrium measurements [43, 49]. In both cases, data is usually obtained by analyzing concentration profiles determined by optical absorbance, resulting in volume-weighted particle size distributions. In time-dependent measurements, sedimentation coefficients can be obtained if the solvent viscosity is known. Although sedimentation coefficients largely depend on particle size and density, other factors such as shape contribute to sedimentation velocity [87, 94]. Sedimentation-diffusion equilibrium measurements inform on the particle buoyant mass or magnetic moment, depending on whether sedimentation occurs in a gravitational or magnetic field.

VSM measurements inform on the total magnetic moment of the nanoparticle from which the particle volume can be calculated, provided that the bulk magnetization of the material is known. VSM measurements are volume-weighted, as the measured quantity is magnetic moment which scales with particle volume [84].

In this research, citrate-coated maghemite particles are analyzed using a range of methods. Results are interpreted using a simple particle model assuming a core of iron oxide, which is partially magnetic and partially nonmagnetic, surrounded by a shell of surfactant and immobilized solvent. A combination of TEM, VSM and x-ray absorbance is used to characterize the particle cores, and the hydrodynamic shell of the particles is investigated using magnetic and nonmagnetic sedimentation experiments as well as DLS.

5.2 Experimental

5.2.1 Preparation of Ferrofluid

All chemicals used were of p.a. grade. Iron salts were obtained from Sigma-Aldrich, and all other chemicals were obtained from Merck. Water used in this research was Milli-Q water. Ferrofluid was prepared following an adapted Massart protocol [16, 17].

5.19 g of $FeCl_3 \cdot 6H_2O$ and 1.92 g of $FeCl_2 \cdot 4H_2O$ were dissolved in 130 mL of water and 3.0 g NaOH in 20 mL of water was rapidly added while the mixture was stirred. The solution was stirred for 5 more minutes, after which the black precipitate was collected using a magnet and the supernatant was poured off. The sediment was redispersed in 24 mL of 2M HNO_3, and 5.10 g of $Fe(NO_3)_3 \cdot 9H_2O$ in 36 mL of water was added. The suspension was refluxed at 90 °C for 1 hour, after which the particles were gathered by magnet and the supernatant was poured off. After the particles were washed with 2M HNO_3 twice, approximately half of the sediment was taken and redispersed in 10 mL of water. To this suspension, 6 mL of 1M trisodium citrate was added and the mixture was refluxed at 90 °C for 15 minutes. After this, acetone was added to precipitate the particles, which were gathered by magnet, and the sediment was redispersed in 10 mM NaCl in water. This washing step was repeated three times. After the fourth washing cycle, the sediment was redispersed in approximately 10 mL of 10 mM NaCl in water. The suspension was left on a cylindrical neodymium magnet (45 mm diameter, 30 mm thickness) for 15 minutes in order to remove aggregates, after which the top 8 mL of liquid was taken apart and the rest of the liquid discarded.

5.2.2 Physical Measurements

Transmission electron microscopy was performed using a Tecnai 20 microscope at 200 kV. For the particle size distribution, approximately 200 particles were analyzed using the ImageJ software.

Magnetization curves were determined using a Microsense EZ-9 vibrating sample magnetometer. Measurements were performed on samples containing approximately 60 µL of liquid, weighed using a calibrated analytical balance. Hysteresis loops were measured between +1.5 and –1.5 T. The VSM was cal-

ibrated before each measurement session. Measurements were performed at room temperature, approximately 20 °C.

Dynamic light scattering measurements were performed on a Malvern Instruments Zetasizer Nano ZS using a 633 nm laser. DLS measurements were performed at 20 °C and scattered light was collected at an angle of 173°. For each measurement, 15 runs of 10 seconds each were performed and reported values are the average of 20 measurements. Samples were diluted to an iron oxide volume fraction of approximately $1{\cdot}10^{-5}$.

Analytical centrifugation experiments were performed using a Beckman Coulter ProteomeLab XL-I. A sample of ferrofluid was diluted to an iron oxide volume fraction of approximately $1{\cdot}10^{-4}$ with 10 mM NaCl in water and was put in a cell with 3 mm optical path length. Absorbance was measured at a wavelength of 376 nm against a reference cell containing 10 mM NaCl in water. The experiment was performed at a rotational rate of 16,000 rpm at 20 °C (20000 g at 7.0 cm from the rotor axis). In order to obtain a distribution of sedimentation coefficients, scans were analyzed using Sedfit software version 16.1c, fitting a continuous $c(s)$ distribution model. In the fitting the bottom was kept at a fixed value, and the meniscus, the frictional coefficient and the baseline were floated.

Magnetic sedimentation experiments were performed by centering ferrofluid samples in a plastic cuvette (internal cross section 3 mm × 10 mm; filled to 10 mm height) on top of a cylindrical neodymium magnet (diameter 4 mm, thickness 30 mm). Concentration profiles were measured by x-ray transmission at 17.48 keV using a LUMiReader X-ray (LUM, Berlin, Germany). For each measurement, samples were carefully taken from the magnet and placed in the LUMiReader X-ray for measurement. After measurement, samples were carefully placed back on the magnets. Measurements were performed at room temperature, approximately 20 °C and for each experiment, three identical samples were analyzed.

5.3 Results and Discussion

5.3.1 Iron Oxide Core Analysis

The size of the iron oxide cores of the particles was determined from TEM measurements, see figure 5.1. Since the particles are synthesized by coprecipitation and it gives a good fit, a lognormal particle size distribution is assumed [84]. In a lognormal distribution, the probability of finding a particle with diameter D in a population is given by equation 5.1.

$$P(D, \tilde{D}, s) = \frac{1}{\sqrt{2\pi}\beta(s)D} \cdot \exp\left(-\frac{\ln^2(D/\tilde{D})}{2\beta(s)^2}\right) \tag{5.1}$$

Here, $\tilde{D}$ is the median diameter and $\beta(s) = \sqrt{\ln(1+s^2)}$, with polydispersity index s defined as the standard deviation divided by the average diameter.

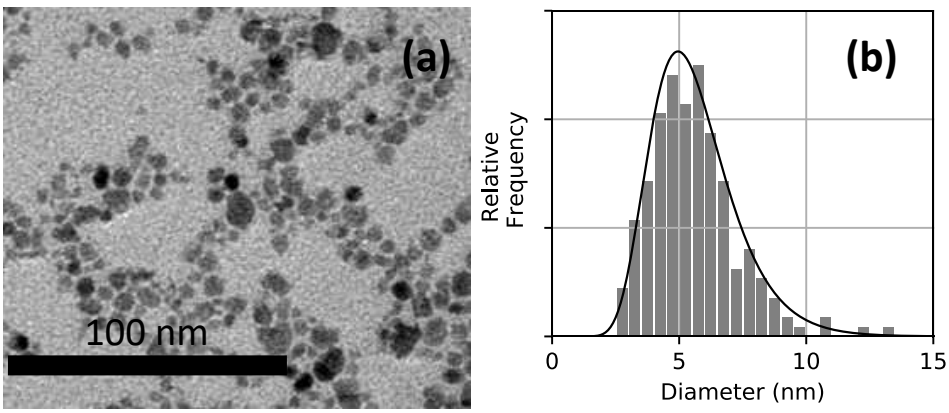

Figure 5.1: (a) Typical TEM image of iron oxide nanoparticles. (b) Histogram of the number distribution of particle diameters determined by TEM analysis. The black line represents a lognormal particle size distribution with a median diameter of 5.4 nm and a standard deviation of 30%.

Magnetization curves were measured for multiple samples of the ferrofluid. As no hysteresis was observed, for clarity only the positive part of the magnetization curves is shown in figure 5.2. The magnetization as a function of field for a sample with known size distribution is given in equation 5.2.

$$M(H) = M_{\text{sat}} \int_{D_{\min}}^{D_{\max}} L(D, H) \cdot P_{\text{vol}}(D, \tilde{D}_{\text{vol}}, s) \cdot \mathrm{d}D \tag{5.2}$$

Here, $M(H)$ is the magnetization of the sample in external field H, M_{sat} the saturation magnetization of the sample and $L(D, H)$ the Langevin factor, defined as:

$$L(H) = \coth\left(\frac{\mu_0 \mu_{\text{np}} H}{k_{\text{B}} T}\right) - \frac{k_{\text{B}} T}{\mu_0 \mu_{\text{np}} H} \tag{5.3}$$

where $k_{\text{B}}T$ is the thermal energy, μ_0=$4\pi \cdot 10^{-7}$ m kg s^{-2}A^{-2} is the permeability of free space and μ_{np} the magnetic dipole moment of the particles (in Am^2) defined as $\pi D^3 m_{\text{bulk}}/6$ with m_{bulk} the bulk magnetization of the material (in A/m). The particle size distribution $P_{\text{vol}}(D, \tilde{D}_{\text{vol}}, s)$ is given in terms of a volume-weighted median diameter, since the magnetic dipole moment of the particle scales with the particle volume. For lognormal particle size distributions, the conversion from number-weighted $P(D, \tilde{D}_{\text{num}}, s)$ to volume-weighted $P_{\text{vol}}(D, \tilde{D}_{\text{vol}}, s)$ particle size distribution is done via equation 5.4. Changing the moment of a lognormal distribution does not influence the shape, but only the value of the median. The polydispersity index s remains constant [95].

$$\tilde{D}_{\text{vol}} = \tilde{D}_{\text{num}} \cdot \exp(3\beta(s)^2) \tag{5.4}$$

Here, $\tilde{D}_{\text{vol}}$ is the volume-weighted median diameter and $\tilde{D}_{\text{num}}$ is the number-weighted median diameter.

From magnetization curves, particle size distributions were calculated, assuming a bulk magnetization of 430 kA/m for maghemite [85] and a lognormal particle size distribution. Comparison with TEM size distribution requires a conversion, since the particle size distribution obtained with this method is volume-weighted and TEM size distribution is number-weighted. A direct comparison of number-weighted particles size distributions is given in figure 5.3(a).

The size distribution as found by fitting VSM data results in an average diameter approximately 1.2 nm smaller than that found by TEM. The difference in sizes might in principle be explained in two ways, (1) a lower bulk magnetization of the iron oxide in the nanoparticle cores compared to the bulk magnetization of pure maghemite, or (2) the presence of a shell of nonmagnetic iron oxide around a core of magnetic iron oxide. Our measurements do not allow one to discriminate between the two interpretations. For our model,

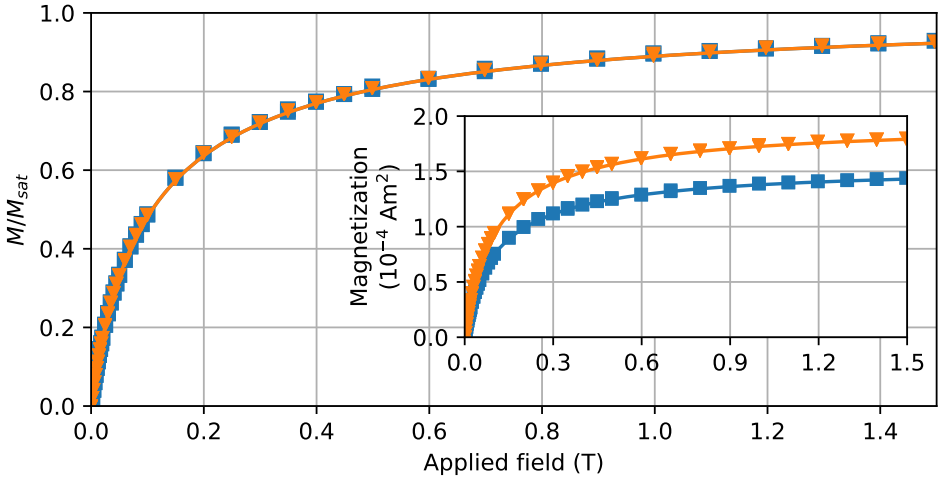

Figure 5.2: Magnetization curves as measured for two separate samples, scaled to saturation magnetization. The symbols represent measured points and the lines represent fitted curves. Inset: magnetization curves for the same two samples, before scaling to saturation magnetization. Sample weights were 58.2 mg and 71.8 mg for the blue squares and orange triangles, respectively.

we chose the second interpretation because a lower overall magnetization is most likely to originate from surface spin disorder and anisotropy, as is shown in other work [96, 97, 98].

This interpretation leads to a layer of 0.6 nm non-magnetic iron oxide material around a core of magnetic maghemite as shown in figure 5.3(b), on the order of the distance between iron atoms in a maghemite crystal [85]. Based on the data presented here, it is not possible to determine whether the thickness of the nonmagnetic shell depends on the size of the magnetic domain. However, since surface effects are not expected to scale with the size of the domain underneath, we assume the nonmagnetic layer to be of the same thickness, independent of the size of the magnetic cores of the particles.

The offset between the size of the iron oxide core and the magnetic domain is not only found by comparing VSM measurements to TEM images, but it is also observed when other methods are used to determine the size of the iron oxide cores. For instance, characterization of these systems using SANS [17] or SAXS [12] results in a particle size slightly larger than that found from magnetic analysis.

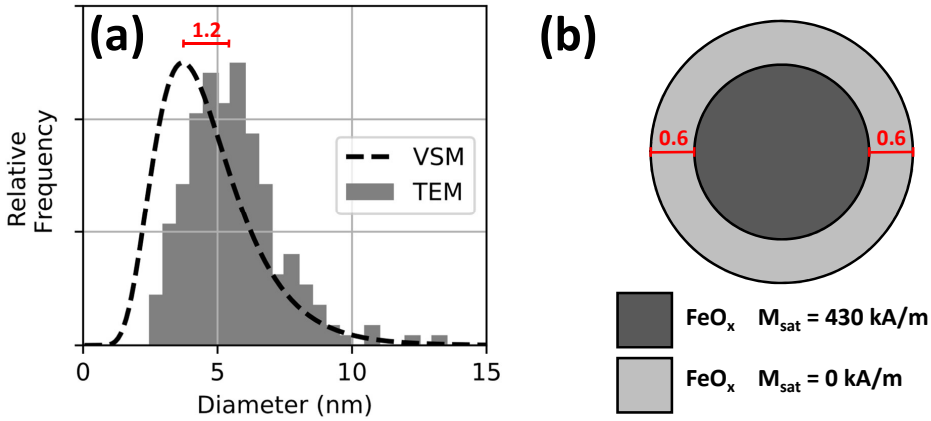

Figure 5.3: (a) Number-weighted particle size distribution from TEM analysis (gray bars) and as found by fitting VSM curves (dashed line). VSM fit gives a lognormal distribution with a median diameter of 4.3 nm and a polydispersity of 40%. (b) Simple model of particle composition. A core of magnetic iron oxide material with a saturation magnetization similar to bulk maghemite, surrounded by a shell of nonmagnetic iron oxide. The thickness of the nonmagnetic shell is given by the offset between the size distributions found by VSM and TEM.

To determine the ratio of magnetic to nonmagnetic iron oxide in an independent way, we measured the x-ray absorbance at 17.48 keV as a function of concentration of magnetic material (see figure 5.4). Using literature values for the mass attenuation coefficient and density of maghemite (26.2 cm^2/g [99]; 4.9 $\cdot 10^3$ kg/m^3 [100]) and water, the average bulk magnetization of all iron oxide was calculated to be 229 kA/m. Assuming the simple model shown in figure 5.3(b) with a core of magnetic iron oxide surrounded by a layer of nonmagnetic iron oxide, this gives a volume fraction of 0.53 magnetic iron oxide in the core of the particle, corresponding to a layer of approximately 0.5 nm around a core of 4 nm diameter. This increase in diameter of 2×0.5 nm is comparable to the offset of 1.2 nm between diameters observed by TEM and diameters found from VSM measurements.

5.3.2 Hydrodynamic Size

Without magnetic field, the hydrodynamic size of the particles was determined by analytical (ultra)centrifugation (AUC). This was done by fitting a distri-

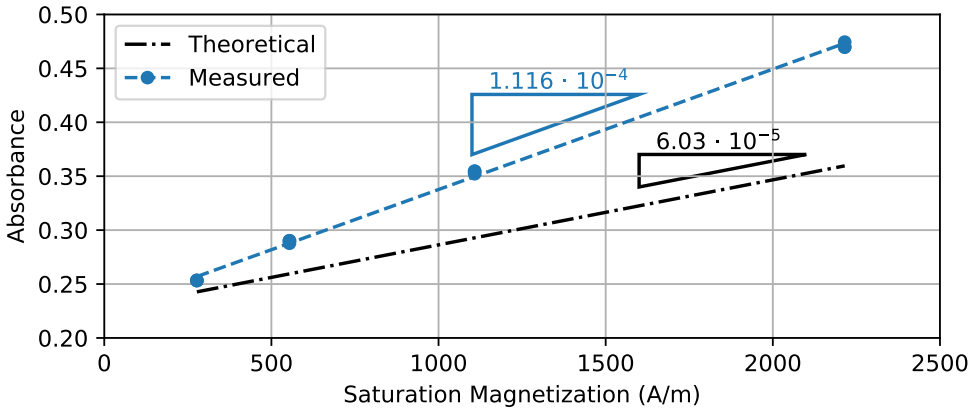

Figure 5.4: X-ray absorbance (defined as minus the natural logarithm of transmittance; 17.48 keV; 2 mm path length through the liquid) plotted against the saturation magnetization of the ferrofluid. The blue line indicates the fit to the experimental data (blue points), and the black line indicates the slope found from literature values assuming only magnetic iron oxide.

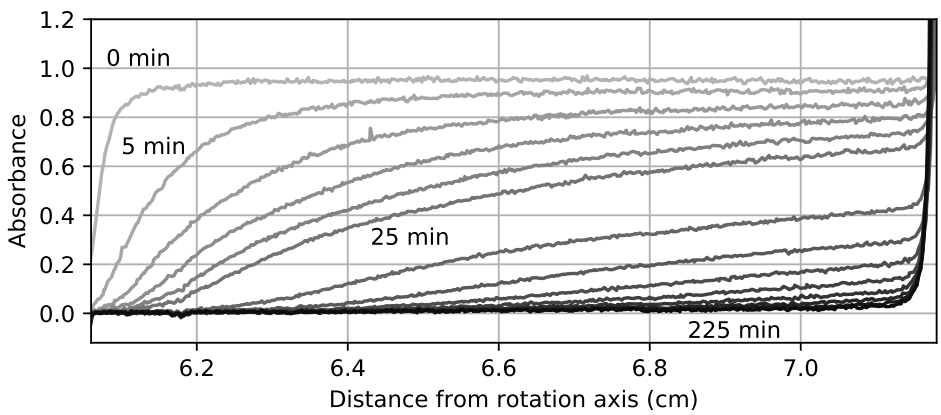

Figure 5.5: Selection of absorbance profiles used for fitting of sedimentation coefficients from analytical centrifugation. From 0 to 25 minutes, profiles are shown with 5 minute intervals, and from 25 to 225 minutes, profiles are shown with 25 minute intervals. The experiment was performed at 20 °C and 16000 rpm, with scans taken every minute.

bution of sedimentation coefficients to the measured concentration profiles. A selection of measured concentration profiles is shown in figure 5.5.

The sedimentation coefficient s_{AUC} is defined as the sedimentation velocity of a particle divided by the centrifugal acceleration, resulting in a value

independent of rotational rate and rotor size:

$$s_{\mathrm{AUC}} = \frac{v}{\omega^2 r} \tag{5.5}$$

Here, s_{AUC} is the sedimentation coefficient in Svedberg (10^{-13} s), v the sedimentation velocity of the particle, ω the angular velocity and r the distance to the axis of rotation. In order to determine a particle size from the sedimentation coefficient, assumptions on the structure of the particle have to be made. In the simple case of a homogeneous sphere, the size can be found by equation 5.6.

$$s_{\mathrm{AUC}} = \frac{\Delta\rho V}{3\pi\eta D} = \frac{\Delta\rho D^2}{18\eta} \tag{5.6}$$

Here, V is the particle volume, $\Delta\rho$ the density difference between the particle and the solvent, and η the solvent viscosity. For the particles studied here, this model is not accurate, due to the inhomogeneity of the particles. In the core-shell model used in this research, an iron oxide core is assumed, surrounded by a shell of surfactant and immobilized solvent. Assuming the density of the outer shell of surfactant and solvent to be equal to the density of the solvent, equation 5.6 was modified to apply to this model:

$$s_{\mathrm{AUC}} = \frac{\Delta\rho_{\mathrm{FeO_x}} V_{\mathrm{FeO_x}}}{3\pi\eta D_{\mathrm{hydrodynamic}}} = \frac{\Delta\rho_{\mathrm{FeO_x}} D^3_{\mathrm{FeO_x}}}{18\eta D_{\mathrm{hydrodynamic}}} \tag{5.7}$$

where $\Delta\rho_{\mathrm{FeO_x}}$=3.9·$10^3$ kg/m^3 is the density difference between the iron oxide core and the solvent, $V_{\mathrm{FeO_x}}$ the volume of the iron oxide core, $D_{\mathrm{hydrodynamic}}$ the hydrodynamic diameter and $D_{\mathrm{FeO_x}}$ the diameter of the iron oxide core of the particle. The hydrodynamic diameter was found by fitting the sedimentation coefficients using the particle size distribution obtained by TEM as the diameter of the iron oxide core. The sedimentation coefficient distribution found by AUC is noisy at higher sedimentation coefficients, corresponding to the fastest moving fraction of the sample. Since the major fraction of the particles is found in the lower sedimentation coefficient range, the position of the highest peak was used for fitting a hydrodynamic shell size, as shown in figure 5.6b. Since profiles are measured using optical transmittance, the distribution of sedimentation coefficients is volume-weighted and the size distribution ob-

tained by TEM was transformed to a volume-weighted size distribution using equation 5.4 for the fitting. The thickness of the hydrodynamic shell found with this method is 1.0 nm, which is in line with values of 0.7-1.0 nm found by AFM for citrate layers on flat gold substrates and XPS analysis on gold nanoparticles [101, 102].

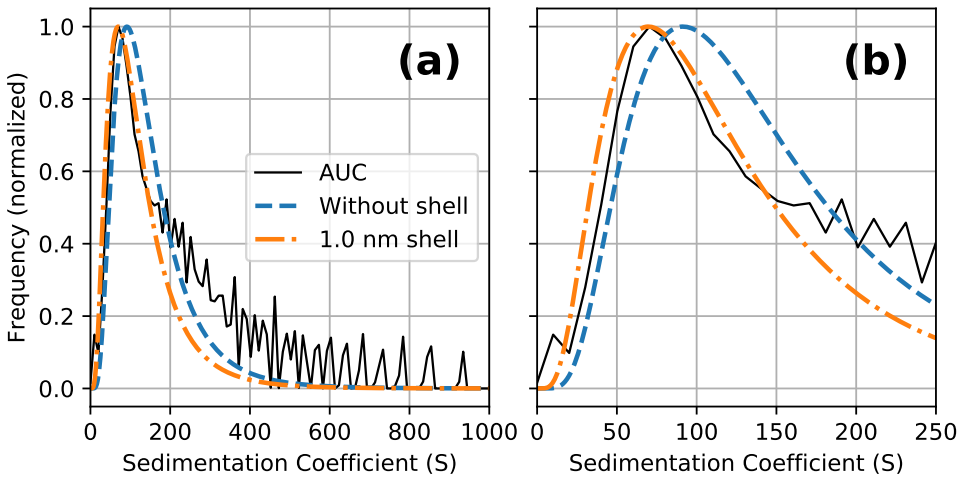

Figure 5.6: (a) Distributions of sedimentation coefficients of the nanoparticles obtained by AUC (solid black line), compared to distributions calculated from the core size found by TEM without shell (blue dashed line) or with a shell of 1.0 nm thickness (orange dashed line). (b) Enlarged view of the position of the peak, used for fitting the hydrodynamic size.

From magnetic sedimentation data, the effective hydrodynamic size was obtained using a method described in chapter 4. In short, concentration profiles at several points in time are fitted to concentration profiles simulated using a relatively simple model. In this model, the size of the magnetic cores is determined from the concentration profile in sedimentation-diffusion equilibrium and the hydrodynamic size was adjusted to fit the time-dependent data. For ease of interpretation, the concentration-weighted average height is calculated for each profile using equation 5.8.

$$< h >= \frac{\int_{h_{\min}}^{h_{\max}} c(h) \cdot h \mathrm{d}h}{\int_{h_{\min}}^{h_{\max}} c(h) \mathrm{d}h} \tag{5.8}$$

The concentration-weighted average particle height decreases as particles

sediment, with an initial slope equal to the average sedimentation velocity of the particles. Over time an increasing concentration gradient counteracts magnetic sedimentation and the average particle height tends to its equilibrium value, as shown in figure 5.7.

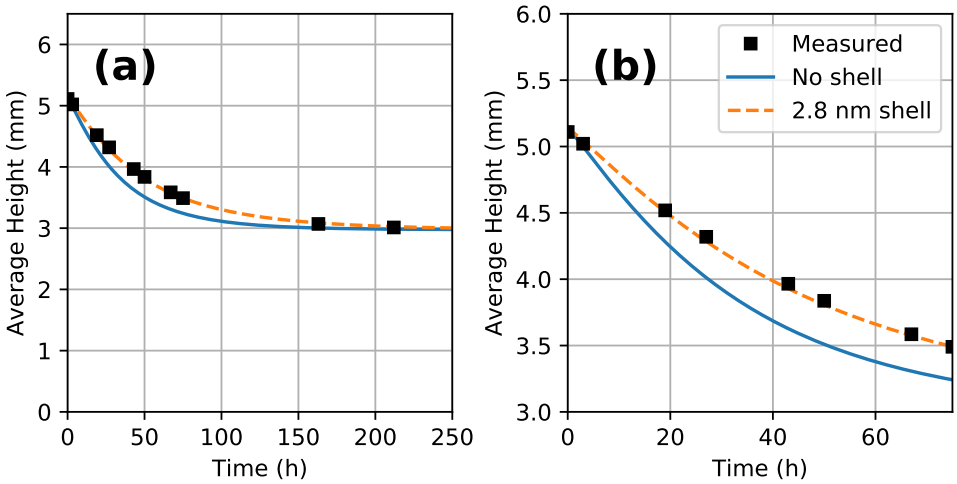

Figure 5.7: (a) Concentration-weighted average particle height as measured (black squares), compared to simulations without shell (solid blue line) or with a shell of 2.8 nm thickness (orange dashed line). (b) Enlarged view of the initial part of the experiment.

As shown in figure 5.8 there is a discrepancy of approximately 2 nm in the effective hydrodynamic diameters of the particles found by the nonmagnetic and magnetic sedimentation methods. In light of the possibility of magnetic field-induced dipolar structure formation, it was expected that the magnetic sedimentation might possibly be faster than predicted from the hydrodynamic size found in the absence of magnetic field, but surprisingly, the inverse is the case: the magnetic sedimentation is slower. The reason for this is unclear. Long-range interparticle interactions should affect both types of measurements in the same way, and at a typical concentration of 0.1 volume percent, the average distance between particles is about 0.5 µm, much more than the Debye length of 3 nm at 10 mM ionic strength. One fundamental difference between the two types of sedimentation experiments is that whereas a gravitational force is in the same direction independent of particle orientation, magnetic field in principle can exert a magnetic torque that depends on the particle's

dipolar orientation, possibly affecting the flow field around the particle. In our approach, we assume a steady-state magnetic force found by the time-averaged orientation of the magnetic moment of the nanoparticle, as provided by a magnetization curve. This approach seems to be warranted, however, since the time scale of field flow adjustment is expected to be of the order of the time required for a particle to sediment across a distance equal to its diameter, here about 20 s (sedimentation at 0.2 nm/s and 4 nm radius), and since the Brownian rotation of the dipole moment inside the particles via the Néel mechanism is expected to be faster by several orders of magnitude [103]. It is remarked that in 20 s, particles with a radius of $a = 4$ nm diffuse across a distance $\sqrt{2Dt}$ of about 50 µm in sedimentation direction, assuming a diffusion coefficient D given by $k_\mathrm{B}T/(6\pi\eta a)$, with $k_\mathrm{B}T$ the thermal energy and η the viscosity of the solvent. Magnetic sedimentation is so slow that a tiny bit of thermal convection might suffice to slow it down even further.

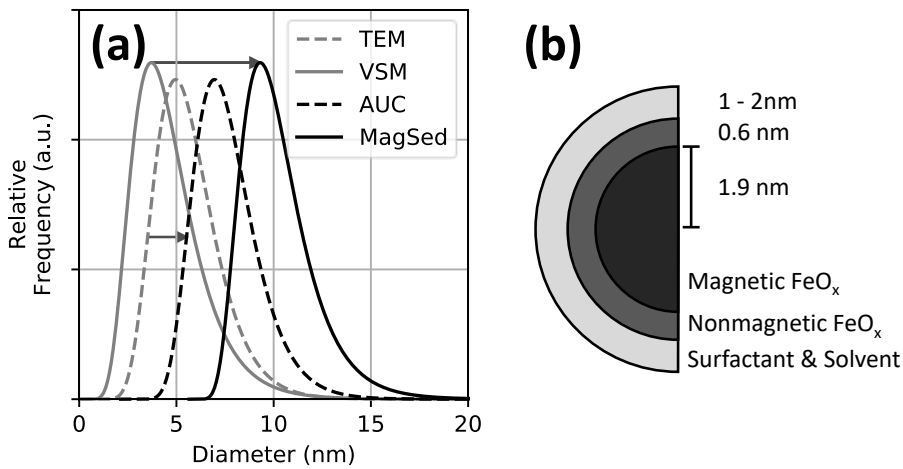

Figure 5.8: (a) Number-weighted particle size distribution as found from AUC (dashed black line), obtained using the size distribution found by TEM (light gray dashed line) and from magnetic sedimentation (solid black line) starting from the size distribution found by VSM (light gray solid line). (b) Schematic representation of the particle model, with indications for the sizes of the core and shells of the particle. Size indications are for the most frequent particle size, since the system is polydisperse.

Another effect may be that the size distributions for the iron oxide cores is assumed to be lognormal, with a fixed thickness of the nonmagnetic iron oxide

shell. Consequently, the magnetic domain size distribution cannot be strictly lognormal. By fitting to a lognormal size distribution, an error is introduced in the precise shape of the size distribution, which may influence the obtained hydrodynamic shell thickness from magnetic sedimentation.

Nanoparticles in water are in the Stokes regime, so that the friction force is determined by the radius of the particle. However, the effective hydrodynamic size of a particle is also determined by the shape of the particle. As shown in figure 5.1 the particles used in this research are roughly spherical, but they do deviate from exact spheres. These deviations cause an increased the friction factor, which can be described as an increased effective hydrodynamic size. The magnitude of this contribution to the effective hydrodynamic radius may vary depending on the precise shape of a single particle. As an indication, cubic particles have a friction factor increased by approximately 8% compared to a sphere of equal volume [87]. A magnetic-field induced effect on the time-averaged orientation of the particles might also be a fundamental difference with sedimentation in the absence of magnetic field.

Table 5.1: Overview of the number-weighted size distribution found using different analysis techniques. For the VSM and X-ray analyses, the ratio between magnetic iron oxide and total iron oxide is shown.

Technique	Average Diameter (nm)	Polydispersity (%)	Magnetic FeO_x fraction
TEM	5.4	30	
VSM	4.3	40	0.50
X-ray			0.53
AUC	7.4	30	
Mag	9.9	40	
DLS	13.0	31	

The hydrodynamic size of the particles was also investigated using dynamic light scattering, giving a number-weighted average diameter of 13.0 ± 1.3 nm, with a standard deviation of 4.0 ± 0.2 nm (see Appendix). This is significantly larger than the hydrodynamic size as found from sedimentation methods, and would imply a layer of immobilized solvent of approximately 4 nm around the iron oxide cores of the particles. Since such larger than expected particle diameters are also found by other research groups using similar particles in

DLS analysis [34], we explain this discrepancy by a combination of factors which are assumed in usual DLS analysis, such as spherical particle shape, absence of light absorption and optical homogeneity. One effect that plays a role here is the optical heterogeneity of the particles. The iron oxide core of the particles scatters light much stronger than the surrounding hydrodynamic shell, which causes the intensity of scattered light to scale with a_{core}^6 instead of $a_{\text{hydrodynamic}}^6$ as is assumed in DLS. Since a_{core} is smaller than $a_{\text{hydrodynamic}}$ by the thickness of the shell, this intensity scaling tends to underrepresent the small particles and overrepresent large particles more than the normal intensity scaling, increasing the observed average diameter. Another effect here might be the higher dilution necessary for DLS measurements, compared to other methods. Samples were diluted using 10 mM NaCl in water, to keep ionic strength constant. Although the dilution for DLS is only higher by one order of magnitude when compared to the AUC measurements, small aggregates may be formed due to partial desorption of citrate from the particles' surface [17].

Yet another possible explanation might be that light scattered at 173° towards the detector combines with light first scattered at small angles and is then reflected towards the detector by the flat wall of the cuvette (heterodyning), an effect that causes the decay time of the correlation function to double [104]. Theoretically, heterodyning leads to a lower contrast which was not observed in the measurements here, but since DLS gives such strongly different results than obtained via the both time-dependent sedimentation techniques and the analysis of magnetic sedimentation-diffusion equilibria, the interpretation of the zetasizer DLS results on these samples merits further attention. Earlier DLS results on oil-based ferrofluids with homebuilt DLS equipment were in good agreement with TEM [94], possibly suggesting that reflections at the flat cuvette wall of the zetasizer equipment might affect measurements differently than the cylindrical wall in earlier measurements using homebuilt equipment [94].

5.4 Conclusions and Outlook

The structure of magnetic nanoparticles was investigated by a combination of analysis techniques, interpreted using a simple particle model. The particle model assumes an iron oxide core, consisting of magnetic and nonmagnetic iron oxide. The size of the core and the relative amount of magnetic and nonmagnetic iron oxide were investigated by TEM, VSM, and x-ray absorbance measurements, which provided a consistent picture of the particles, with nonmagnetic shell of about 0.5 nm in thickness. However, for the determination of the hydrodynamic diameter, the three applied techniques —AUC, magnetic sedimentation, and DLS— gave different results. For now, our results obtained by these techniques raise more questions about the interpretation and inherent assumptions of the methods than that they answer about the hydrodynamic size of the particles.

It will be useful to repeat the DLS experiments with other equipment, of the type used in the past when good agreement was found between DLS and TEM size analysis of comparable ferrofluids.

5.5 Appendix: DLS Data

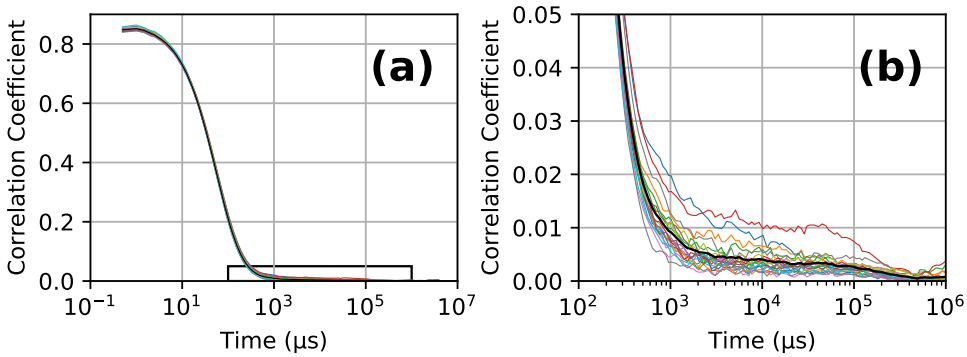

Figure 5.9: (a) Intensity correlation function obtained by DLS. The black rectangle indicates the area enlarged in panel (b). Each colored line represents a single measurement of 15 runs of 10 seconds each. The black line shows the average of all measurements shown.

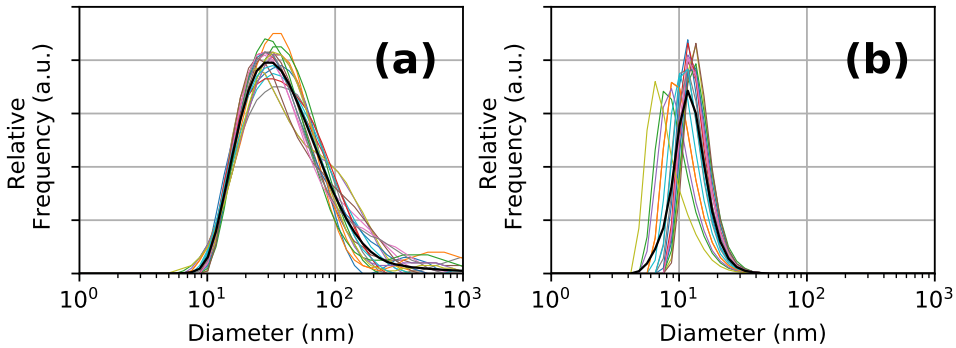

Figure 5.10: (a) Intensity weighted size distribution obtained by DLS. (b) Number weighted size distribution obtained by DLS. Each colored line represents a single measurement of 15 runs of 10 seconds each. The black lines show the average of all measurements shown.

The DLS data show an essentially monomodal distribution, with practically no particles larger than those in the 10 to 100 nm range. It is noteworthy that the the peak in the intensity weighted size distribution shown in figure 5.10(a) is wider than the peak in the number weighted size distribution shown in figure 5.10(b), while the polydispersity index in a lognormal size distribution is expected to be independent of the moment of the distribution.

Chapter 6

Summary / Samenvatting

6.1 Summary

Magnetic Density Separation (MDS) is a recycling technology that can separate several different materials in a single processing step. This requires a dilute ferrofluid that ideally should remain homogeneous in external magnetic field. In practice, magnetic sedimentation and the resulting loss in homogeneity of dilute ferrofluids are an issue. Nevertheless, the practical impact of sedimentation can be limited by minimizing the sedimentation rate, which depends on colloidal stability and size of the particles. In this thesis, the main objectives are: (1) to characterize the rate of magnetic sedimentation in dilute aqueous ferrofluids of potential interest to MDS and (2) to understand the rate at which sedimentation occurs. Several methods for measurement and modelling of sedimentation of magnetic nanoparticles in magnetic fields are presented.

In the experiments, three types of dilute aqueous ferrofluid are analyzed, two ferrofluids received from Urban Mining Corporation, a company developing the MDS technique, and one ferrofluid synthesized in the Van 't Hoff Laboratory in Utrecht via a well-known method to prepare citrate-stabilized ferrofluids. Sedimentation rates of these ferrofluids show significant differences, with the ferrofluid synthesized in our laboratory showing sedimentation rates as expected for nanoparticles dispersed as single particles. The other two ferrofluids show significantly faster sedimentation rates.

In **chapter 1**, an overview is presented of the background of this project. The societal relevance and necessity for MDS are mentioned, and a brief overview is given of the working principle of the technology. Ferrofluids are introduced, as well as basic aspects of magnetic sedimentation. The synthesis method followed to prepare aqueous ferrofluid in our laboratory is discussed, with a brief explanation of the chemical processes happening in each of the synthesis steps.

In **chapter 2**, sedimentation of nanoparticles in the ferrofluids is monitored using magnetic measurements. A magnetic field sensor is placed between a cylindrical neodymium magnet and a ferrofluid sample in order to detect changes in the local magnetic field. Time-dependent measurements are interpreted using a simple model in which the ferrofluid is represented by a stack of three columns: (1) a top layer of solvent, in which no magnetic particles

are present, (2) a middle layer with the same concentration of nanoparticles as in the initial sample, and (3) a layer of concentrated magnetic nanoparticles at the bottom of the vial. In this approach a well-defined sedimentation front is assumed, neglecting diffusion. For this reason, the main result of the measurements is the initial sedimentation rate. The time-dependent magnetic measurements provide too little information to justify interpreting them using a more elaborate model.

In **chapter 3**, sedimentation of nanoparticles is monitored in magnetic fields up to 10 tesla, with magnetic field gradients up to 100 tesla per meter. Ferrofluids are brought into the bore of a Bitter magnet and sedimentation is observed by optical imaging. From the images, concentration profiles are obtained as a function of time and sedimentation velocities are calculated. The sedimentation velocity is studied as a function of magnetic field and magnetic field gradient, two parameters selected independently via the electrical current through the magnet and the position of the sample.

For a stable ferrofluid, such as the citrate-stabilized maghemite ferrofluids synthesized in our laboratory, the sedimentation velocity scales linearly with the field gradient and is independent of field strength above approximately 1 tesla, when magnetization approaches saturation. Moreover, the equilibrium profiles obtained after prolonged sedimentation correspond well to the presence of individually dispersed particles. In ferrofluids where aggregates are present, an increase in optical attenuation is observed as soon as the field is turned on, and rapid sedimentation occurs. These observations are explained by the field-induced formation of dipolar structures inside the ferrofluid.

Sedimentation rates and colloidal stability of particles at magnetic fields of 0.3 to 0.5 tesla correlate well with sedimentation rates and colloidal stability at much higher magnetic fields. The practical implication is that experiments performed using neodymium magnets may provide enough information to predict colloidal stability at magnetic fields of several tesla.

In **chapter 4**, a theoretical model is developed to describe sedimentation of polydisperse magnetic nanoparticles in the dilute regime. In this model, three main forces on a nanoparticle are considered: (1) a magnetic force towards higher magnetic field, (2) an osmotic force, due to the gradient in chemical potential that forms as sedimentation occurs, and (3) a frictional force that

scales with solvent viscosity as well as the velocity and hydrodynamic radius of the particles. Setting the sum of these forces to zero, the average velocity of the particles is found in finite volume elements at different height. Starting from a homogeneous concentration profile, subsequent profiles are numerically calculated by displacing particles to and from neighboring volume elements according to the local average velocities, in discrete time steps. This theoretical model neglects particle interactions, and stable polydisperse particle systems are modelled as a sum of monodisperse particle systems, weighted by their relative occurrence in the polydisperse system.

Numerical calculations performed at different magnetic fields and field gradients are compared to experimentally obtained data. For the most stable ferrofluids, whose magnetic nanoparticles are dispersed individually, the numerical method is found to give an accurate description of the sedimentation of magnetic nanoparticles in magnetic fields ranging from 0.3 to 10 tesla and at gradients ranging from 15 to 100 tesla per meter. Sedimentation velocity of the magnetic nanoparticles was the same in numerical calculations and experiments when an effective hydrodynamic shell of approximately 3 nm thickness was assumed. Because particle interactions are neglected, the model is not accurate for systems containing aggregates or systems with field-induced structure formation. For a stable ferrofluid, the model makes it possible to predict sedimentation on other length scales, for instance those of an industrial MDS installation.

In **chapter 5**, the particle-scale model for the sedimentation rate of magnetic nanoparticles is investigated in more detail. A citrate-stabilized ferrofluid is investigated using a combination of transmission electron microscopy, vibrating sample magnetometry, x-ray absorbance, analytical (ultra)centrifugation, magnetic sedimentation, and dynamic light scattering. Results are interpreted using a core-shell-shell model, in which the particles consist of a magnetic iron oxide core, surrounded by a first shell of iron oxide that is nonmagnetic and a second shell consisting of adsorbed citrate molecules and immobilized solvent. For the characterization of the iron oxide core, agreement in the ratio between magnetic and nonmagnetic iron oxide is found for all methods used. However, for the determination of the hydrodynamic size of the particles discrepancies are found between the three used methods. These discrepancies are discussed

in terms of the practical limitations and interpretative uncertainties of the methods.

In conclusion of this thesis, the work confirms that aggregation must be prevented to minimize the magnetic sedimentation rate in dilute ferrofluids. In the experimental characterization of sedimentation, time-dependent measurements of the concentration profile are the most instructive. Sedimentation equilibrium profiles enable a clearcut conclusion whether the nanoparticles are dispersed individually in external magnetic field, and the average sedimentation rate in polydisperse ferrofluids can be modelled well on the basis of the size-dependent magnetohydrodynamic properties of the individual particles.

6.2 Samenvatting

Magnetische Dichtheid Scheiding (MDS) is een recycling technologie waarmee verschillende materialen in een enkele processtap te scheiden zijn. MDS maakt gebruik van een verdunde magnetische vloeistof die idealiter homogeen zou moeten blijven in extern magneetveld. In de praktijk, echter, is het niet mogelijk om magnetische sedimentatie te voorkomen en worden verdunde magnetische vloeistoffen in de loop der tijd steeds minder homogeen. Desalniettemin kan men ervoor zorgen dat dit proces zo traag mogelijk gebeurt, via een optimale colloïdale stabiliteit en kleine afmeting van de magnetische nanodeeltjes. In dit proefschrift zijn de meest belangrijke vragen: (1) op welke manier de snelheid van magnetische sedimentatie kan worden gemeten en (2) of we de gemeten sedimentatiesnelheid kunnen begrijpen. Verschillende meetmethoden en theoretische modellen voor de sedimentatie van magnetische nanodeeltjes in magneetvelden worden gepresenteerd.

In de experimenten worden drie soorten magnetische vloeistof geanalyseerd: twee vloeistoffen die ontvangen zijn van Urban Mining Corporation, een bedrijf dat de industriële toepassing van MDS ontwikkelt, en een vloeistof die gemaakt is in het Van 't Hoff Laboratorium in Utrecht. Significante verschillen in sedimentatiesnelheid zijn gevonden tussen de verschillende vloeistoffen, waarbij de vloeistof die in ons eigen laboratorium gemaakt is een sedimentatiesnelheid heeft zoals verwacht wordt voor nanodeeltjes die zich als losse deeltjes in de vloeistof bevinden. Bij de andere twee vloeistoffen worden significant hogere sedimentatiesnelheden gevonden.

Een overzicht van de achtergrond van dit project wordt gegeven in **hoofdstuk 1**. De maatschappelijke relevantie en de noodzaak voor MDS worden besproken, gevolgd door een korte uitleg over de werking van MDS. Hierna volgt een korte inleiding tot magnetische vloeistoffen, ook wel ferrofluïda genoemd, waarna enige basisaspecten van magnetische sedimentatie worden samengevat. De chemische methode waarmee de zelfgemaakte magnetische vloeistoffen zijn bereid wordt besproken, met toelichting van de chemische processen in iedere stap van de synthese.

In **hoofdstuk 2** wordt de sedimentatie van magnetische vloeistoffen geanalyseerd met behulp van magnetische metingen. Tussen een cilindrische neodymium magneet en een monster van magnetische vloeistof wordt een

magnetisch veld sensor geplaatst, die veranderingen in het lokale magneetveld meet. Tijdsafhankelijke metingen worden geïnterpreteerd aan de hand van een simpel model, waarin de magnetische vloeistof wordt voorgesteld als een stapel van drie cilinders: (1) een toplaag met oplosmiddel waarin zich geen magnetische nanodeeltjes bevinden, (2) een middelste laag waarin de concentratie van magnetische nanodeeltjes gelijk is aan de initiële concentratie van het systeem en (3) een laag met geconcentreerd sediment op de bodem van het monster. Deze aanpak gaat uit van een scherp sedimentatiefront, en negeert daarmee diffusie van de deeltjes. Om deze reden informeert deze methode vooral over de beginsnelheid van de sedimentatie. Interpretatie via een complexer model lijkt niet zinvol, omdat de meetdata daarvoor te weinig informatie bevatten.

Sedimentatie van deeltjes in sterke magneetvelden wordt bestudeerd in **hoofdstuk 3**. Hierin wordt sedimentatie van magnetische vloeistoffen gemeten in magneetvelden tot 10 tesla met gradiënten tot 100 tesla per meter. Dit wordt gedaan door capillairen gevuld met magnetische vloeistof in een Bitter magneet te plaatsen en deze optisch in beeld te brengen. Vanuit de beelden worden tijdsafhankelijke concentratieprofielen bepaald, waaruit de sedimentatiesnelheid wordt bepaald. De sedimentatiesnelheid wordt systematisch bepaald voor verschillende magneetvelden en magneetveldgradiënten, welke apart in te stellen zijn via de stroomsterkte door de magneet en de afstand van de meetobjecten tot het veldcentrum van de magneet.

Voor een stabiele magnetische vloeistof, zoals de vloeistof gemaakt in ons eigen laboratorium, schaalt de sedimentatiesnelheid lineair met de veldgradiënt. De sedimentatiesnelheid is onafhankelijk van magneetveldsterkte mits deze hoger is dan 1 tesla, omdat de magnetische vloeistoffen dan hun verzadigingsmagnetisatie benaderen. Bij magnetische vloeistoffen met geaggregeerde deeltjes neemt de hoeveelheid doorgelaten licht af zodra een magneetveld wordt aangelegd en is de sedimentatie ongeveer twee ordes van grootte sneller dan die van losse deeltjes. Deze observaties worden verklaard door de vorming van dipolaire structuren in de vloeistof.

Voor de vloeistoffen die gebruikt zijn in dit onderzoek, geven experimenten die zijn uitgevoerd bij magneetvelden van 0,3 tot 0,5 tesla een goede indicatie voor de sedimentatiesnelheid en colloïdale stabiliteit bij hogere velden. Dit impliceert dat het gedrag van magnetische vloeistoffen in sterke magneetvelden

kan worden voorspeld aan de hand van metingen met relatief simpele opstellingen en permanente magneten.

Een theoretisch model voor de sedimentatie van magnetische nanodeeltjes wordt gepresenteerd in **hoofdstuk 4**. In dit model voor verdunde magnetische vloeistoffen worden drie krachten op een magnetisch deeltje beschouwd, (1) een magnetische kracht in de richting van hoger magneetveld, (2) een osmotische kracht vanwege het gradiënt in chemische potentiaal dat ontstaat door sedimentatie van deeltjes, en (3) een wrijvingskracht die afhankelijk is van de snelheid waarmee het deeltje zich door de vloeistof beweegt. Door de som van deze krachten gelijk aan nul te stellen wordt de gemiddelde snelheid van de deeltjes bepaald als functie van hoogte. Beginnend vanuit een homogene vloeistof, worden volgende profielen in de tijd berekend door deeltjes in kleine tijdstapjes dt te verplaatsen van en naar aangrenzende volume elementen volgens de lokale snelheden van de aanwezige deeltjes. Voor ieder nieuw concentratieprofiel wordt weer de gemiddelde snelheid van de deeltjes berekend op iedere hoogte en het proces wordt herhaald. Op deze manier wordt het concentratieprofiel als functie van tijd berekend. In dit model worden interacties tussen deeltjes niet meegenomen. Verdunde polydisperse systemen worden gemodelleerd als een verzameling van monodisperse systemen waarvan een gewogen gemiddelde wordt genomen op basis van hun relatieve frequentie in het polydisperse systeem.

De berekeningen zijn uitgevoerd voor verschillende magneetvelden en magneetveldgradiënten, waarna de resultaten zijn vergeleken met experimentele resultaten in vergelijkbare velden en gradiënten. Voor stabiele magnetische vloeistoffen, waarvan de deeltjes individueel gedispergeerd zijn, komen de theoretische en experimentele resultaten overeen in magneetvelden van 0,3 tot 10 tesla, en gradiënten van 15 tot 100 tesla per meter. Hiervoor wordt een hydrodynamische schil rondom de kernen van deeltjes aangenomen met een dikte van 3 nm. Omdat in dit model interacties tussen deeltjes niet wordt meegenomen, is dit model niet geschikt voor het modelleren van vloeistoffen waarin zich geaggregeerde deeltjes bevinden of voor systemen waarin dipolaire structuren gevorm worden in magneetveld. Voor een stabiele magnetische vloeistof kan het model worden gebruikt om te voorspellen hoe de sedimentatie zal optreden op de lengteschaal van een industriële MDS opstelling.

In **hoofdstuk 5** wordt in meer detail bestudeerd hoe de magnetische sedimentatiesnelheid in relatie staat tot de afmeting en structuur van de magnetische nanodeeltjes. Een magnetische vloeistof, bestaand uit maghemiet nanodeeltjes gestabiliseerd met citraatgroepen, wordt geanalyseerd met elektronenmicroscopie, magnetometrie, röntgenextinctie, analytische (ultra)centrifugatie, magnetische sedimentatie en dynamische lichtverstrooiing. Resultaten van deze analyses worden geïnterpreteerd met behulp van een deeltjesmodel, waarin de magnetische nanodeeltjes bestaan uit een magnetische kern, omringd door een schil van niet-magnetisch ijzeroxide, wat op zijn beurt weer wordt omringd door een hydrodynamische schil van geadsorbeerd citraat en gebonden oplosmiddel.

Voor de analyse van de magnetische kern en de schil van niet-magnetisch ijzeroxide laten verschillende methoden overeenkomende resultaten zien, waarin de schil van niet-magnetisch ijzeroxide ongeveer 0,6 nm dik is. De analyse van de hydrodynamische afmeting levert echter verschillende resultaten op voor diverse analysemethoden. Deze onderlinge afwijkingen worden besproken aan de hand van de inherente eigenschappen en aannames van de gebruikte methoden.

Als algemene conclusie van dit proefschrift blijkt dat het samenklonteren van de nanodeeltjes moet worden voorkomen om de magnetische sedimentate in verdunde ferrofluïda zo traag mogelijk te laten verlopen. Tijdsafhankelijke metingen van het hoogte-afhankelijke concentratieprofiel geven de meest leerzame informatie over de magnetische sedimentatiesnelheid. Uit het evenwichtsprofiel valt zonder ambiguïteit te concluderen of de nanodeeltjes in extern magneetveld los van elkaar zijn verspreid in de vloeistof. Tevens is het mogelijk om de sedimentatiesnelheid van polydisperse magnetische vloeistoffen te modelleren in termen van de magnetohydrodynamische eigenschappen van de individuele deeltjes van verschillende grootten.

Bibliography

[1] "Innovative magnetic density separation for the optimal use of resources and energy," https://www.nwo.nl/onderzoek-en-resultaten/programmas/perspectief/Perspectief-programmas/2015/programma+1, accessed: 2020-03-23.

[2] "Plastics - the facts 2019," PlasticsEurope, Tech. Rep., 2020.

[3] "Plastics - the facts 2018," PlasticsEurope, Tech. Rep., 2019.

[4] L. L. Vatta, "Floating diamonds with nanomagnetic particles," *Macromolecular Symposia*, vol. 225, no. 1, pp. 221–228, 2005.

[5] J. Svoboda, "Densimetric separation of coal using magnetic fluids," *Physical Separation in Science and Engineering*, vol. 13, no. 3-4, pp. 127–139, 2004.

[6] D. Lin, M. Leroux, and J. Finch, "Batch magnetohydrostatic separations with a modified Frantz separator," *Minerals Engineering*, vol. 8, no. 3, pp. 283–292, 1995.

[7] K. Raj, Y. Hirota, and T. Black, "Current and emerging applications of ferrofluids," *Magnetohydrodynamics (0024-998X)*, vol. 49, 2013.

[8] R. E. Rosensweig, *Ferrohydrodynamics*. Cambridge University Press, Cambridge, 1985.

[9] S. Tajfirooz, PhD Candidate at Eindhoven University of Technology, member of the MDS research program.

[10] "Plastic Recycling Amsterdam," https://plasticrecyclingamsterdam.nl/, accessed: 2020-03-23.

[11] H. Shokrollahi, "A review of the magnetic properties, synthesis methods and applications of maghemite," *Journal of Magnetism and Magnetic Materials*, vol. 426, pp. 74–81, 2017.

[12] B. Luigjes, S. M. Woudenberg, R. de Groot, J. D. Meeldijk, H. M. Torres Galvis, K. P. de Jong, A. P. Philipse, and B. H. Erné, "Diverging geometric and magnetic size distributions of iron oxide nanocrystals," *The Journal of Physical Chemistry C*, vol. 115, no. 30, pp. 14 598–14 605, 2011.

[13] M. Klokkenburg, B. H. Erné, V. Mendelev, and A. Ivanov, "Magnetization behavior of ferrofluids with cryogenically imaged dipolar chains," *Journal of Physics: Condensed Matter*, vol. 20, no. 20, p. 204113, 2008.

[14] G. G. Stokes, *On the effect of the Internal Friction of Fluids on the Motion of Pendulums.* Pitt Press Cambridge, 1851, vol. 9.

[15] M. Klokkenburg, B. H. Erné, J. D. Meeldijk, A. Wiedenmann, A. V. Petukhov, R. P. Dullens, and A. P. Philipse, "In situ imaging of field-induced hexagonal columns in magnetite ferrofluids," *Physical Review Letters*, vol. 97, no. 18, p. 185702, 2006.

[16] R. Massart, "Preparation of aqueous magnetic liquids in alkaline and acidic media," *IEEE Transactions on Magnetics*, vol. 17, no. 2, pp. 1247–1248, 1981.

[17] E. Dubois, V. Cabuil, F. Boué, and R. Perzynski, "Structural analogy between aqueous and oily magnetic fluids," *The Journal of Chemical Physics*, vol. 111, no. 15, pp. 7147–7160, 1999.

[18] A. P. LaGrow, M. O. Besenhard, A. Hodzic, A. Sergides, L. K. Bogart, A. Gavriilidis, and N. T. K. Thanh, "Unravelling the growth mechanism of the co-precipitation of iron oxide nanoparticles with the aid of synchrotron x-ray diffraction in solution," *Nanoscale*, vol. 11, no. 14, pp. 6620–6628, 2019.

[19] M. A. Blesa and E. Matijević, "Phase transformations of iron oxides, oxohydroxides, and hydrous oxides in aqueous media," *Advances in Colloid and Interface Science*, vol. 29, no. 3-4, pp. 173–221, 1989.

[20] H. Lyklema, "Pair interactions," in *Fundamentals of Interface and Colloid Science*. Elsevier, 2005, vol. 4, pp. 3–1.

[21] F. A. Tourinho, R. Franck, and R. Massart, "Aqueous ferrofluids based on manganese and cobalt ferrites," *Journal of Materials Science*, vol. 25, no. 7, pp. 3249–3254, 1990.

[22] "National center for biotechnology information. pubchem database. citric acid, cid=311," https://pubchem.ncbi.nlm.nih.gov/compound/Citric-acid, accessed: 2020-05-05.

[23] W. Boon, "Concentration profiles of ferrofluids in magnetic fields," Master's thesis, Utrecht University, 2018.

[24] C. Cornelissen, "Colloidal stability of aqueous ferrofluids with iron oxide nanoparticles sterically stabilized by phosphorylated polyethylene glycol," Master's thesis, Utrecht University, 2018.

[25] M. Hogeboom, "High gradient magnetic separation of magnetic fluids," Bachelor's thesis, Utrecht University, 2018.

[26] H. Oppermann, "Coating nanoparticles for the stabilisation of magnetic fluids," Bachelor's thesis, Utrecht University, 2018.

[27] R. Koschny, "Optical analysis and theoretical modelling of colloidal maghemite sedimentation in magnetic field," Master's thesis, Utrecht University, 2019.

[28] K. Dreijer, "Dipolar chain formation of magnetically levitated holes under magnetic density separation conditions," Bachelor's thesis, Utrecht University, 2020.

[29] S. Odenbach, *Colloidal Magnetic Fluids: Basics, Development and Application of Ferrofluids*. Springer, 2009, vol. 763.

[30] L. Vékás, D. Bica, and M. V. Avdeev, "Magnetic nanoparticles and concentrated magnetic nanofluids: synthesis, properties and some applications," *China Particuology*, vol. 5, no. 1-2, pp. 43–49, 2007.

[31] C. Scherer and A. M. Figueiredo Neto, "Ferrofluids: properties and applications," *Brazilian Journal of Physics*, vol. 35, no. 3A, pp. 718–727, 2005.

[32] K. Raj and R. Moskowitz, "Commercial applications of ferrofluids," *Journal of Magnetism and Magnetic Materials*, vol. 85, no. 1-3, pp. 233–245, 1990.

[33] S. Serranti, V. Luciani, G. Bonifazi, B. Hu, and P. C. Rem, "An innovative recycling process to obtain pure polyethylene and polypropylene from household waste," *Waste Management*, vol. 35, pp. 12–20, 2015.

[34] B. Chanteau, J. Fresnais, and J.-F. Berret, "Electrosteric enhanced stability of functional sub-10 nm cerium and iron oxide particles in cell culture medium," *Langmuir*, vol. 25, no. 16, pp. 9064–9070, 2009.

[35] S. Laurent, D. Forge, M. Port, A. Roch, C. Robic, L. Vander Elst, and R. N. Muller, "Magnetic iron oxide nanoparticles: synthesis, stabilization, vectorization, physicochemical characterizations, and biological applications," *Chemical Reviews*, vol. 108, no. 6, pp. 2064–2110, 2008.

[36] M. Klokkenburg, R. P. Dullens, W. K. Kegel, B. H. Erné, and A. P. Philipse, "Quantitative real-space analysis of self-assembled structures of magnetic dipolar colloids," *Physical Review Letters*, vol. 96, no. 3, p. 037203, 2006.

[37] L. N. Donselaar, P. M. Frederik, P. Bomans, P. A. Buining, B. M. Humbel, and A. P. Philipse, "Visualisation of particle association in magnetic fluids in zero-field," *Journal of Magnetism and Magnetic Materials*, vol. 201, no. 1-3, pp. 58–61, 1999.

[38] R. Chantrell, J. Popplewell, and S. Charles, "Measurements of particle size distribution parameters in ferrofluids," *IEEE Transactions on Magnetics*, vol. 14, no. 5, pp. 975–977, 1978.

[39] A. O. Ivanov, S. S. Kantorovich, E. N. Reznikov, C. Holm, A. F. Pshenichnikov, A. V. Lebedev, A. Chremos, and P. J. Camp, "Magnetic

properties of polydisperse ferrofluids: A critical comparison between experiment, theory, and computer simulation," *Physical Review E*, vol. 75, no. 6, p. 061405, 2007.

[40] V. Mendelev and A. Ivanov, "Magnetic properties of ferrofluids: an influence of chain aggregates," *Journal of Magnetism and Magnetic Materials*, vol. 289, pp. 211–214, 2005.

[41] M. Bonini, E. Fratini, and P. Baglioni, "SAXS study of chain-like structures formed by magnetic nanoparticles," *Materials Science and Engineering: C*, vol. 27, no. 5-8, pp. 1377–1381, 2007.

[42] M. Klokkenburg, B. Erné, A. Wiedenmann, A. Petukhov, and A. Philipse, "Dipolar structures in magnetite ferrofluids studied with small-angle neutron scattering with and without applied magnetic field," *Physical Review E*, vol. 75, no. 5, p. 051408, 2007.

[43] J.-F. Berret, O. Sandre, and A. Mauger, "Size distribution of superparamagnetic particles determined by magnetic sedimentation," *Langmuir*, vol. 23, no. 6, pp. 2993–2999, 2007.

[44] H. D. Young, R. A. Freedman, T. Sandin, and A. L. Ford, *University Physics*. Addison-Wesley Reading, MA, 1996, vol. 9.

[45] Q. A. Pankhurst, J. Connolly, S. K. Jones, and J. Dobson, "Applications of magnetic nanoparticles in biomedicine," *Journal of Physics D: Applied Physics*, vol. 36, no. 13, p. R167, 2003.

[46] Langevin, P., "Sur la théorie du magnétisme," *J. Phys. Theor. Appl.*, vol. 4, no. 1, pp. 678–693, 1905.

[47] P. C. Hiemenz and P. C. Hiemenz, *Principles of Colloid and Surface Chemistry*. M. Dekker New York, 1986, vol. 188.

[48] B. D. Cullity and C. D. Graham, *Introduction to Magnetic Materials*. John Wiley & Sons, 2011.

[49] B. Luigjes, D. M. Thies-Weesie, A. P. Philipse, and B. H. Erné, "Sedimentation equilibria of ferrofluids: I. Analytical centrifugation in ultra-

thin glass capillaries," *Journal of Physics: Condensed Matter*, vol. 24, no. 24, p. 245103, 2012.

[50] B. Luigjes, D. M. Thies-Weesie, B. H. Erné, and A. P. Philipse, "Sedimentation equilibria of ferrofluids: II. Experimental osmotic equations of state of magnetite colloids," *Journal of Physics: Condensed Matter*, vol. 24, no. 24, p. 245104, 2012.

[51] E. Bakker, P. Rem, and N. Fraunholcz, "Upgrading mixed polyolefin waste with magnetic density separation," *Waste Management*, vol. 29, no. 5, pp. 1712–1717, 2009.

[52] J. De Koning, E. Bakker, and P. Rem, "Sorting of vegetable seeds by magnetic density separation in comparison with liquid density separation," *Seed Science and Technology*, vol. 39, no. 3, pp. 593–603, 2011.

[53] "Urban Mining Corporation," http://www.umincorp.com/, accessed: 2019-11-6.

[54] A. F. Pshenichnikov, E. A. Elfimova, and A. O. Ivanov, "Magnetophoresis, sedimentation, and diffusion of particles in concentrated magnetic fluids," *The Journal of Chemical Physics*, vol. 134, no. 18, p. 184508, 2011.

[55] C. Vasilescu, M. Latikka, K. D. Knudsen, V. M. Garamus, V. Socoliuc, R. Turcu, E. Tombácz, D. Susan-Resiga, R. Ras, and L. Vékás, "High concentration aqueous magnetic fluids: structure, colloidal stability, magnetic and flow properties," *Soft Matter*, vol. 14, no. 32, pp. 6648–6666, 2018.

[56] L. Shen, P. E. Laibinis, and T. A. Hatton, "Bilayer surfactant stabilized magnetic fluids: synthesis and interactions at interfaces," *Langmuir*, vol. 15, no. 2, pp. 447–453, 1999.

[57] N. Jain, Y. Wang, S. K. Jones, B. S. Hawkett, and G. G. Warr, "Optimized steric stabilization of aqueous ferrofluids and magnetic nanoparticles," *Langmuir*, vol. 26, no. 6, pp. 4465–4472, 2010.

[58] G. D. Mendenhall, Y. Geng, and J. Hwang, "Optimization of long-term stability of magnetic fluids from magnetite and synthetic polyelectrolytes," *Journal of Colloid and Interface Science*, vol. 184, no. 2, pp. 519–526, 1996.

[59] C. Guibert, V. Dupuis, V. Peyre, and J. Fresnais, "Hyperthermia of magnetic nanoparticles: experimental study of the role of aggregation," *The Journal of Physical Chemistry C*, vol. 119, no. 50, pp. 28 148–28 154, 2015.

[60] B. Frka-Petesic, J. Fresnais, J.-F. Berret, V. Dupuis, R. Perzynski, and O. Sandre, "Stabilization and controlled association of superparamagnetic nanoparticles using block copolymers," *Journal of Magnetism and Magnetic Materials*, vol. 321, no. 7, pp. 667–670, 2009.

[61] V. Petrenko, O. Artykulnyi, L. Bulavin, L. Almásy, V. Garamus, O. Ivankov, N. Grigoryeva, L. Vékás, P. Kopcansky, and M. Avdeev, "On the impact of surfactant type on the structure of aqueous ferrofluids," *Colloids and Surfaces A: Physicochemical and Engineering Aspects*, vol. 541, pp. 222–226, 2018.

[62] T. Kruse, H.-G. Krauthäuser, A. Spanoudaki, and R. Pelster, "Agglomeration and chain formation in ferrofluids: Two-dimensional x-ray scattering," *Physical Review B*, vol. 67, no. 9, p. 094206, 2003.

[63] E. Dubois, R. Perzynski, F. Boué, and V. Cabuil, "Liquid- gas transitions in charged colloidal dispersions: small-angle neutron scattering coupled with phase diagrams of magnetic fluids," *Langmuir*, vol. 16, no. 13, pp. 5617–5625, 2000.

[64] V. S. Mendelev and A. O. Ivanov, "Ferrofluid aggregation in chains under the influence of a magnetic field," *Physical Review E*, vol. 70, no. 5, p. 051502, 2004.

[65] C. Rablau, P. Vaishnava, C. Sudakar, R. Tackett, G. Lawes, and R. Naik, "Magnetic-field-induced optical anisotropy in ferrofluids: A time-dependent light-scattering investigation," *Physical Review E*, vol. 78, no. 5, p. 051502, 2008.

[66] Y. Hwang and X. Wu, "Quasi-two-dimensional domain structures of magnetic particles in a static field," *Physical Review E*, vol. 49, no. 4, p. 3102, 1994.

[67] J. Jin, D. Song, J. Geng, and D. Jing, "Time-dependent scattering of incident light of various wavelengths in ferrofluids under external magnetic field," *Journal of Magnetism and Magnetic Materials*, vol. 447, pp. 124–133, 2018.

[68] C. Holm and J.-J. Weis, "The structure of ferrofluids: A status report," *Current Opinion in Colloid & Interface Science*, vol. 10, no. 3-4, pp. 133–140, 2005.

[69] M. Lakić, L. Andjelković, M. Šuljagić, P. Vulić, M. Perić, P. Iskrenović, I. Krstić, M. M. Kuraica, and A. S. Nikolić, "Optical evidence of magnetic field-induced ferrofluid aggregation: Comparison of cobalt ferrite, magnetite, and magnesium ferrite," *Optical Materials*, vol. 91, pp. 279–285, 2019.

[70] "High Field Magnet Laboratory, Radboud University Nijmegen," https://www.ru.nl/hfml/use-our-facility/magnet-specifications/, accessed: 2019-11-6.

[71] A. van Silfhout and B. Erné, "Magnetic detection of nanoparticle sedimentation in magnetized ferrofluids," *Journal of Magnetism and Magnetic Materials*, vol. 472, pp. 53–58, 2019.

[72] J. Kestin, M. Sokolov, and W. A. Wakeham, "Viscosity of liquid water in the range –8 °C to 150 °C," *Journal of Physical and Chemical Reference Data*, vol. 7, no. 3, pp. 941–948, 1978.

[73] A.-H. Lu, E. L. Salabas, and F. Schüth, "Magnetic nanoparticles: synthesis, protection, functionalization, and application," *Angewandte Chemie International Edition*, vol. 46, no. 8, pp. 1222–1244, 2007.

[74] S. Khalafalla and G. Reimers, "Separating nonferrous metals in incinerator residue using magnetic fluids," *Separation Science*, vol. 8, no. 2, pp. 161–178, 1973.

[75] A. P. Philipse, "Colloidal sedimentation (and filtration)," *Current Opinion in Colloid & Interface Science*, vol. 2, no. 2, pp. 200–206, 1997.

[76] T. Sobisch and D. Lerche, "Thickener performance traced by multisample analytical centrifugation," *Colloids and Surfaces A: Physicochemical and Engineering Aspects*, vol. 331, no. 1-2, pp. 114–118, 2008.

[77] G. Iglesias, L. F. Ruiz-Morón, J. I. Monesma, J. Durán, and A. Delgado, "An experimental method for the measurement of the stability of concentrated magnetic fluids," *Journal of Colloid and Interface Science*, vol. 311, no. 2, pp. 475–480, 2007.

[78] W. Huang and X. Wang, "Study on the properties and stability of ionic liquid-based ferrofluids," *Colloid and Polymer Science*, vol. 290, no. 16, pp. 1695–1702, 2012.

[79] D. Jiles, *Introduction to Magnetism and Magnetic Materials.* CRC press, 2015.

[80] J.-C. Boyer, M.-P. Manseau, J. I. Murray, and F. C. Van Veggel, "Surface modification of upconverting $NaYF_4$ nanoparticles with PEG- phosphate ligands for NIR (800 nm) biolabeling within the biological window," *Langmuir*, vol. 26, no. 2, pp. 1157–1164, 2010.

[81] C. Lu, L. R. Bhatt, H. Y. Jun, S. H. Park, and K. Y. Chai, "Carboxyl–polyethylene glycol–phosphoric acid: a ligand for highly stabilized iron oxide nanoparticles," *Journal of Materials Chemistry*, vol. 22, no. 37, pp. 19 806–19 811, 2012.

[82] H. B. Na, I. S. Lee, H. Seo, Y. I. Park, J. H. Lee, S.-W. Kim, and T. Hyeon, "Versatile PEG-derivatized phosphine oxide ligands for water-dispersible metal oxide nanocrystals," *Chemical Communications*, no. 48, pp. 5167–5169, 2007.

[83] Z. Jia and C. Tian, "Quantitative determination of polyethylene glycol with modified dragendorff reagent method," *Desalination*, vol. 247, no. 1-3, pp. 423–429, 2009.

[84] J. van Rijssel, B. W. M. Kuipers, and B. H. Erné, "Bimodal distribution of the magnetic dipole moment in nanoparticles with a monomodal distribution of the physical size," *Journal of Magnetism and Magnetic Materials*, vol. 380, pp. 325–329, 2015.

[85] R. M. Cornell and U. Schwertmann, *The iron oxides: structure, properties, reactions, occurrences and uses.* John Wiley & Sons, 2003.

[86] F. Concha and A. Barrientos, "Settling velocities of particulate systems, 4. Settling of nonspherical isometric particles," *International Journal of Mineral Processing*, vol. 18, no. 3-4, pp. 297–308, 1986.

[87] G. R. Carmichael, "Estimation of the drag coefficient of regularly shaped particles in slow flows from morphological descriptors," *Industrial & Engineering Chemistry Process Design and Development*, vol. 21, no. 3, pp. 401–403, 1982.

[88] S. Tsuda and R. E. Rosensweig, "Ferrofluid centered voice coil speaker," Jun. 1 2010, US Patent 7,729,504.

[89] W. L. Prater, "Ferrofluid seal for actuator bearing," May 8 2001, US Patent 6,229,676.

[90] H. Borchert, E. V. Shevchenko, A. Robert, I. Mekis, A. Kornowski, G. Grübel, and H. Weller, "Determination of nanocrystal sizes: a comparison of TEM, SAXS, and XRD studies of highly monodisperse $CoPt_3$ particles," *Langmuir*, vol. 21, no. 5, pp. 1931–1936, 2005.

[91] K. Takahashi, H. Kato, T. Saito, S. Matsuyama, and S. Kinugasa, "Precise measurement of the size of nanoparticles by dynamic light scattering with uncertainty analysis," *Particle & Particle Systems Characterization*, vol. 25, no. 1, pp. 31–38, 2008.

[92] B. Khlebtsov and N. Khlebtsov, "On the measurement of gold nanoparticle sizes by the dynamic light scattering method," *Colloid Journal*, vol. 73, no. 1, pp. 118–127, 2011.

[93] D. Mahl, J. Diendorf, W. Meyer-Zaika, and M. Epple, "Possibilities and limitations of different analytical methods for the size determination of a

bimodal dispersion of metallic nanoparticles," *Colloids and Surfaces A: Physicochemical and Engineering Aspects*, vol. 377, no. 1-3, pp. 386–392, 2011.

[94] A. Philipse, "Particulate colloids: aspects of preparation and characterization," in *Fundamentals of Interface and Colloid Science.* Elsevier, 2005, vol. 4, pp. 2–1.

[95] J. Heintzenberg, "Properties of the log-normal particle size distribution," *Aerosol Science and Technology*, vol. 21, no. 1, pp. 46–48, 1994.

[96] X. Batlle and A. l. Labarta, "Finite-size effects in fine particles: magnetic and transport properties," *Journal of Physics-London-D Applied Physics*, vol. 35, no. 6, pp. R15–R42, 2002.

[97] R. Kodama, "Magnetic nanoparticles," *Journal of Magnetism and Magnetic Materials*, vol. 200, no. 1-3, pp. 359–372, 1999.

[98] P. Hendriksen, S. Linderoth, C. Oxborrow, and S. Morup, "Ultrafine maghemite particles. II. The spin-canting effect revisited," *Journal of Physics: Condensed Matter*, vol. 6, no. 16, p. 3091, 1994.

[99] C. Chantler, K. Olsen, R. Dragoset, J. Chang, A. Kishore, S. Kotochigova, and D. Zucker, "X-ray form factor, attenuation and scattering tables (version 2.1).[online] available: http://physics. nist. gov/ffast [monday, 29-jul-2013 23:22:42 EDT]. National Institute of Standards and Technology, Gaithersburg, MD. Originally published as Chantler CT," *J Phys Chem Ref Data*, vol. 29, pp. 597–1048, 2000.

[100] J. Anthony, R. Bideaux, K. Bladh, and M. Nichols, "Maghemite," *Handbook of Mineralogy III (Halides, Hydroxides, Oxides)*, 1997.

[101] S. Biggs, P. Mulvaney, C. Zukoski, and F. Grieser, "Study of anion adsorption at the gold-aqueous solution interface by atomic force microscopy," *Journal of the American Chemical Society*, vol. 116, no. 20, pp. 9150–9157, 1994.

[102] J.-W. Park and J. S. Shumaker-Parry, "Structural study of citrate layers on gold nanoparticles: role of intermolecular interactions in stabiliz-

ing nanoparticles," *Journal of the American Chemical Society*, vol. 136, no. 5, pp. 1907–1921, 2014.

[103] P. Fannin, "Wideband measurement and analysis techniques for the determination of the frequency-dependent, complex susceptibility of magnetic fluids," *Advances in Chemical Physics*, vol. 104, pp. 181–292, 1998.

[104] G. Grübel, A. Madsen, and A. Robert, "X-ray photon correlation spectroscopy," pp. 954–955, 2008.

List of Publications

The following publications are based on the content of this thesis:

Chapter 2:
A. M. van Silfhout, B. H. Erné, "Magnetic Detection of Nanoparticle Sedimentation in Magnetized Ferrofluids", *Journal of Magnetism and Magnetic Materials*, vol. 472, pp. 53-58, 2019.

Chapter 3:
A. M. van Silfhout, H. Engelkamp, B. H. Erné, "Sedimentation of Aqueous Iron Oxide at High Fields and Gradients in a Bitter Magnet", submitted.

Chapters 3 and 4:
A. M. van Silfhout, H. Engelkamp, B. H. Erné, "Colloidal Stability of Aqueous Ferrofluids at 10 T", *Journal of Physical Chemistry Letters*, vol. 11, pp. 5908-5912, 2020.

Chapters 4 and 5:
A. M. van Silfhout, H. Engelkamp, B. H. Erné, "Magnetic Sedimentation Velocities and Equilibria in Dilute Aqueous Ferrofluids", *Journal of Physical Chemistry B*, 2020 (accepted).

Acknowledgements

The work described in this thesis would not have been possible without the support of many people. I want to sincerely thank each person who helped or supported me in this journey. Because there are so many people to thank, I cannot mention each person individually here. For all the people not mentioned by name: thank you very much!

First of all, I would like to thank my promotor and copromotor. Albert, thank you for the opportunity to do the research at the Van 't Hoff laboratory, and for the useful input for my research. Ben, thank you for the excellent guidance and the always constructive and positive feedback. The door to your office was always open, and you were always willing to help with anything I was stuck with.

Additionally, I want to thank the assessment committee for spending their time to assess my thesis: prof. dr. Bruijnincx, prof. dr. Kegel, prof. dr. Krijgsman, prof. dr. ir. Sprakel, and prof. dr. ir. Tuinier. Thank you!

I also thank the user committee of my project and the people at Urban Mining Corporation. It was very enjoyable to work with you to convert the scientific results into a practial application, something that I had no experience with before. Switching between the more fundamental research at the university and the applied research was very nice.

In the last 4 years I had the opportunity to supervise a number of student projects. I learned many things from each of you and I hope you also learned a little bit from me. Thank you Cedric, Georgia, Hannah, Kim, Myrthe, Richard and Willem.

I thank all of the people I worked with at FCC for the nice working environment. Especially my office mates Chris, Pepijn, Riande and Didier: thanks for being part of the best decorated office in FCC! Marina, thanks for the nice

company and the many, many liters of coffee. Thank you Bonny and Kanvaly for the help with solving all the daily problems in the lab and office. Dominique, thanks for the help in many things, not just the lab. I want to thank Hans Meeldijk and Chris Schneijdenberg for all the help around the TEM measurements. Frans, thanks! Not only for proofreading the entire thesis but also for the many laughs and occasional drink we might have had.

Voor mijn familie (en vooral mijn ouders): bedankt! Zonder jullie zou ik dit nooit hebben kunnen doen. Niet alleen de afgelopen 4 jaar, maar mijn hele leven hebben jullie altijd voor me klaar gestaan. Ik ben jullie daar enorm dankbaar voor en ik ben blij dat ik in zo'n fijne omgeving heb mogen opgroeien.

Ook mijn vrienden wil ik graag bedanken. Het is enorm fijn om vrienden te hebben waar je terecht kan, niet alleen voor een gezellige avond maar ook voor serieuzere dingen. Bedankt daarvoor!

Riande, ik vond het erg fijn om kantoorgenoten te zijn. Zo was het kantoor niet alleen een plek voor werk maar ook een stuk gezelligheid. Martin, hartelijk bedankt voor de vele jaren vriendschap (al sinds de kleuterschool)! Ik vind het erg fijn dat jullie naast me willen staan bij mijn verdediging.

About the Author

Alexander Marius van Silfhout was born on June 14th, 1992 in Ede, the Netherlands. He grew up in Ede, where he went to the Stadhouder Willem III school from 1996 to 2004. He attended the Jacobus Fruytier Scholengemeenschap in Apeldoorn from 2004 to 2010, where he received his gymnasium degree.

From 2010 to 2014, he studied Molecular Life Science at Wageningen University, with a minor in healthy aging in humans and model species. His bachelor thesis was on the characterization of force distribution in colloidal Wigner crystals under the supervision of dr. R. F. Higler and prof. dr. ir. J. H. B. Sprakel.

In 2016, he obtained his master's degree in Molecular Life Science, with a specialization in Physical Chemistry from the Wageningen University. During his master, he worked on a project investigating the synthesis of melamine resin microspheres under the supervision of prof. dr. ir. J. H. B. Sprakel. For his master's thesis he joined the laboratory of BioNanoTechnology at the Wageningen University, where he worked on the design and fabrication of NMR microcoil probes under the supervision of dr. V. Saggiomo and prof. dr. A. H. Velders. In his internship, he worked on the synthesis and conjugation of gold nanoparticles at Aurion, a company located in Wageningen.

In 2016, he joined the Van 't Hoff laboratory at the Utrecht University where he started his PhD work presented in this thesis under the supervision of dr. B. H. Erné and prof. dr. A. P. Philipse.